Eclética Química Journal

Volume 44 • number 1 • year 2019

A review on the state-of-the-art advances for CO_2 electro-chemical reduction using metal complex molecular catalysts

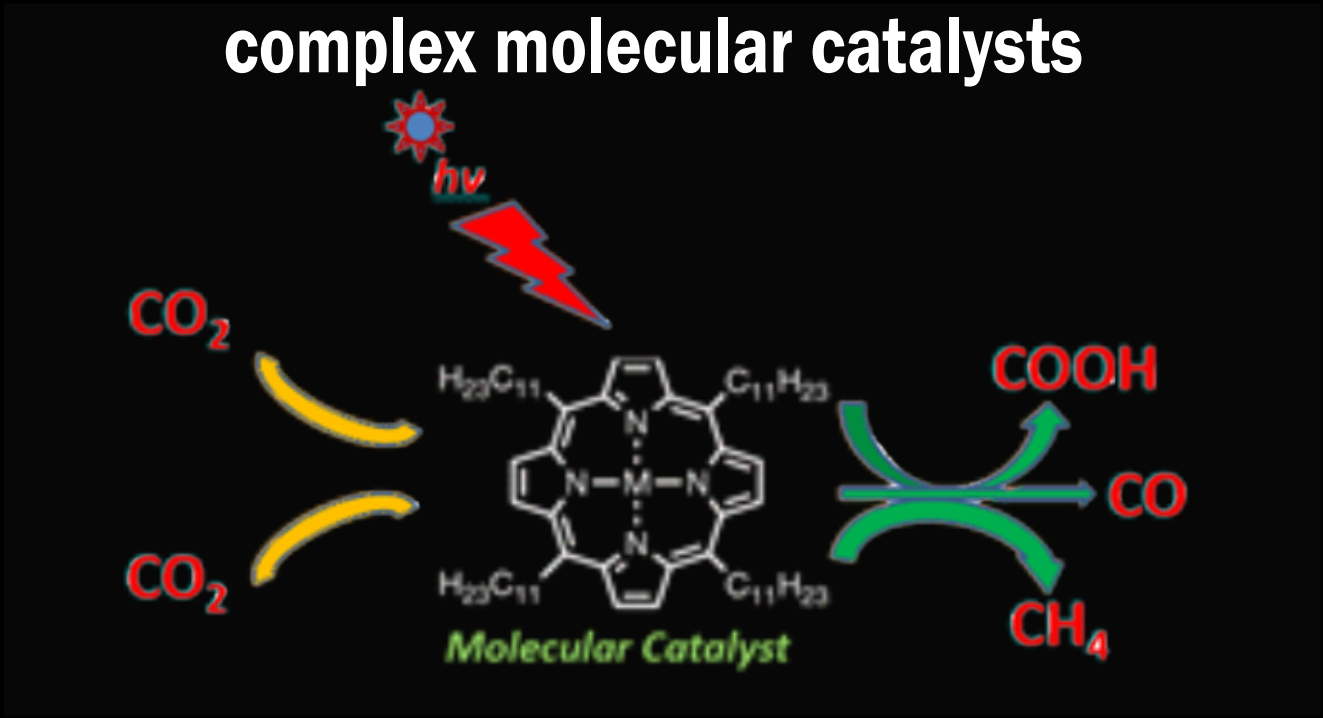

Digital

Chromium speciation in leather samples: an experiment using digital images, mobile phones and environmental concepts

Ecotoxicity

Electrochemical remediation of industrial pharmaceutical wastewater containing hormones in a pilot scale treatment system

Voltammetry

Voltammetric method for the quantification of cadmium using non-commercial electrodes and minimal instrumentation

unesp
UNIVERSIDADE ESTADUAL PAULISTA
"JÚLIO DE MESQUITA FILHO"

Instituto de Química
UNESP
Araraquara
ISSN 1678-4618

UNIVERSIDADE ESTADUAL PAULISTA

Reitor

Sandro Roberto Valentini

Vice-reitor

Sergio Roberto Nobre

Pró-reitor de Planejamento Estratégico e Gestão

Leonardo Theodoro Büll

Pró-reitora de Graduação

Gladis Massini-Cagliari

Pró-reitor de Pós-Graduação

João Lima Sant'Anna Neto

Pró-reitora de Extensão Universitária

Cleopatra da Silva Planeta

Pró-reitor de Pesquisa

Carlos Frederico de Oliveira Graeff

INSTITUTO DE QUÍMICA

Diretor

Eduardo Maffud Cilli

Vice-Diretora

Dulce Helena Siqueira Silva

Eclética Química Journal

Editorial Team
iq.unesp.br/ecletica

| Vol. 44 | n. 1 | 2019 |

Editorial Team

Eclética Química Journal

Editorial
iq.unesp.br/ecletica

| Vol. 44 | n. 1 | 2019 |

Editorial

The Editor is very happy to announce the first issue of Eclética Química Journal of 2019, hoping from now on the dawn of a new era for EQJ. This issue contains a review on the state-of-the-art advances for CO_2 electro-chemical reduction using metal complex molecular catalysts**.** For this purpose, the authors claimed that in order to increase metal complexes molecular catalysts application, it is imperative to overcome their poor stability which is a significant challenge. Following this review, the readers can find a description of a new method for the elimination of residual drugs from pharmaceutical and domestic sources, based on electrocoagulation techniques, consisting of a pilot prototype development and its application to remove these contaminants and decrease significantly the toxicity of treated water. In sequence, the quantification of cadmium with an acceptable repeatability and good accuracy was presented employing noncommercial electrodes and minimal instrumentation, which can be accessed by many laboratories with scarce economic resources. In the last article, a new and simple method for Cr speciation and Cr(VI) determination in leather samples is described using the capture of digital images with a mobile phone and their processing with a free app called PhotoMetrix, and the results are compared to the reference methods.

The Editor and his team thank all authors for their valuable contributions, and reviewers for their outstanding collaboration.

Assis Vicente Benedetti
Editor-in-Chief of EQJ

Eclética Química Journal

Author guidelines
iq.unesp.br/ecletica

| Vol. 44 | n. 1 | 2019 |

Instructions for Authors

Preparation of manuscripts

• **Only manuscripts in English will be accepted.** British or American usage is acceptable, but they should not be mixed.

• **The corresponding author should submit the manuscript online**: http://revista.iq.unesp.br/ojs/index.php/ecletica/author

• **Manuscripts must be sent in editable files as** *.doc, *.docx or *.odt. The text must be typed using font style Times New Roman and size 11. Space between lines should be 1.5 mm and paper size A4.

• **The manuscript should be organized in sections as follows:** Introduction, Experimental, Results and Discussion, Conclusions, and References. Sections titles must be written in bold and numbered sequentially; only the first letter should be in uppercase letter. Subsections should be written in normal and italic lowercase letters. For example: **1. Introduction**; *1.1 History;* **2. Experimental**; *2.1 Surface characterization; 2.1.1 Morphological analysis.*

• **The cover letter should include**: the authors' full names, e-mail addresses, ORCID code and affiliations, and remarks about the novelty and relevance of the work. The cover letter should also contain a declaration of the corresponding author, on behalf of the other authors, that the article being submitted is original and its content has not been published previously and is not under consideration for publication elsewhere, that no conflict of interest exists and if accepted, the article will not be published elsewhere in the same form, in any language, without the written consent of the publisher. Finally, the cover letter should also contain the suggestion of 3 (three) suitable reviewers (please, provide full name, affiliation, and e-mail).

• **The first page of the manuscript** should contain the title, abstract and keywords. ***Please, do not give authors names and affiliation, and acknowledgements since a double-blind reviewer system is used. Acknowledgements should be added to the proof only*.**

• **All contributions should include** an Abstract (200 words maximum), three to five Keywords and a Graphical Abstract (8 cm wide and 4 cm high) with an explicative text (2 lines maximum).

• **References should be numbered** sequentially in superscript throughout the text and compiled in brackets at the end of the manuscript as follows:

***Journal*:**

[1] Adorno, A. T. V., Benedetti, A. V., Silva, R. A. G. da, Blanco, M., Influence of the Al content on the phase transformations in Cu-Al-Ag Alloys, Eclet. Quim. 28 (1) (2003) 33-38. https://doi.org/10.1590/S0100-46702003000100004.

***Book*:**

[2] Wendlant, W. W., Thermal Analysis, Wiley-Interscience, New York, 3rd ed., 1986, ch1.

***Chapter in a book*:**

[3] Ferreira, A. A. P., Uliana, C. V., Souza Castilho, M. de, Canaverolo Pesquero, N., Foguel, N. V., Pilon dos Santos, G., Fugivara, C. S., Benedetti, A. V., Yamanaka, H., Amperometric Biosensor for Diagnosis of Disease, In: State of the Art in Biosensors - Environmental and Medical Applications, Rinken, T., ed., InTech: Rijeka, Croatia, 2013, Ch. 12.

***Material in process of publication*:**

[4] Valente Jr., M. A. G., Teixeira, D. A., Lima Azevedo, D., Feliciano, G. T., Benedetti, A. V., Fugivara, C. S., Caprylate Salts Based on Amines as Volatile Corrosion Inhibitors for Metallic Zinc: Theoretical and Experimental Studies, Frontiers in Chemistry. https://doi.org/10.3389/fchem.2017.00032.

• Figures, Schemes, and Tables should be numbered sequentially and presented at the end of the manuscript.

• Nomenclature, abbreviations, and symbols should follow IUPAC recommendations.

• Figures, schemes, and photos already published by the same or different authors in other publications may be reproduced in manuscripts of **Eclet. Quim. J.** only with permission from the editor house that holds the copyright.

• Graphical Abstract (GA) should be a high-resolution figure (900 dpi) summarizing the manuscript in an interesting way to catch the attention of the readers and accompanied by a short explicative text (2 lines maximum). GA must be submitted as *.jpg, *.jpeg or *.tif.

• **Communications** should cover relevant scientific results and are limited to 1,500 words or three pages of the Journal, not including the title, authors' names, figures, tables and references. However, Communications suggesting fragmentation of complete contributions are strongly discouraged by Editors.

• **Review articles** should be original and present state-of-the-art overviews in a coherent and concise form covering the most relevant aspects of the topic that is being revised and indicate the likely future directions of the field. Therefore, before beginning the preparation of a Review manuscript, send a letter (1page maximum) to the Editor with the subject of interest and the main topics that would be covered in Review manuscript. The Editor will communicate his decision in two weeks. Receiving this type of manuscript does not imply acceptance to be published in **Eclet. Quím. J.** It will be peer-reviewed.

• **Short reviews** should present an overview of the state-of-the-art in a specific topic within the scope of the Journal and limited to 5,000 words. Consider a table or image as corresponding to 100 words. Before beginning the preparation of a Short Review manuscript, send a letter (1page maximum) to the Editor with the subject of interest and the main topics that would be covered in the Short Review manuscript.

• **Technical Notes**: descriptions of methods, techniques, equipment or accessories developed in the authors' laboratory, as long as they present chemical content of interest. They should follow the usual form of presentation, according to the peculiarities of each work. They should have a maximum of 15 pages, including figures, tables, diagrams, etc.

• **Articles in Education in Chemistry and chemistry-correlated areas**: research manuscript related to undergraduate teaching in Chemistry and innovative experiences in undergraduate and

graduate education. They should have a maximum of 15 pages, including figures, tables, diagrams, and other elements.

• **Special issues** with complete articles dedicated to Symposia and Congresses can be published by **Eclet. Quim. J.** under the condition that a previous agreement with Editors is established. All the guides of the journal must be followed by the authors.

• **Eclet. Quim. J.** Ethical Guides and Publication Copyright:

Before beginning the submission process, please be sure that all ethical aspects mentioned below were followed. Violation of these ethical aspects may prevent authors from submitting and/or publishing articles in **Eclet. Quim. J.**

- The corresponding author is responsible for listing as authors only researchers who have really taken part in the work, and for informing them about the entire manuscript content and for obtaining their permission for submitting and publishing.

- Authors are responsible for carefully searching for all the scientific work relevant to their reasoning irrespective of whether they agree or not with the presented information.

- Authors are responsible for correctly citing and crediting all data used from works of researchers other than the ones who are authors of the manuscript that is being submitted to **Eclet. Quim. J.**

- Citations of Master's Degree Dissertations and PhD Theses are not accepted; instead, the publications resulting from them must be cited.

- Explicit permission of a non-author who has collaborated with personal communication or discussion to the manuscript being submitted to **Eclet. Quím. J.** must be obtained before being cited.

- Simultaneous submission of the same manuscript to more than one journal is considered an ethical deviation and is conflicted to the declaration has been done below by the authors.

- Plagiarism, self-plagiarism, and the suggestion of novelty when the material was already published are unaccepted by **Eclet. Quim. J.**

- The word-for-word reproduction of data or sentences as long as placed between quotation marks and correctly cited is not considered ethical deviation when indispensable for the discussion of a specific set of data or a hypothesis.

- Before reviewing a manuscript, the *turnitin* anti-plagiarism software will be used to detect any ethical deviation.

- The corresponding author transfers the copyright of the submitted manuscript and all its versions to **Eclet. Quim. J.**, after having the consent of all authors, which ceases if the manuscript is rejected or withdrawn during the review process.

- Before submitting manuscripts involving human beings, materials from human or animals, the authors need to confirm that the procedures established, respectively, by the institutional committee on human experimentation and Helsinki's declaration, and the recommendations of the animal care institutional committee were followed. Editors may request complementary information on ethical aspects.

- When a published manuscript in EQJ is also published in other Journal, it will be immediately withdrawn from EQJ and the authors informed of the Editor decision.

• Manuscript Submissions

For the first evaluation: the manuscripts should be submitted in three files: the cover letter as mentioned above, the graphical abstract and the entire manuscript.

The entire manuscript should be submitted as *.doc, *.docx or *.odt files.

The Graphical Abstract (GA) 900 dpi resolution is mandatory for this Journal and should be submitted as *.jpg, *.jpeg or *.tif files as supplementary file.

The cover letter should contain the title of the manuscript, the authors' names and affiliations, and the relevant aspects of the manuscript (no more than 5 lines), and the suggestion of 3 (three) names of experts in the subject: complete name, affiliation, and e-mail).

• Reviewing

The time elapsed between the submission and the first response of the reviewers is around 3 months. The average time elapsed between submission and publication is 7 months.

• **Resubmission** (manuscripts "rejected in the present form" or subjected to "revision"): **A LETTER WITH THE RESPONSES TO THE COMMENTS/CRITICISM AND SUGGESTIONS OF REVIEWERS/EDITORS SHOULD ACCOMPANY THE REVISED MANUSCRIPT. ALL MODIFICATIONS MADE TO THE ORIGINAL MANUSCRIPT MUST BE HIGHLIGHTED.**

• Editor's requirements

Authors who have a manuscript accepted in **Eclética Química Journal** may be invited to act as reviewers.

Only the authors are responsible for the correctness of all information, data and content of the manuscript submitted to **Eclética Química Journal**. Thus, the Editors and the Editorial Board cannot accept responsibility for the correctness of the material published in **Eclética Química Journal**.

• Proofs

After accepting the manuscript, **Eclet. Quim. J.** technical assistants will contact you regarding your manuscript page proofs to correct printing errors only, i.e., other corrections or content improvement are not permitted. The proofs shall be returned in 3 working days (72 h) via e-mail.

• Authors Declaration

The corresponding author declares, on behalf of the other authors, that the article being submitted is original and has been written by the stated authors who are all aware of its content and approve its submission. Declaration should also state that the article has not been published previously and is not under consideration for publication elsewhere, that no conflict of interest exists and if accepted, the article will not be published elsewhere in the same form, in any language, without the written consent of the publisher.

• Appeal

Authors may only appeal once about the decision regarding a manuscript. To appeal against the Editorial decision on your manuscript, the corresponding author can send a rebuttal letter to the editor, including a detailed response to any comments made by the reviewers/editor. The editor will consider the rebuttal letter, and if dimmed appropriate, the manuscript will be sent to a new reviewer. The Editor decision is final.

• Contact

Gustavo Marcelino de Souza (ecletica@journal.iq.unesp.br)

Submission Preparation Checklist

As part of the submission process, authors are required to check off their submission's compliance with all of the following items, and submissions may be returned to authors that do not adhere to these guidelines.

In **Step 1**, select the appropriate section for this submission.

Be sure that Authors' names, affiliations and aknowledgements were removed from the manuscript. The manuscript must be in *.doc, *.docx or *.odt format before uploading in **Step 2**.

In **Step 3**, add the full name of each author including the ORCID IDs in its full URL ONLY WITH HTTP, NOT HTTPS (eg. http://orcid.org/0000-0002-1825-0097).

Add the authors in the same order as they appear in the manuscript in **step 3**.

Be sure to have the COVER LETTER and GRAPHICAL ABSTRACT (according to the Author Guildelines) to upload them in **Step 4**.

Check if you've followed all the previous steps before continuing the submission of your manuscript.

Copyright Notice

The corresponding author transfers the copyright of the submitted manuscript and all its versions to **Eclet. Quim. J.**, after having the consent of all authors, which ceases if the manuscript is rejected or withdrawn during the review process.

Self-archive to institutional, thematic repositories or personal web page is permitted just after publication.

Eclética Química Journal

Summary
iq.unesp.br/ecletica

| Vol. 44 | n. 1 | 2019 |

SUMMARY

Eclética Química Journal

Original review
iq.unesp.br/ecletica

| Vol. 44 | n. 1 | 2019 |

A review on the state-of-the-art advances for CO_2 electro-chemical reduction using metal complex molecular catalysts

Hitler Louis[1, 2+], Ozioma Udochukwu Akakuru[2, 3], Philip Monday[1], Oyebanji Oluwatomisin Funmilayo[4]

[1] University of Chinese Academy of Sciences, National Centre for Nanoscience and Technology, CAS Centre for Excellence in Nanoscience, CAS Key Laboratory for Nanosystem and Hierarchical Fabrication, Beijing, China.
[2] University of Calabar, Faculty of Physical Sciences, Department of Pure and Applied Chemistry, Calabar, Cross River State, Nigeria
[3] University of Chinese Academy of Sciences, Ningbo Institute of Materials Technology and Engineering, Zhejiang, P.R. China
[4] University of Ibadan, Faculty of Physical Sciences, Department of Chemistry, Ibadan, Nigeria

[+] Corresponding author: Hitler Louis, phone: +86 15 001075832, e-mail address: louismuzong@gmail.com; louis@nanoctr.cn

ARTICLE INFO

Article history:
Received: October 18, 2018
Accepted: December 25, 2018
Published: January 28, 2019

Keywords:
1. metal complex
2. molecular catalyst
3. photocatalysis
4. mechanism
5. CO_2 electrochemical

ABSTRACT: Significantly, global warming which is caused by CO_2 emission and energy shortage are global problems resulting from artificial photosynthesis because it required many functions (light harvesting, Z water, and oxidation scheme). Therefore, photocatalytic systems development for CO_2 reduction is germane in this field. Metal complexes molecular catalyst have become prevalent homogeneous catalysts for carbon dioxide (CO_2) photocatalytic reduction since it was initially known as CO_2 reduction catalysts in the 70s and the 80s, while utmost part involved macrocyclic cobalt(II) and nickel(II) complexes. This review article presents a broad understanding on some active catalysts recently reported as a metal complex molecular catalytic schemes for CO_2 reduction, alongside catalytic activity, stability, selectivity under electro-reduction, and photoreduction circumstances. The progress of *in situ* spectroelectrochemical methods, typically supported via theoretical calculations, helped to access this know-how by providing information which enabled researchers to acquire more in-depth perception into unveiling the catalytic reaction and mechanisms intermediates.

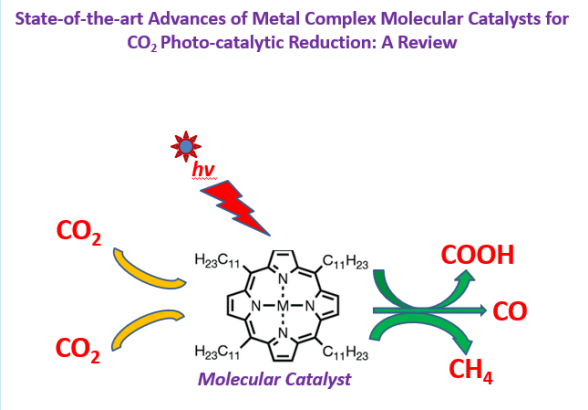

1. Introduction

The increasing level of atmospheric CO_2 concentration and fossil resources diminishing are sources of global environmental problems, hence, restoring environmental paradigm requires: atmospheric CO_2 level monitoring and renewable energy sources exploration for alternative uses CO_2 to value-added products[1-3]. For instance, CO_2 conversion for other uses (e.g., fuel or chemical feedstock compounds) could fundamentally reduce CO_2 emissions and fossil fuel consumption causing climate change and other related environmental problems[1]. Moreover, the reliability of electrocatalytic reduction of CO_2 method has been reported, because: (i) operates under ambient conditions and (ii) could exert electricity produced from renewable energy sources[2]. Selective photocatalytic CO_2 reduction to CO is one promising process because CO is an essential feedstock chemical for liquid hydrocarbons and methanol production[4]. Several materials (e.g.

metals - Cu, Au, Ag, and Zn)[5-8], metal oxide semiconductors – ZnO, SnO_2[9, 10], metal dichalcogenides – MoS_2 and WSe_2[11, 12], and transition-metal-based molecular complexes: Mn-, Fe-, Co-, Ni-, Cu-, Ru-, and Re-based complexes[13-15], have been utilized for catalyzing electro-reduction of CO_2 to liquid fuel hydrocarbons. It has been widely known and generally accepted that there are three significant steps in photocatalysis: solar light harvesting, charge separation and transportation, and surface reactions. By using the CO_2 reduction catalysts, significant progress has been made in optimizing the first two steps as they involve the same issues in solar-driven water splitting and CO_2 reduction reaction systems[16-22]. The primary difference between these two photoconversion systems is the surface reaction of charge carriers (electrons for reduction and holes for oxidation). Scientists have devoted an enormous effort in order to improve the efficiency of the third step in solar water splitting, much more than in CO_2 photoreduction[23, 24].

Generally, two types of materials (homogeneous metal complexes [coordination and organometallic complexes] and solid materials) are revealed in recent CO_2 reduction catalyst studies. At the same time, while acknowledging the significance of former approach, our interest in this review would address the mechanisms and benefits of metal complex molecular catalysts; a common model for fine-tuning reactivity by ligands synthetic modifications. Molecular catalysts attributes must include the ability to store multiple reducing equals over-mediated multi-electron/multi-proton transformations essential for catalytic CO_2 reduction. This can be achieved either by reducing the metal center, which then obliges a proficient ligand field to stabilize the reduced metal ions or by lessening the ligand scaffold, with the metal operating as a mediator for electron relay[25-28]. Nonetheless, it is challenging to transform a "conventional" catalyst into an electrochemical type owing to preconditions and design rules/set[26, 27]. Notably, the catalyst conduction band edge requires a suitable range, while the catalyst reduced form is adequately stable, and the chemical step is obtainable under the desired electrolysis conditions. Expectedly, the operating state of homogeneous electrocatalyst should adjoin the thermodynamic reaction potential of the proposed catalysis, while fast chemical step kinetics is mandatory for rapid turnover frequency. For metal-organic compounds, these factors are adjustable consequent to anticipated electrolysis conditions of an appropriate metal choice and ligand tuning optimization. In the last few decades, remarkable advancement has been achieved both in the electrocatalytic performance optimization as well on mechanistic aspects.

2. Background of molecular catalyst

2.1 Principles

Most electrochemical reactions are conducted in a pair, indicating that reaction at the anode (anodic reaction) is paired with a reaction occurring at the cathode (cathodic reaction) in the photoelectrochemical cell (PEC). The co-reaction of two electrochemical, separately provides valuable, important product or intermediate for chemical synthesis, and constitutes a universal sustainable production plan for chemicals[29]. Past studies have recorded weighty examples for paired electro-organic syntheses[29-31]. However, the most prevalent paired process is chloro alkali electrolysis. Such a method can be practical to recover the energy efficiency and the atom economy in comparison to distinctly conducted processes. Achieving a maximum Faradaic efficiency (200%) is realizable since the passed electric charge is primarily used twice. However, in CO_2 reduction, the conventional approach for up-scaled reactors is the coupling to water oxidation (oxygen evolution reaction, OER)[32-36].

Electrocatalysts *sensu lato* are perfect electron transfer agents that function near the thermodynamic potential of the intended driven (products/substrates). Because, the overpotential is the difference between the applied potential ($V_{applied}$) necessary to produce certain current density at a time t, and the thermodynamic potential (E^o) of the studied system, direct electrochemical CO_2 reduction on virtually all electrode surfaces requires a tremendous over-potential, which consequently decreases the conversion efficiency because the amount of voltage applied is greater as compared to the thermodynamic required voltage. Interestingly, at this state, both thermodynamic and kinetic considerations are essential. Apparently, the function of catalysts is to minimize overpotentials and for that, their development is based on the following requirements: (a) to possess formal potentials (E^o $(C^{atn+/0})$, well matched to reactions

Eclética Química Journal, vol. 44, n. 1, 2019, 11-39
ISSN: 1678-4618
DOI: 10.26850/1678-4618eqj.v44.1.2019.p11-39

[E^o] (products/substrates), and (c) appreciable constants rate, for substrates chemical reduction to products at the present state. In addition, the heterogeneous rate constant for electrocatalyst reduction at the electrode surface must be high[37]. A general method for an electrocatalytic system is presented in Figure 1.

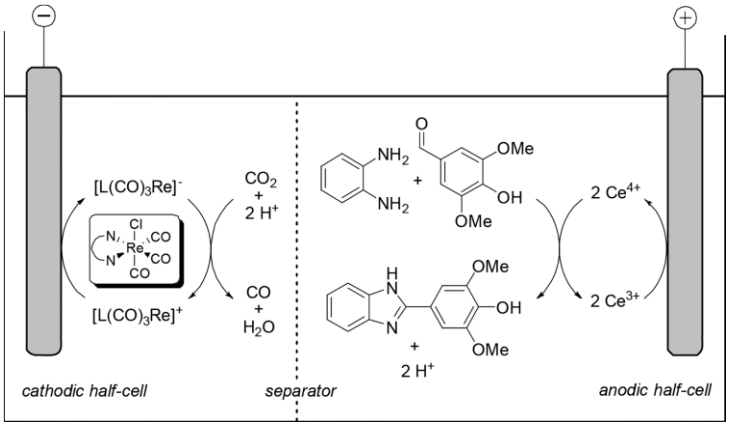

Figure 1. Diagrammatic illustration of a paired electrolysis relating cathodic CO_2-to-CO conversion catalyzed with a Re complex and anodic synthesis of a 2-substituted benzimidazole mediated by ceric ammonium nitrate[38]. Modified by the authors.

2.2 Carbon dioxide coordination Chemistry

2.2.1 Electronic structure of CO_2

The electrocatalytic CO_2 reduction is activated by the interactions of the active form of the catalyst and the substrate molecule through a process of activation. Carbon dioxide (16e^- molecule), belongs to $D_{\infty h}$ symmetry group with linear geometry at the ground state or gaseous phase. Regardless the molecular nature (nonpolar molecule and chemical stability), it encompasses two polar bonds, with two orthogonal orbital (π) sets. Previously CO_2 is assumed to be a poor ligand, however topical scientific studies on CO_2 has improved this understanding which are the display of various coordination mode and several coordination sites in its complexes. The carbon atom (LUMO orbital), has a Lewis acid character and can be described as an electrophilic center, while the oxygen atoms (HOMO orbitals) are weak Lewis bases and defined as nucleophiles[39]. Noteworthy, most CO_2 catalytic reactions involve a concurrent acid-base activation, with the carbon atom and one of the oxygen atoms tangled in the interface with the metal[40]. The two double bonds include π electrons that can interrelate per transition metals electrons in a Dewar – Chatt – Duncanson bonding scheme Figure 2[41]. When the CO_2 LUMO orbitals are engaged (through electron transfer), the least energy state and a bent geometry are equivalent, reflected in the bond length increase, bond angle decrease, and a negative charge determined by the degree of CO_2 adsorption and activation.

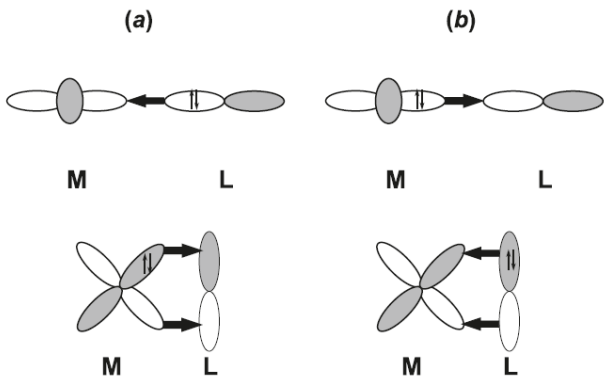

Figure 2. Schematic representation of (*a*) the Dewar–Chatt–Duncanson model and (*b*) the reversed Dewar–Chatt–Duncanson model[41]. *Reprinted with permission from Goedecke, et al., The Dewar–Chatt–Duncanson model reversed—Bonding analysis of group-10 complexes [(PMe3)2M–EX3] (M = Ni, Pd, Pt; E = B, Al, Ga, In, Tl; X = H, F, Cl, Br, I), Can. J. Chem. 87 (10) (2009) 1470-1479, © Canadian Science Publishing.*

2.2.2 Carbon monoxide binding modes

There are four basic CO_2 coordination approaches [(C, O), and binding modes [Figure 3, ref. 39]. The coordination mode involves a significant charge transfer between a metal orbital

Eclética Química Journal, vol. 44, n. 1, 2019, 11-39
ISSN: 1678-4618
DOI: 10.26850/1678-4618eqj.v44.1.2019.p11-39

and the antibonding CO_2 orbital. This bonding mode is made easier via additional weak interaction between one or two CO_2 oxygen atoms with a Lewis acid center positioned in the metal coordination domain and more partial with nucleophilic (electron-rich) metals. The η^1-CO_2 complexes are not strong; mostly, their isolation entails glove box or Schlenk techniques, exclusion of oxygen and water[40-42]. Following past records of Herskovitz[43, 44] on η^1 complexes, it becomes requisite to pressurize the system with CO_2 in order to attain complexes (iridium and rhodium). Nevertheless, ligand displacement does not occur in the forming process of these compounds. In the (C, O) bonding mode, there is a double bonding structure involving bond from the CO_2 orbital to an empty metal orbital, alongside a "back-bonding" from a filled d_{xy} metal orbital to the empty CO_2 orbital. Aresta and Nobile[45] reported the η^2 complex $[Ni(CO_2)(PCy_3)_2]$ made by reaction of $Ni(PCy_3)_3$ or $[Ni(PCy_3)_3]N_2$, in toluene, with CO_2 at atmospheric pressure and obtained as toluene solvate. The η^1 (O) end-on coordination mode is ideal with electron poor metals, and the CO_2 molecule may persist as linear or bent weakly. The (O, O) coordination mode can be defined as a metal carboxylate with an ionic bond and regularly encountered with alkali or alkaline-earth metals or, with metal surfaces in the CO_2 adsorption, for instance. Also, η^2-CO_2 complex synthesis was conveyed by Karsch[46] from the reaction of $Fe(PMe_3)_4$ with CO_2 in pentane; a second product, $Fe(PMe_3)_3(CO)(CO_3)$ was likewise attained. Recently, features of the complex $Fe(CO_2)(depe)_2$, fully characterized by Komiya *et al.*[47], buttressed the formulation of the first compound (Karsch[46]).

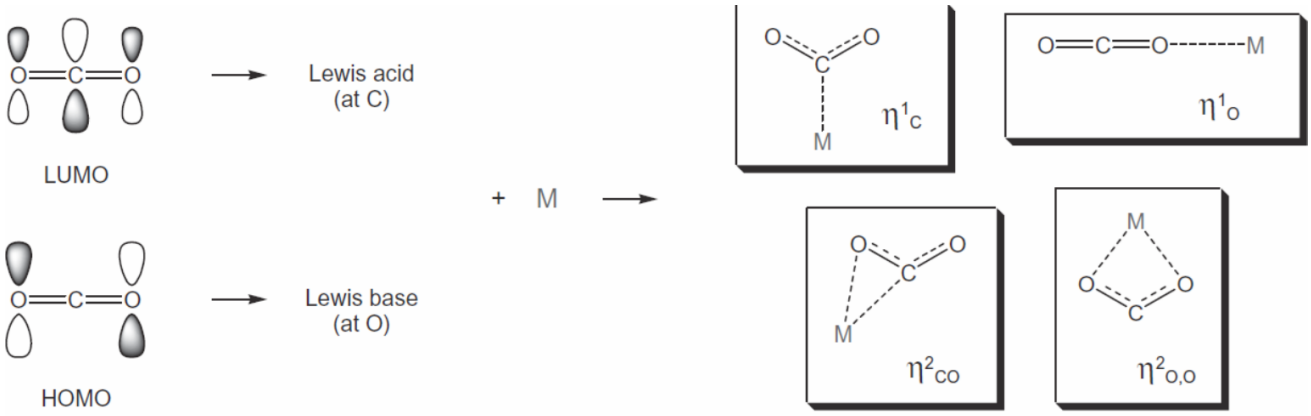

Figure 3. CO_2 coordination modes to a single metal center[39-42].

2.3 Recent Advances of CO_2 Reduction using Molecular Catalyst

2.3.1 Iron-based Molecular Catalyst

As previously explained, electrochemical CO_2 reduction to hydrocarbon fuel plays a significant part in climate change and energy cycle[48]. For instance, in the Fischer-Tropsch process carbon monoxide and hydrogen can be converted to liquid fuels. Molecular catalysts (homogenous or heterogeneous) in electrochemical or photochemical conditions are typically useful in the field[49]. In past years, iron porphyrins and metal-organic structures have received vast attention for electrocatalytic and photo electro-catalytic CO_2 reduction[50]. Applications of various modern methods and modification through synthesis to enhance the reactivity and product selectivity afforded homogeneous electro-catalysts to be one of the preferred approaches. Past results of Taheri *et al.*[51] on "an iron electrocatalyst for selective reduction of CO_2 to formate in the water" stated that with low applied overpotential, formate is produced with a high current density and Faradaic efficiency (96%). Besides, those studies explicated catalysis mechanism by means of cyclic voltammetry, and structurally categorized a key reaction intermediate, that is the reduced hydride.

Combination of investigational data in $MeCN/H_2O$ (95:5) and aqueous solution point to a mechanism for CO_2 reduction where the electrocatalyst (Fig. 4) is reduced from $\mathbf{1}^-$ to $\mathbf{1}^{2-}$ and then protonated to produce $(H{-}\mathbf{1})^-$. A further selective reaction of $(H{-}\mathbf{1})^-$ with CO_2 to yield a C−H bond resulted in formate.

Eclética Química Journal, vol. 44, n. 1, 2019, 11-39
ISSN: 1678-4618
DOI: 10.26850/1678-4618eqj.v44.1.2019.p11-39

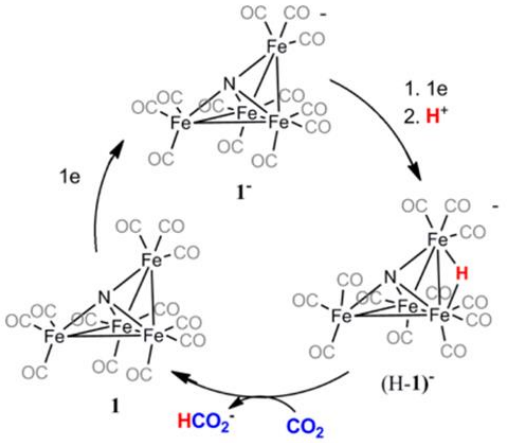

Figure 4. Projected Mechanism for Reduction of CO_2 to Formate by **1**$^-$ in the Existence of Protons[51]. *Reprinted with permission from Taheri et al., An iron electrocatalyst for selective reduction of CO_2 to formate in water: including thermochemical insights, ACS Catalysis 5 (12) (2015) 7140-7151. ACS Catal. 2015, 5, 7140−7151. Copyright (2015) American Chemical Society.*

Ambre *et al.*[52] explored the "molecular engineering for effectual and discriminating iron porphyrin catalysts for the electrochemical reduction of CO_2 to CO". Here, ester groups (*para*, *meta*, and *ortho* positions) of Fe-porphyrin were introduced and set iron porphyrins Fe-*p*E, Fe-*m*E, and Fe-*o*E. The electrochemical reduction of CO_2 to CO by these catalysts was studied. The Faradaic efficiency [(FE) - exclusive 65% and quasi-exclusive 98%] for CO was accomplished by Fe-*m*E and Fe-*o*E in CO_2 saturated electrolyte with addition of 2 mol L^{-1} H_2O, after 2 h bulk electrolysis. Also, the *meta*-substituted derived (**FE-*m*E**) is extremely selective for CO production giving FE (65%) lacking competitive H_2 production while the *para* substituted (**Fe-*p*E**) generated only H_2 (FE, 84%) as a key product of bulk electrolysis.

The cyclic voltammograms (CVs) results of these Fe porphyrins specify that Fe-*p*E, Fe-*m*E, and Fe-*o*E in DMF exhibited distinctive iron porphyrins redox behaviors. Notably, the $E(Fe^{I/0})$ of Fe-*o*E is apparently more negative than those of Fe-*p*E and Fe-*m*E, perhaps consequence of its dipole. Therefore, the Fe^0 species of Fe-*o*E is the most robust reducing catalyst between these four Fe porphyrins. Congruently, Savéant and co-workers also discussed that the reduction of CO_2 is simplified by Fe(0) species at Fe(I)/Fe(0) redox wave under CO_2 atmosphere[53-55].

Further, Rao *et al.*[56] studied the "visible-light-driven methane formation from CO_2 with a molecular iron catalyst". They observed functionalization of iron tetraphenylporphyrin complex with trimethylammonio groups, which is the most common, competent and selective molecular electrocatalyst for CO_2 conversion to CO[57-59]. This catalyst is also able to catalyze the eight-electron CO_2 reduction to methane upon distinguishable light radioactivity at ambient temperature and pressure. In addition, the catalytic system functioned in an acetonitrile solution covering a photosensitizer and sacrificial electron donor and works stably over several days. Direct CO_2 photoreduction reaction produces CO as the principal product, nonetheless, a two-pot method that first reduces CO_2 to CO and then reduces CO to methane with a selectivity (ca. 82%) and quantum yield (0.18%). Figure 5 presents conceivable mechanism illustration based on obtained results and experimental considerations, including the assumption of formyl intermediate[60, 61], which could be steadied through space interactions between the trimethylammonium group's positive charges and fractional negative charge on the CHO species bounded to the metal.

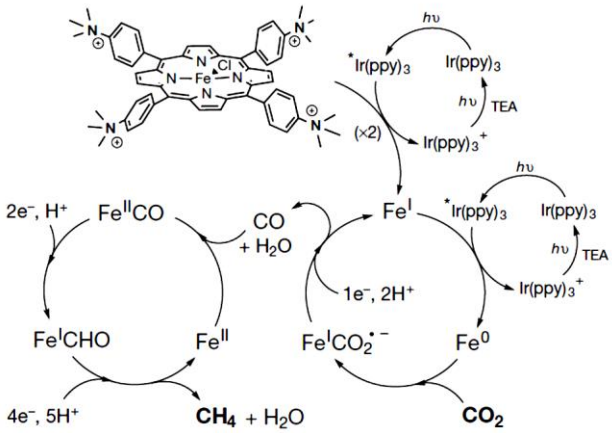

Figure 5. Illustration of the mechanism for CO_2 reduction to CH_4[56]. *Reprinted with permission from Rao et al., Visible-light-driven methane formation from CO_2 with a molecular iron catalyst, Nature 548 (2017) 74-77. Spinger Nature and Copyright (2017) Clearance Center.*

The description of the suggested mechanism includes; the reduction of proceeding Fe^{3+} porphyrin (top left) with three electrons to the catalytically active Fe^0 species. The CO_2 is reduced with Fe^0 species, regenerating FeI due to electron

Eclética Química Journal, vol. 44, n. 1, 2019, 11-39
ISSN: 1678-4618
DOI: 10.26850/1678-4618eqj.v44.1.2019.p11-39

transfer from the excited photosensitizer (right-hand side cycle). The resulting CO binds to Fe^{2+} and further lessened with six electrons (transferred from the excited sensitizer) and protons to make methane, from a guessed FeI-formyl (FeICHO) intermediate (left-hand side cycle).

Lately, Pan and co-workers[62] experimented the "active sites of CO_2 reduction on nitrogen-coordinated and atomically isolated iron and cobalt catalysts." They observed that Fe−N_4 sites are inherently extra efficient than Co−N_4 sites in M−N−C catalysts for CO_2 reduction to CO with high FE, more positive onset potential, and ample. Likewise, they computationally acknowledged (Figure 6) that the edge-hosted (M−N_{2+2}−C_8) sites bridging two armchair-like graphitic layers were dynamic moiety for the CO_2RR. Unambiguously, the M centers and C atoms, floppy bonds and following N are the vigorous *CO and *OH adsorb sites in the C−O bond cleavage throughout the CO_2RR, correspondingly.

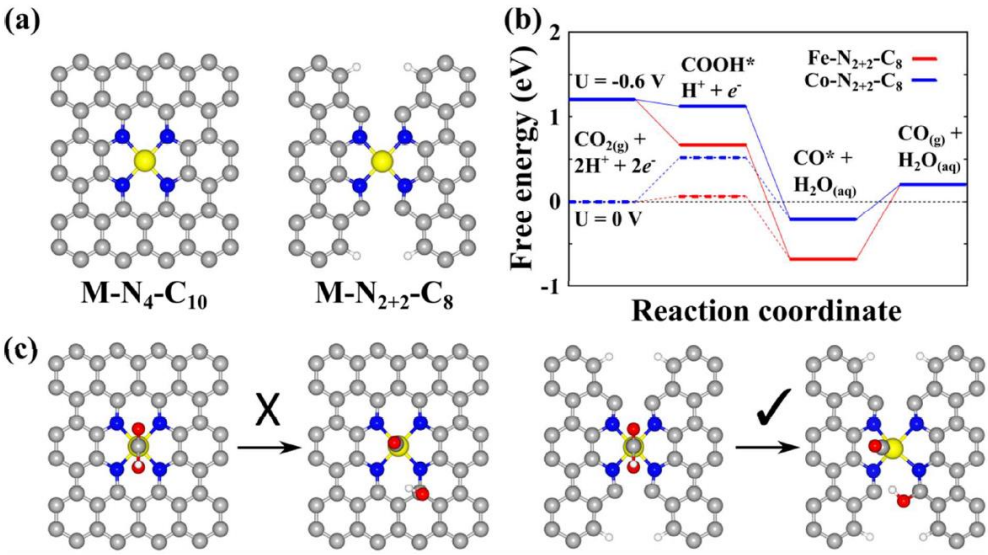

Figure 6. Atomic structure of M−N_4−C_{10} and M−N_{2+2}−C_8 (M=Fe or Co) active sites. (b) Calculated free energy evolution of CO_2 reduction to CO on M−N_{2+2}−C_8 sites under useful electrode potential (U) of 0 V and −0.6 V. (c) The initial and final state for the COOH dissociation reaction on M−N_4−C_{10} and M−N_{2+2}−C_8 sites. In the figure, the gray, blue, yellow, red, and white balls represent C, N, M, O, and H atoms, respectively[62]. *Reprinted with permission from Pan et al., Unveiling Active Sites of CO_2 Reduction on Nitrogen-Coordinated and Atomically Dispersed Iron and Cobalt Catalysts, ACS Catal. 8 (4) (2018) 3116-3122. Copyright (2018) American Chemical Society.*

The positional secondary organization dependence sphere groups on the reactivity of a conserved chief iron porphyrin core for electrochemical CO_2 reduction were investigated by Nichols *et al.*[63]. Thereby, four positional isomers (Figure 7) were synthesized, changing the position of the second-sphere amide group *ortho*- and *para*-, likewise proximal and distal, to the porphyrin plane.

In an atmosphere of CO_2 and in existence of phenol (acid source), CO_2 reduction catalytic responses suggestive is examined using cyclic voltammetry for all catalysts. Comparatively, when phenol (100 mmol L^{-1}) was used, Fe–ortho-1-amide display a catalytic onset that is somewhat more positive than Fe–ortho-2-amide, while both evinces meaningfully higher catalytic responses than the equivalent para-functionalized positional un-functionalized Fe-TPP.

For a better understanding of CO_2 reduction catalyzed by this series of amide-functionalized porphyrins, the pragmatic constants rate determined by FOWA were reviewed as a function of phenol and CO_2 concentration. All four functionalized catalysts reveal first-order dependence on phenol concentration under pseudo-first order circumstances. Fe–ortho-2-amide has the most momentous experimental constants rate of all catalysts studied. Nonetheless, displays non-linearity at higher phenol concentrations, probably as a result of catalyst inhibition or local depletion of CO_2. The Fe–ortho-1-amide has the next highest values (K_{obs}), trailed by Fe–para-2-amide while

Eclética Química Journal, vol. 44, n. 1, 2019, 11-39
ISSN: 1678-4618
DOI: 10.26850/1678-4618eqj.v44.1.2019.p11-39

Fe–para-1-amide is the least. To appraise the catalytic efficacy, it is mandatory to examine the overpotential (η) vs. log (TOF) relationships exhibited by the catalytic Tafel plot[64]. Operative catalysts function with higher TOFs at lower overpotentials (upper left portion of such plots. Fe–ortho-2-amide demonstrate higher TOFs above all over potential values than Fe–ortho-1-amide that exhibits higher TOFs compared to Fe-TPP and both *para*-substituted porphyrins. The values at the peak of the curves depict the maximum turnover frequency realizable at large over potential. It crucial to emphasize the difference in E_{0cat} values amongst catalysts when aiming to resolute optimal second-sphere pendant location queries. Previously[65, 66], the electrochemical CO_2 reduction driving force is habitually pretentious by electron retreating or bequeathing substituents on the porphyrin aryl rings (E_{0cat}). In such event, a linear scaling relationship among log(TOF_{max}) and its observations (E_{0cat}), moreover, larger TOFs is achieved wherever there are catalysts with high negative values (E_{0cat}). Nonconformity arises when second-sphere interactions either inhibit or promote catalysis, as previously recorded for electrostatic effects[67].

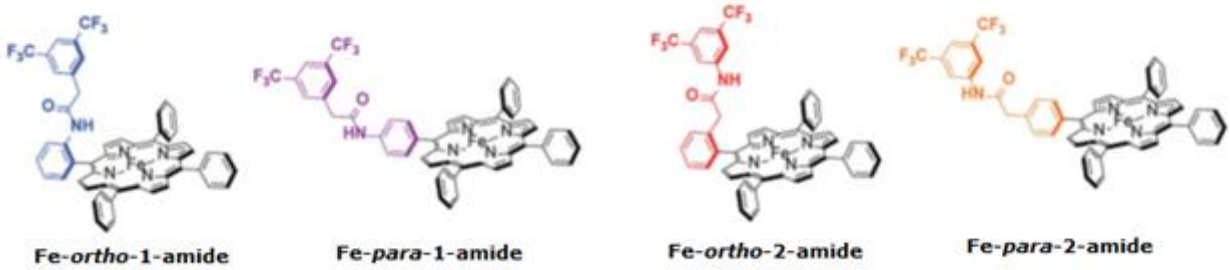

Figure 7. Positional isomers of amide-functionalized iron tetraphenylporphyrins[63]

2.3.2 Zn-based Metal Complex Molecular Catalyst

In terms of price, abundance, and toxicity of the metal center, the use of zinc-based systems is of significant interest. Hence, it is amazing that only a handful examples of zinc catalyzed hydrosilylation of CO_2 have been reported in literature: two cationic, N-heterocyclic carbene (NHC) zinc complexes, a dicationic NHC-stabilized zinc hydride cluster, including the tris(thiopyridyl) methane based [Tptm] ZnH and the tris[(1-isopropylbenzimidazol-2-yl)dimethylsilyl] methane-based [TismPriBenz] ZnH complexes catalytically reacted with CO_2[68-72]. The synthesis and evaluation of two new Zn(II) complexes for their ability to stimulate and reduce CO_2 have been stated by Donovan *et al.*[73]. The electrochemical characteristics of dichloro[phenyldi(2-pyridyl)phosphine-κ^2-*N*,*N*'] zinc(II) and dichloro[diphenyl-(2-pyridyl)phosphine-κ^1-*N*]zinc(II) complexes are contrasted with cyclic voltammetry.

To explore the reactivity of these complexes (dichloro[phenyldi(2-pyridyl)phosphine-κ^2-*N*,*N*'] zinc(II) and dichloro[diphenyl-(2-pyridyl)phosphine-κ^1-*N*]zinc(II)) with CO_2, samples of each complex were exposed to bubbling CO_2 as 0.20 mol L^{-1} solutions in THF. Afterward, the solid materials isolated from these solutions were placed on KBr windows via solvent evaporation at CO_2 room temperature. Comparatively, the results showed that dichloro[phenyldi(2-pyridyl)phosphine-κ^2-*N*,*N*'] zinc(II) complex lacks a continuous CO_2 adduct form since no changes were observed in the IR spectrum while dichloro[diphenyl-(2-pyridyl)phosphine-κ^1-*N*]zinc(II) complex showed a novel stretching band (1726 cm^{-1}) after 30 min at room temperature reaction time. This implies the formation of a novel compound species, **2-CO_2**. Cyclic voltammetry was used to confirm if dichloro[diphenyl-(2-pyridyl)phosphine-κ^1-*N*]zinc(II) complex could reduce the overpotential required to reduce CO_2[74]. In the ambient CO_2 atmosphere, the reduction peak onset shifted anodically (approximately 0.6 V) when a potential negative bias was utilized to dichloro[diphenyl-(2-pyridyl)phosphine-κ^1-*N*]zinc(II) complex. There is concordance between the voltammogram and the IR data as it advocates the existence of CE mechanism. Intriguingly, carbon monoxide

Eclética Química Journal, vol. 44, n. 1, 2019, 11-39
ISSN: 1678-4618
DOI: 10.26850/1678-4618eqj.v44.1.2019.p11-39

evolution was ascertained in the mass spectra acquired before and after bulk electrolysis. The electrolysis cell headspace was determined for gas composition in an airtight syringe and injected into a GC/MS instrument. The attained spectrum prior to controlled potential electrolysis (CPE), showed the superseding peak (44 *m/z*) assigned to CO_2 with the other negligible peaks in the spectrum result. Besides, the CO_2 obtained was an insignificant product in the mass spectrum and topmost (28 *m/z* is leading) after 4 hours of CPE. Summarily, it is evident that dichloro[diphenyl-(2-pyridyl)phosphine-κ^1-*N*]zinc(II) complex is the first organometallic Zn complex that improves the CO_2 electrochemical conversion to CO and sinking the required overpotential (approximately 0.6 V). Moreover, this transformation is earned at a glassy carbon electrode; more desirable compared to expensive Pt or Pd alternatives often used for electrocatalysis of this kind.

Wu *et al.*[75] reported heterogeneous zinc−porphyrin complex (zinc (II) 5,10,15,20-tetramesitylporphyrin) as an electrocatalyst that consigns a relatively high turnover frequency (14.4 sites^{-1}s^{-1}) and a Faradaic efficiency (95%) for CO_2 electro-reduction to CO at −1.7 V *vs.* usual hydrogen electrode in an organic/water mixed electrolyte. The PorZn electrodes were studied for electrochemical CO_2 reduction at different potentials in a CO_2-saturated solvent system including 0.1 mol L^{-1} tetrabutylammonium hexafluorophosphate hexafluorophosphate ($TBAPF_6$) in DMF/H_2O. The fractional current CO production densities and matching Faradaic efficiencies at various potentials are represented (Figure 8A, left). Positive potentials above −1.4 V *vs.* SHE, resulted in H_2 as the only product. CO_2 conversion to CO observation begins at −1.4 V, with a CO 22% Faradaic efficiency. Notably, applications of more negative potentials are corresponded to increase in both the current density and CO Faradaic efficiency. The supreme CO Faradaic efficiency (95%, −1.7 V *vs.* SHE) with a current density (ca. 2.1 mA/cm^2). Equally, the CO Faradaic efficiency and total current density can be reserved (at least 4 hours at −1.7 V, Figure 8B, left). Certain that Zn metal is an active recognized catalytic for electrochemical CO_2 reduction to CO[76-78], it is important to ignore the metallic Zn formation, and its catalyzing reaction.

To observe oxidation state vagaries and Zn center electronic structure in electrochemical CO_2 reaction situations, *in situ* and operando XAS extents was conducted with the reaction cell previously reported[79]. This method has been magnificently used to scrutinize the Co oxidation state in a solid-state (cobalt−porphyrin-based catalyst material) in electrocatalysis[80]. No obvious variations in the Zn K-edge X-ray absorption close to edge structure (XANES) spectra are detected as the active electrode potential is tuned from open circuit voltage (OCV, −1.7 V *vs.* SHE) (Figure 8A, right) and thereafter to +0.2 V *vs.* SHE, depicting no changes of Zn center oxidation state in the PorZn catalyst at the tested potential range. The high-quality data afforded us a clearer understanding of the PorZn local structures. As presented in Figure 8B (right), slight variations in the Zn coordination number and bond distances are recorded at the examined potentials and during electrolysis. The inconsequential alterations in the Zn local structure could be attributed to the reduction of the porphyrin ligand or binding of molecules on the Zn site. This shows that the Zn center is influential to the PorZn catalytic activity, despite that it is still redox-innocent during electrocatalysis.

The PorZn porphyrin ligand is therefore likely to be the impetus for the two-electron reduction of CO_2 to CO. The PorZn CV in saturated electrolyte shows a reduction wave that begins near −1.4 V *vs.* SHE, corresponding with the CO_2 reduction to CO observation at the potential. The cyclic voltammograms in Ar-saturated electrolyte exhibit a comparable wave linked with PorZn reduction, perhaps joined with protonation[81-84]. The utmost surprising alteration among the two CVs is the reversing wave pattern. The CV in CO_2-saturated electrolyte presents anodic wave that is weak (about −1.45 V) equivalent to the reduction wave (about −1.6 V). In contrast, the CV in Ar-saturated electrolyte presents three anodic waves (about −1.53 V, −1.17 V, and −0.43 V *vs.* SHE). Similar event (three anodic waves) was recorded in an investigation of zinc(II) 5,10,15,20-tetraphenylporphyrin studied at the same scan rate[83]. Following precedent literature[83], these anodic waves are presumed to conform with subsequent oxidation and deprotonation of the reduced porphyrin ring. For deeper understanding in PorZn-catalyzed CO_2 reduction, Wu and co-workers conducted PorZn chemical reduction using solution under inert situations and adopt one or two equals of sodium naphthalene in tetrahydrofuran (NaNap, ca. −2.4 V *vs.* SHE in THF[85]) as the reducing agent. The reduced PorZn

Eclética Química Journal, vol. 44, n. 1, 2019, 11-39
ISSN: 1678-4618
DOI: 10.26850/1678-4618eqj.v44.1.2019.p11-39

species display absorption bands at 710, 820, and 920 nm in the UV−Vis spectra, which are features of transiently generated zinc−porphyrin compounds with reduced ligands[81, 86]. Upon exposure of the reduced PorZn species to air, the rapid PorZn renaissance was reported in the UV−Vis spectroscopy. Thus far, the wavering of these reduced species has precluded full characterization. This experiment discloses the first molecularly structured Zn-based catalyst for electrochemical CO_2 reduction to CO with significant product selectivity. The Zn(II) center, implies redox-inactive though intrinsic to the catalysis, which separates the studied catalyst from transition metal-based molecular catalysts previously reported.

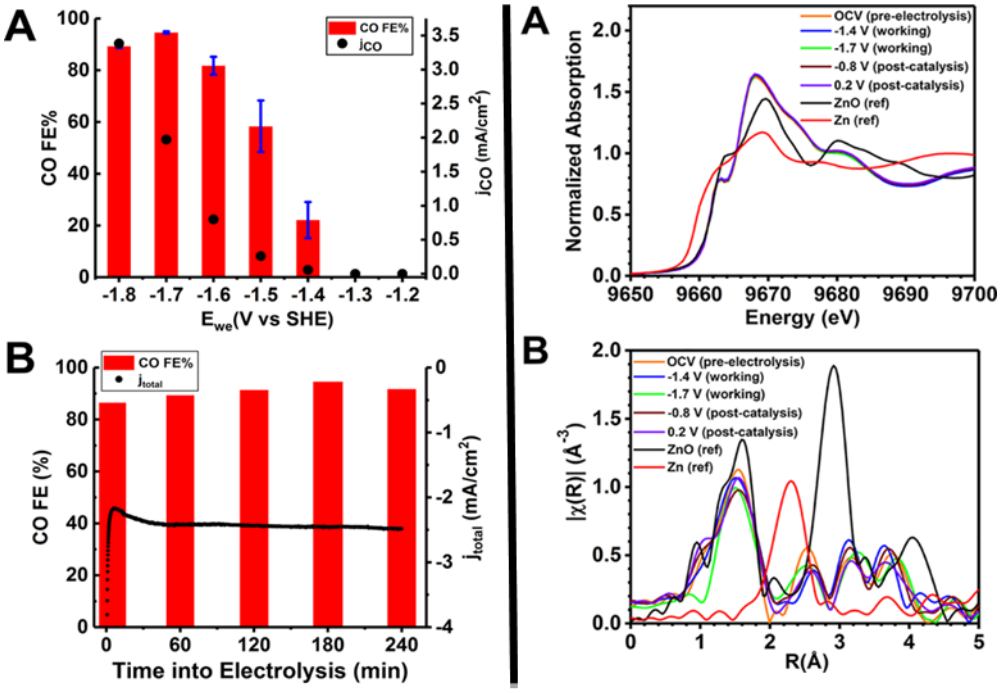

Figure 8: (Left) Electrochemical CO_2 reduction catalyzed by the PorZn electrode in 0.1 mol L^{-1} $TBAPF_6$ DMF/H_2O solution. (A) CO Faradaic efficiencies and CO partial current densities at different potentials averaged from three measurements. (B) CO Faradaic efficiencies and total current densities after 5, 60, 120, 180, and 240 min of electrolysis at −1.7 V *vs.* SHE. (right) (A) Zn K-edge XANES spectra and (B) Fourier transforms of Zn K-edge EXAFS spectra of the PorZn catalyst electrode at different potentials (V *vs.* SHE)[75]. *Reprinted with permission from Wu et al., Electroreduction of CO_2 Catalyzed by a Heterogenized Zn-Porphyrin Complex with a Redox-Innocent Metal Center, ACS Central Science 3 (8) (2017) 847-852. Copyright (2017) American Chemical Society.*

Wang *et al.*[87] studied aqueous electrocatalytic reduction of CO_2 of several synthesized ZIF–8 nanomaterials, having uncommon properties e.g., large surface area, uniform pore size, well-defined morphology, and strong coordination. Upon CO_2 electrochemical reduction, ZIF–8 nanocomposites are substantiated to be effective and proposed (ZIF–8 metal nodes) as active catalysis sites. The synthesis of CO_2 reduction electrochemical employing the nanomaterials (ZIF–8) braced on glassy carbon (GC) electrodes was assessed using CV in 0.5 mol L^{-1} NaCl aqueous solution. CV traces of different ZIF–8 materials in Ar and CO_2 exhibit magnified current and positively shifted beginning potential of catalysis in CO_2 for both nanomaterials (ZIF–8^{SO4} and ZIF–8^{NO3}) For ZIF–8^{SO4}, the positive potential shift is ca. 400 mV and ZIF–8^{AC} presents slightly less current in CO_2 compared to Ar. Notwithstanding, the current of ZIF–8^{AC} decreases a bit, yet distinguishable from other two materials (ZIF–8^{SO4} and ZIF–8^{NO3}) at the surface loading uniformity. Further, when combined with electrolysis results, ZIF–8^{AC} demonstrated high current for hydrogen evolution, and not CO_2 reduction.

The Controlled-potential electrolysis (CPE) were observed under CO_2 to understand the

Eclética Química Journal, vol. 44, n. 1, 2019, 11-39
ISSN: 1678-4618
DOI: 10.26850/1678-4618eqj.v44.1.2019.p11-39

distribution of product and the FE. The potential utilized current between –1.4 V and –1.9 V *vs.* SCE using similar electrode. For gaseous analysis and liquid phase products, gas chromatography (GC) and nuclear magnetic resonance spectroscopy (NMR) was applied. Three discoveries were reported: (i) all ZIF-8 materials, (ii) important products (H_2 and CO) and (iii) only a small amount of formate in the liquid phase was discovered. The used potential increase the FE for CO primarily increases till maximum attainment, and then lessening with further utilized potentials Various CO Faradaic efficiency were obtained (highest = ZIF–8^{SO4}[65.5%], ZIF–8^{NO3}[69.8%] & ZIF–8^{AC} [57.7%] at –1.8 V *vs.* SCE, however, ZIF–8^{SO4} displays the most extensive potential range appropriate for CO production (–1.5 to –1.9 V *vs.* SCE. The current densities of H_2 and CO products for ZIF-8 materials at –1.8 V *vs.* SCE has been also investigated[87]. The heightened partial CO current density justified that ZIF–8^{SO4} is a highly efficient catalyst for CO_2 reduction compared to ZIF–8^{NO3} and ZIF–8^{AC}.Many synthesized ZIF–8 nanocomposites were proven to be impressive CO_2 reduction catalysts. Through zinc sources regulation, ZIF–8 chemical reactivity can be modulated, and ZIF–8^{SO4} generates excellent CO selectivity. Likewise, the electrolyte performs a vital role for high CO selectivity. The Cl^- anion improves and yields the best CO_2 reduction reactivity, probably due to superficial anion exchange and small hydrated range. These observances propound ZIF-8s as effective electrocatalysts for CO_2 reduction.

2.3.3 Mn-based Metal Complex Molecular Catalyst

The most persistent manganese oxidation state occurs in +2, +4, and +7 of the compounds complete range formed by manganese. The Mn^{+7} oxidation state is sturdy, frequently lessened to Mn^{+2}. The oxidation state of Mn^{+1} is less common, but normally ensues within manganese-based organometallic complexes; d^6 Mn^I tricarbonyl complexes have become important in the catalysis field[88, 89]. Typically, complexes like the archetypal *fac*-[Mn(bpy) $(CO)_3Br$] uncover a HOMO controlled by a Mn 3d-orbital and a diimine-based LUMO. The electronic and photophysical character state of analogous Mn^I complexes can be better adjusted through diimine ligand chemical structure modification hence adapting the LUMO energy. Application of manganese as a catalyst is due to chemical similarities with rhenium (same group, oxidation states, and geometries). Nonetheless, manganese is 1.3 million times more abundant in the Earth's crust than rhenium[90].

There are several reviews on transition metals and manganese-based systems for CO_2[91-94] until recent review (Sinopoli *et al.*[90]) which unveiled the efficiency, feature and strategy of Mn carbonyl schemes for CO_2 electro- and photoreduction. In the same way, Stanbury and colleagues[95] reported in a comprehensive survey of all the Mn carbonyl systems reported as being active catalysts for CO_2 reduction, based on activity, stability, and selectivity under electro-reduction and photoreduction circumstances. In their review, they uncovered that Mn-based carbonyl complexes display an elevated capacity for CO_2 catalysis through electro-, photo- or photo electro-reduction, with activities (TON, TOF) that can contend with the Re analogs.

Fei *et al.*[96] reported the post-synthetic metallation of a robust Zr(IV)-based metal-organic framework (MOF) with open bpy metal-chelating linkers to obtain isolated Mn(bpy)-$(CO)_3Br$ moieties in the MOF. Most significantly, in conjunction with $[Ru(dmb)_3]^{2+}$ as a redox photosensitizer and 1-benzyl-1,4-dihydronicotinamide (BNAH) as a propitiatory reducing agent, the resultant [UiO-67 Mn(bpy)$(CO)_3Br$] was realized to be immensely active and selective for the photocatalytic reduction of CO_2 to formate with a turnover number (TON) of 110 through 18 h of catalysis.

The suggested mechanism for the photocatalytic reaction is presented in this review (Figure 9). In these reactions, BNAH assists as the conciliatory reducing agent, reducing the excited Ru(II) photosensitizer and starting the photocatalytic reaction. There is an electron transmission from the reduced photosensitizer to the Mn catalyst, forming an absorbable Mn(0) during catalysis. The UiO-67[97-99] large pores, are copious to allow electron transfer amongst the Ru(II) photosensitizer and the Mn complex within the MOF, as the Ru(II) photosensitizer have the strength to allow the interior of UiO-67. TEOA plausibly improves the reaction by contributing a yielded proton and electron (i.e., a hydrogen atom) for the time of catalysis through a Hofmann-type degradation process (Figure 9)[100]. It is unaffirmed whether or not TEOA harmonizes the Mn center in the course of this process; nevertheless, co-joining

Eclética Química Journal, vol. 44, n. 1, 2019, 11-39
ISSN: 1678-4618
DOI: 10.26850/1678-4618eqj.v44.1.2019.p11-39

of CO_2 with the metal center is aided by TEOA, constituting an O-bound Re−OC(O)$OCH_2CH_2NR_2$ complex, this was made known in past studies with Re bipyridine catalysts[101]. Fei and co-workers propose TEOA giving one proton and one electron to the catalytic reaction, devising a Mn(I)−H complex. CO_2 can insert into the Mn−H bond, making a Mn(I)−OC(O)H complex. Formate (or formic acid after further protonation) can then be liberated from the Mn center renewing the starting Mn(I) complex. These conclusions are from the bulk of previously published work on photosensitized catalysis impelled by sacrificial reducing agents[102-107].

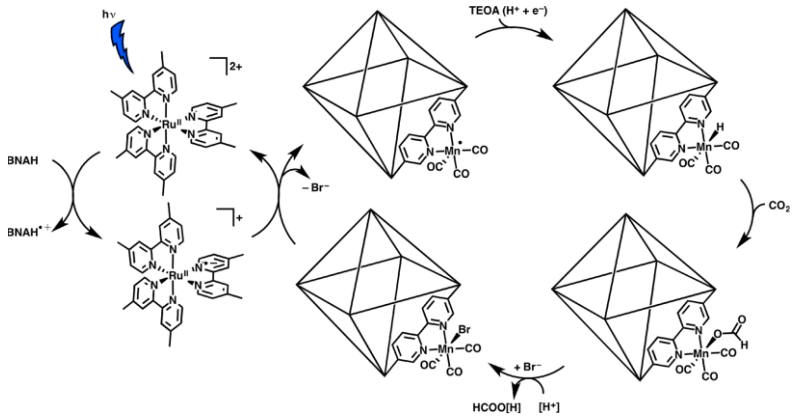

Figure 9. Suggested mechanism for the formation of formate from the photocatalytic reaction with UiO-67-Mn(bpy)$(CO)_3$Br[96]. *Reprinted with permission from Fei et al., Photocatalytic CO_2 Reduction to Formate Using a Mn(I) Molecular Catalyst in a Robust Metal–Organic Framework, Inorg. Chem. 54 (14) (2015) 6821-6828. Copyright (2015) American Chemical Society.*

According to Franco *et al.*[108], the first pure organometallic *fac*-[MnI$(CO)_3$(bis-MeNHC)Br] complex with the revolutionary operation for selective electrocatalytic CO_2-to-CO reduction, overreaching 100 turnovers CO with outstanding FE yields (ηCO~95%) in anhydrous CH_3CN. During similar state, CV was used determined maximum turnover frequency (TOF_{max}) of 2100 s^{-1}, thus, evidently greater than the values described for other Mn-based catalysts.

Experimental results account for the direct transformation of the [MnI$(CO)_3$(bis-MeNHC)Br] species (Figure 10), into five-coordinate [Mn$(CO)_3$(bis-MeNHC)]$^-$, the core product formed upon reduction. Importantly, the energy of the experimental CO stretching of [Mn$(CO)_3$(bis-MeNHC)]$^-$ show a powerfully localized negative charge over the Mn atom persistent with the bis-MeNHC ligand redox innocence. In fact, Kohn-Sham orbitals of [Mn$(CO)_3$(bis-MeNHC)]$^+$ to [Mn$(CO)_3$(bis-MeNHC)]• and [Mn$(CO)_3$(bis-MeNHC)]$^-$ indicate that the reduction occurs particularly over the metal center. The HOMO orbital geometry ([Mn$(CO)_3$(bis-MeNHC)]$^-$**)** is openly accessible to undertake a nucleophilic attack in contrast with [Mn$(CO)_3$(py-MeNHC)]$^-$. To summarize, the first family of organometallic NHC-based tricarbonyl Mn^I complexes active for electrocatalytic CO_2 reduction to CO was reported by Franco and co-workers[108]. Here, bis-MeNHC = methylene bis(N-methylimidazolium) ligand and py-MeNHC = N-methyl-N'-2-pyridilimidazolium ligand. Pyridine ring replacement with a NHC unit exceptionally influences the catalytic operation, to improve the TOF_{max} and selectivity for CO production of well-established C^N ligand-based Mn systems significantly. Additionally, the unique bis-NHC catalyst successfully and selectively adapts CO_2 to CO in an anhydrous aprotic organic solvent; differentially, the traditional bpy-based systems mainstream are unveiled to be inert without regard to definite proton source[109-114].

Eclética Química Journal, vol. 44, n. 1, 2019, 11-39
ISSN: 1678-4618
DOI: 10.26850/1678-4618eqj.v44.1.2019.p11-39

$$[MnBr(CO)_3(bis\text{-}MeNHC)] \underset{}{\overset{-Br,\ +L}{\rightleftharpoons}} [Mn(CO)_3(bis\text{-}MeNHC)L]^+ \quad (1a)$$

$$[Mn(CO)_3(bis\text{-}MeNHC)L]^+ \underset{+L}{\overset{-L}{\rightleftharpoons}} [Mn(CO)_3(bis\text{-}MeNHC)]^+ \quad (1b)$$

$$[Mn(CO)_3(bis\text{-}MeNHC)]^+ \xrightarrow{+e^-} [Mn(CO)_3(bis\text{-}MeNHC)]^0 \quad (1c)$$

$$[Mn(CO)_3(bis\text{-}MeNHC)]^0 \xrightarrow{+e^-} [Mn(CO)_3(bis\text{-}MeNHC)]^- \quad (1d)$$

$$[Mn(CO)_3(bis\text{-}MeNHC)]^- \xrightarrow{+CO_2} [Mn(CO)_3(bis\text{-}MeNHC)(CO_2)]^- \quad (1e)$$

$$[Mn(CO)_3(bis\text{-}MeNHC)(CO_2)]^- \xrightarrow{+CO_2} [Mn(CO)_3(bis\text{-}MeNHC)(CO_2)_2]^- \quad (1f)$$

$$[Mn(CO)_3(bis\text{-}MeNHC)(CO_2)_2]^- \longrightarrow [Mn(CO)_4(bis\text{-}MeNHC)]^+ + CO_3^{2-} \quad (1g)$$

$$[Mn(CO)_4(bis\text{-}MeNHC)]^+ \xrightarrow{+e^-} [Mn(CO)_4(bis\text{-}MeNHC)]^0 \quad (1h)$$

$$[Mn(CO)_4(bis\text{-}MeNHC)]^0 \xrightarrow{-CO} [Mn(CO)_3(bis\text{-}MeNHC)]^0 \quad (1i)$$

bis-MeNHC=methylene bis(N-methylimidazolium); L=acetonitrile

Figure 10. Proposed mechanism of CO_2 reduction to CO by *fac*-[MnI(CO)$_3$(bis-MeNHC)Br] complex [108].

Reuillard *et al.*[115] stated the assemblage of the complex [MnBr(2,2'-bipyridine)(CO)$_3$] attached to a carbon nanotube electrode over a pyrene unit. Molecular catalyst check allows electrocatalytic CO_2 reduction during entire aqueous conditions with a catalytic onset overpotential of η = 360 mV, and restrained potential electrolysis produced turnovers at η = 550 mV greater than 1000. The product selectivity is adjustable by catalyst amendment loading on the nanotube surface.

$$[MnBr(CO)_3(bpy)] + CNT(pyr) \longrightarrow [MnBr(CO)_3(bpy_{pyr})] \quad (2a)$$

$$[MnBr(CO)_3(bpy_{pyr})] \xrightarrow[-Br^-]{+2e^-} [\text{Mn dimer}] \xrightarrow[-CO\ -H_2O]{+CO_2+2H^+} [Mn(CO)_3(bpy_{pyr})] \quad (2b)$$

HCL

$$[MnBr(CO)_3(bpy_{pyr})] \xrightarrow[-Br^-]{+2e^-+2H^+} [\text{Mn hydride}] \xrightarrow[-CO\ -H_2]{+CO_2+2H^+} [Mn(CO)_3(bpy_{pyr})] \quad (2c)$$

LCL

bpy = 2-2'-bipyridine; CNT = carbono nanotube; pyr = pyrene unit of CNT

bpy_{pyr} = bpy bonded to pyrine unit

HCL = high catalyst loading; **LCL** = low catalyst loading

Figure 11. Proposed mechanism of *fac*-[MnBr(bpy_{pyr})(CO)$_3$] immobilized on a CNT sidewall, concentration-dependent dimerization or Mn−H formation, and intermediate-dependent reduction of CO_2 to CO or HCOOH[115].

The complex [MnBr(bpy)(CO)$_3$] (bpy = 2,2'-bipyridine) is a noble metal-free model catalyst for CO_2 reduction consequent to the all-around and direct structure of the bpy ligand[30]. This catalyst displayed high activity (turnover frequency up = 480 s^{-1}) in MeCN, and its catalytic mechanism has been studied greatly by wavering the nature of the substituents on the bpy ligand[116-122]. The Mn catalyst was presently integrated onto CNTs utilizing Nafion[123], onto p-Si through polymerization[124], and onto TiO_2 via a phosphonate anchoring group[125]. The former system showed a

Eclética Química Journal, vol. 44, n. 1, 2019, 11-39
ISSN: 1678-4618
DOI: 10.26850/1678-4618eqj.v44.1.2019.p11-39

record turnover number (TON) for the Mn catalyst of 112 in MeCN[125]. The grafted Mn catalyst form a dimer on the electrode surface[125], as indicated by the UV−Vis spectra electrochemistry (SEC). It has also been enumerated in solution upon electrochemical reduction for this class of catalyst[126]. Despite the observations of these studies, yet, the reported activity is limited to organic solvents and low TONs (maximum of 101) in aqueous conditions[123]. The pyrene unit allowed stable immobilization onto CNTs. The compound, electrocatalytic activity, was the first study approaching the CO_2 reduction in the homogeneous organic solution (MeCN + 5% H_2O) and then in completely aqueous solutions after being heterogenized on the CNT surface. Using CPE and CV, the Mn catalyst modified electrodes were explored. The Mn complex surface loading was disclosed to have a unique effect on the selectivity toward CO or $HCOO^-$ production (Fig. 11). The different catalytic intermediates involved were investigated *in situ* through the application of transmission UV-VIS and surface-sensitive IR SEC in the impaired total reflection (ATR) mode. Selectivity toward either CO or $HCOO^-$ at various surface loadings, accurate formation assignment of one or the other catalytic intermediate is important[116, 122, 124].

2.3.4 Ni-based Molecular Catalyst

Nickel, a non-precious metal (group VIIIB), is considered the best possible alternative instead of palladium or platinum for molecular catalysts[127, 128] owing to its simply achievable oxidation states (e.g., Ni^0, Ni^I, Ni^{II}, Ni^{III}, and Ni^{IV}). The CO_2 reduction performed by nickel catalysts repeatedly required the Ni^{II} reduction to Ni^I, which is linked with the distortion of geometrical from a tetra-dentate, square planar coordination mode fitting for Ni^{II} to a tetrahedral one model for Ni^I [129-131]. Similarly, OER, the Ni^{II} oxidation to Ni^{III} typically allows the structural shift from a square planar to a tetragonal or octahedral geometry[132, 133]. Therefore, the rich redox properties connected with many coordination geometries concede the ligand logical form scaffolds to harmonize with nickel (II) centers, contributing to the nickel complexes with precise catalyst operations[133-138]. Moreover, nickel is an active center in natural enzymes, the well-known {NiFe} hydrogenases for the reversible conversion hydrogen, proton[139, 140], and the {NiFe} CO dehydrogenases (CODHs) for the reversible transformation between CO_2 and CO[141, 142]. These findings further compelled the scientist (mostly energy conversion catalysis), to develop molecular catalysts based on nickel complexes. In spite many insightful reviews on spotlighted earth-abundant metal complexes as catalysts for the HER[143-151], OER[152-154] and CO_2 reduction[155-162], however, details on the Ni-based molecular catalyst is yet to be available in the literature. More recently, Wang, Jia-Wei *et al.*[163] reported a systematical review on the recent developments in the utilization of nickel complexes as molecular catalysts for water splitting and CO_2 reduction. In summary, nickel cyclam complexes display high efficiency and selectivity. Nonetheless, other nickel-based catalysts display moderate activity, and selectivity, while the solvent used, is restricted to non-aqueous solvents.

Niu *et al.*[164] has designed and synthesized a spongy nickel-organic heterogeneous catalyst through the photochemical pathway. The catalyst possesses crystalline network architecture with a high imperfections concentration and active in CO_2 conversion to CO, with ~1.6×10^4 μmol h^{-1} g^{-1} production rate. During the reaction, no measurable H_2 is generated, resulting to approx. 100% selective CO production over the evolution of H_2 and the evolution of CO from these five Ni-organic catalysts in a photocatalytic 6 h response. The spongy Ni(TPA/TEG) (L) composite results to be the highest activity, and the CO amount is 95.2 mmol after a 2 h reaction, yielding to a CO production rate (15,866 μmol h^{-1} g^{-1}), that is many times greater than other samples. The total CO volume produced on the spongy Ni(TPA/TEG) catalyst in 6 h attains 136.9 μmol, giving a turnover of 11.5 for the 6 h reaction. By investigating the CO yield in 2 h on different amounts of Ni(TPA/TEG) catalyst, a roughly linear relationship was obtained between the number of CO evolved and the catalyst amount. However, kinetically, it was found that the CO production rate decrease is proportional to increase in the catalyst amount, where 1.0 mg of the Ni(TPA/TEG) catalyst results to CO production rate of ~26,620 μmol h^{-1} g^{-1} in a similar solution. Thus, implies that more electrons generated from the photosensitizer molecules may perhaps have been transferred to the active catalytic sites. Also, the reusability of the spongy Ni(TPA/TEG) catalyst upon each 2 h of photocatalysis have been tested, where the catalyst retained its activity and

Eclética Química Journal, vol. 44, n. 1, 2019, 11-39
ISSN: 1678-4618
DOI: 10.26850/1678-4618eqj.v44.1.2019.p11-39

selectivity after recycling. In addition, it also displays outstanding architectural stability with no apparent detectable structural change after 24 h of photocatalysis. For further confirmation of the origin of as-produced CO, isotopic $^{13}CO_2$ was used as feedstock gas for the photocatalytic reduction and the products were examined by gas chromatography-mass spectrometry (GC-MS). The study confirms that the detected CO originates from the CO_2 gas source; with the important signal at a mass/charge ratio (29) on the mass spectrum corresponding to ^{13}CO.

Consequence of the previous result, Niu and co-workers proposed the mechanism for the photocatalytic CO_2 reduction reactions on the spongy Ni(TPA/TEG) catalyst (Fig. 12). Based on visible light irradiation, the $[Ru(bpy)_3]^{2+}$ (photosensitizer) is excited and then reductively snuffed out by the sacrificial electron donor [TEOA, 65-167], resulting to the reduced species of $[Ru(bpy)_3]^{2+}$ (Fig. 12). Afterward, the $[Ru(bpy)_3]^{2+}$ reduced species could maybe transfer an electron to the spongy Ni(TPA/TEG) catalyst, which later engages in CO_2 molecules reducing fixed on the catalyst (Fig. 12). The yield tests of CO production in the solution with different Ni(TPA/TEG) amounts for 2 h, revealed that the CO production rate decreases with increase in the catalyst amount, indicating that the electron transfer from $[Ru(bpy)_3]^{2+}$ to the catalyst may be a rate-determining step for the CO_2 reduction reaction, however, limited diffusion scenario may have occurred in this heterogeneous catalytic system[168]. Thereafter, the derivative CO can be reduced to liquid fuels by means of proton-coupled multi-electron reaction processes (Fig. 12). In the electrolyte with a pH value of ~8, it was also suggested conversion pathways resulting to the HCOOH, CH_3COOH, and CH_3CH_2OH formation through proton-coupled one-, four-, and eight-electron steps, respectively.

In the mechanistic CH_3COOH formation route, CO is perpetually hydrated to CHO→CHOH→CH_2OH→CH_3OH, which bonds with the adsorbed CO to form CH_3COOH. With a focus on the CH_3CH_2OH formation, the dehydroxylation of the as-formed CHO may possibly be a crucial rate-limiting step to produce additional C that can be protonated CH→CH_2→CH_3[169], and the C–C coupling in the space separating CH_3 and multi protonated CO could result in the CH_3CH_2OH formation[170]. Frequently, the hydroxyl ions (OH^-) are obtained for the CHO hydroxylation at pH 13, which select the HCOOH formation. Whereas, the facilitated CHO hydroxylation may suppress the kinetics of the CO multi protonation and CHO dihydroxylation, yielding a lower amount of CH_3COOH and CH_3CH_2OH at pH 13. The CH_3OH appearance may present a weak C–C coupling in the space separating CH_3OH and CO at pH 13 (resulting to CH_3COOH at pH 8), hence, may be considered for the next CO_2/CO reduction catalyst design[171].

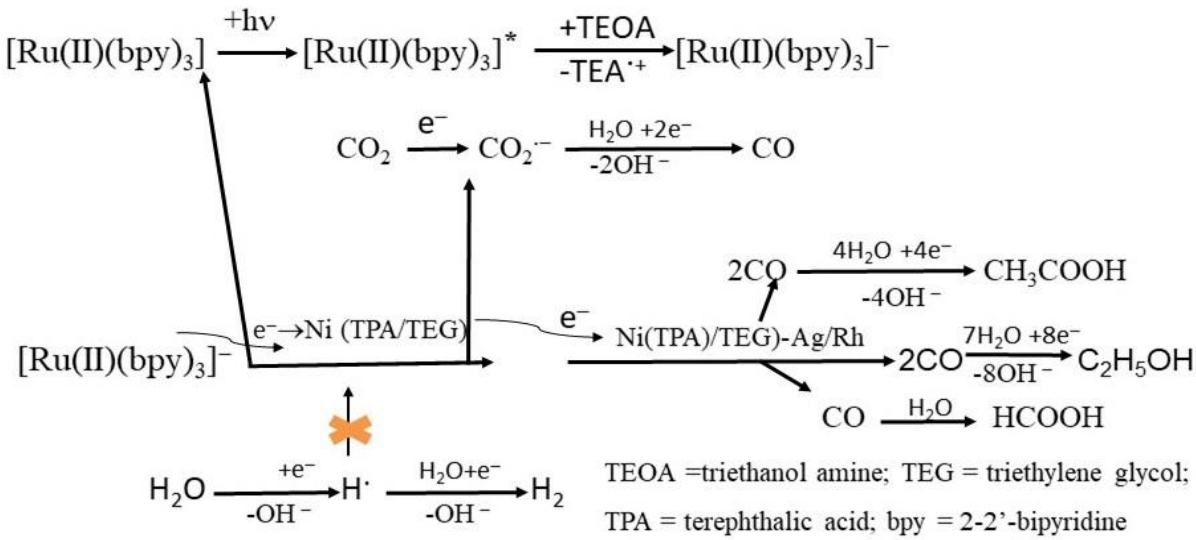

Figure 12. Proposed mechanisms for the photocatalytic reduction of CO_2 to CO and of CO to other liquid products. Visible light reduction of the photosensitizer $[Ru(bpy)_3]^{2+}$, which transfers an electron to the Ni(TPA/TEG) catalyst to convert CO_2 to CO and to Ni(TPA/TEG)-(Ag/Rh) catalysts for the generation of HCOOH, CH_3COOH, and CH_3CH_2OH from further reduction of CO[164].

Eclética Química Journal, vol. 44, n. 1, 2019, 11-39
ISSN: 1678-4618
DOI: 10.26850/1678-4618eqj.v44.1.2019.p11-39

Kuehnel *et al.*[172] investigated a series of self-assembled nickel terpyridine complexes as catalysts for the CO_2 reduction to CO in organic media. Immobilization on CdS quantum dots allows these catalysts to be functional in purely aqueous solution, and photo catalytically reduces CO_2 with > 90% selectivity in UV-filtered simulated solar light irradiation (AM 1.5G, 100 mW cm^{-2}, λ > 400 nm, pH 6.7). The QD-BF4 adjustments were performed in - situ through an additional stock solution of a self-assembled Ni complex to a suspension of QDs in TEOA aqueous solution (0.1 mol L^{-1}). This finally results into H_2O:CH3CN solution composition including 99:1 for $[Ni(terpy)_2]^{2+}$and $[Ni(terpyS)_2]^{2+}$, and 99.5:1 for $[Ni(terpyC)_2]^{2+}$ and $[Ni(terpyP)_2]^{2+}$. Catalyst attachment was affirmed by UV-vis spectroscopy with the anchoring group that involves dependent catalyst loading (Figure 13A). Considerably, the highest loading was accomplished with the thiol derivative, $[Ni(terpyS)_2]^{2+}$, while other anchors were measured with lower affinity (Figure 13B). The determination of main catalyst peaks in the UV-vis and ATR-IR spectra of $[Ni(terpyS)_2]^{2+}$–adjusted CdS QDs immobilized on a mesoporous SnO_2 electrode show that the catalyst maintained its intact chemical structure on the QD surface (Figures 13C). Cyclic voltammetry showed that the anchored catalyst retained its electrochemical response, additional supporting functional integrity on the QD surface (Figure 13D). Therefore, transmission electron microscopy unveiled that anchoring of the catalyst does not affect the particle morphology.

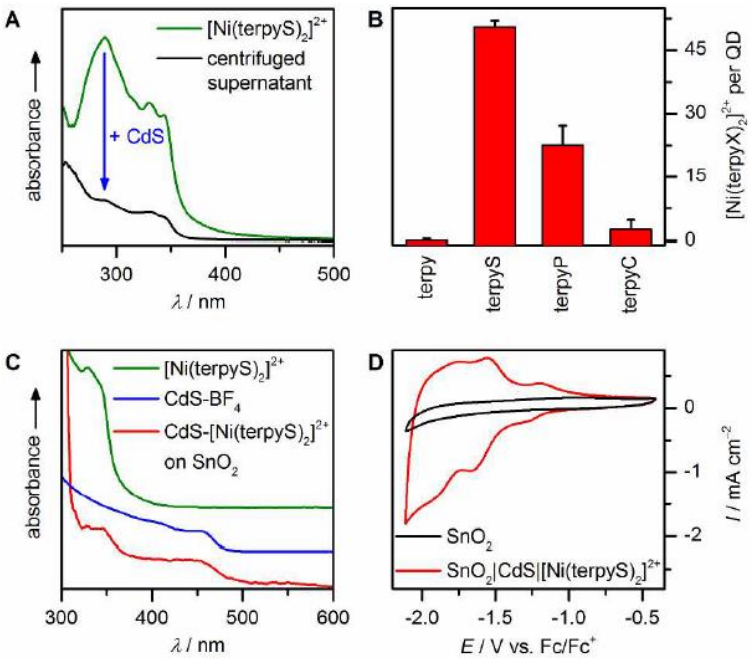

Figure 13. Hybrid photocatalyst assembly from CdS QDs and $[Ni(terpyX)_2]^{2+}$. A) Difference in UV-vis absorption of a $[Ni(terpyS)_2]^{2+}$ solution before and after stirring with CdS QDs; B) Adsorption efficiency of different $[Ni(terpyX)_2]^{2+}$ complexes; C) UV-vis spectra of CdS-$[Ni(terpyS)_2]^{2+}$ hybrid photocatalyst immobilized on a mesoporous SnO_2 electrode and comparison with CdS-BF4 and $[Ni(terpyS)_2]^{2+}$ in solution (spectra scaled and stacked for clarity); D) Cyclic voltammetry of CdS-$[Ni(terpyS)_2]^{2+}$ photocatalyst immobilized on a SnO_2 electrode[172]. *Reprinted with permission from Kuehnel et al., Selective Photocatalytic CO_2 Reduction in Water through Anchoring of a Molecular Ni Catalyst on CdS Nanocrystals, J. Am. Chem. Soc. 139 (21) (2017) 7217-7223. Copyright (2017) American Chemical Society.*

The photocatalytic activity of the congregated CdS-$[Ni(terpyX)_2]^{2+}$ hybrids were investigated in CO_2-saturated water under simulated solar light irradiation in the presence of TEOA (sacrificial electron donor). While the parent CdS-$[Ni(terpy)_2]^{2+}$ catalyst void of an anchoring group mainly yielded H_2 and only traces of CO, the functionalized derivatives displayed higher activities towards CO_2 reduction. $[Ni(terpyS)_2]^{2+}$ revealed both the highest CO_2 reduction activity, product selectivity series (92.2% after 4 h

Eclética Química Journal, vol. 44, n. 1, 2019, 11-39
ISSN: 1678-4618
DOI: 10.26850/1678-4618eqj.v44.1.2019.p11-39

compared to 10.2% and 3.9% for $[Ni(terpyP)_2]^{2+}$ and $[Ni(terpyC)_2]^{2+}$, respectively).

Surprisingly, the selectivity observed does not exhibit the electrocatalytic activity in the homogeneous phase, however, correlates with the adsorption efficiency of each complex to CdS. This behavior affirms that molecular catalyst interfacing with the nanoparticle is important to all-inclusive photocatalytic activity in aqueous solution. At the optimized state, about 20 Ni-based turnovers were obtained with CdS-$[Ni(terpyS)_2]^{2+}$ in 24 h visible light illumination. The CO selectivity continues to exist (> 90%) for the first 8 h prior to slowly decrease that mostly produce H_2 after 24 h. Ion-coupled plasma optical emission spectroscopy (ICP-OES) of QDs isolated from the reaction medium iterates the reducing selectivity co-occurs with a gradual $[Ni(terpyS)_2]^{2+}$ loss of the QD surface, differentially, the $CdSBF_4$ particles remain unchanged. UV-Vis spectra display a slight redshift of the first absorption, presenting limited particle aggregation with no significant photocorrosion. In addition, fresh catalyst after 20 h recovers the CO generation activity and subdue H_2 evolution, while the $Ni(BF4)_2$ addition only promotes H_2 evolution. Conversely, lessening the initial catalyst:QD ratio reduced the CO selectivity, moreover, it did not significantly affect the maximum TONCO (with respect to $[Ni(terpyS)_2]^{2+}$), where it can be inferred that a TONCO of ~20 represents the catalyst stability limit.

3. Conclusions and future perspectives

This general overview of the recent research on metal complex molecular catalysts for CO_2 reduction shows their contributions to the growing and dynamic field that gaining new insights into science at an ever-increasing rate. In order to increase metal complexes molecular catalysts application, it is imperative to overcome their poor stability which is a significant challenge. We suggest that one of the possible means to achieve this stability could be to ensure complexes heterogeneous, through their substrate's immobilization. Notwithstanding, the limited examples we have presented in this review, (e.g., porous structures, or covalent grafting on electrodes through ligand functionalization), suggest that the concept is realizable. Succinctly, the advancing knowledge acquired in several reduction mechanisms might give-way for more efficient selective and prolong metal complex molecular catalysts development. Additionally, most metal complexes molecular catalysts are light sensitive and suffer from photostability issues in any of these two ways; (i) by ligand photodissociation reactions and (ii) photoisomerization. This particular problem is an important obstacle towards the efficient metal complex photocatalysts for CO_2 reduction advancement. Unarguably, more improvements are still required, and other pathways for CO_2 catalytic reduction may perhaps offer ample fruitful opportunities.

5. Acknowledgments

This research did not receive any specific grant from funding agencies in the public, commercial, or not-for-profit organization. However, the authors are grateful to Mr. Abebe Reda of the University of Chinese Academy of Sciences, National Centre for Nanoscience and Technology, Beijing, China for his support and assistance.

6. References

[1] Qiao, J., Liu, Y., Hong, F., Zhang, J., A review of catalysts for the electroreduction of carbon dioxide to produce low-carbon fuels, Chem. Soc. Rev. 43 (2) (2014) 631-675. https://doi.org/10.1039/c3cs60323g.

[2] Liu, G., Hoivik, N., Wang, K., Jakobsen, H., Engineering TiO_2 nanomaterials for CO_2 conversion/solar fuels, Sol. Energ. Mat. Sol. C. (105) (2012) 53-68. https://doi.org/10.1016/j.solmat.2012.05.037.

[3] Costentin, C., Robert, M., Savéant, J.-M., Current Issues in Molecular Catalysis Illustrated by Iron Porphyrins as Catalysts of the CO_2-to-CO Electrochemical Conversion, Acc. Chem. Res. 48 (12) (2015) 2996-3006. https://doi.org/10.1021/acs.accounts.5b00262.

[4] Zhang, Y., Jacobs, G., Sparks, D. E., Dry, M. E., Davis, B. H., CO and CO_2 hydrogenation study on supported cobalt Fischer-Tropsch synthesis catalysts, Catal. Today 71 (3-4) (2002)

411-418. https://doi.org/10.1016/S0920-5861(01)00468-0.

[5] Lu, Q., Rosen, J., Zhou, Y., Hutchings, G. S., Kimmel, Y. C., Chen, J. G., Jiao, F., A selective and efficient electrocatalyst for carbon dioxide reduction, A Nat. Commun. (2014) 5. https://doi.org/3242.10.1038/ncomms4242.

[6] Nie, X., Esopi, M. R., Janik, M. J., Asthagiri, A., Selectivity of CO_2 reduction on copper electrodes: the role of the kinetics of elementary steps, Angew. Chem. 52 (9) (2013) 2459-2462. https://doi.org/10.1002/anie.201208320.

[7] Lu, Q., Rosen, J., Jiao, F., Nanostructured metallic electrocatalysts for carbon dioxide reduction, Chem. Cat. Chem. 7 (1) (2015) 38-47. https://doi.org/10.1002/cctc.201402669.

[8] Hori, Y., Electrochemical CO_2 Reduction on Metal Electrodes. In: Modern Electrochemistry, vol. 42, Vayenas, C. G., White, R. E., Gamboa-Aldeco, M. E., Eds.; Springer New York: New York, NY, 2008; pp 89-189.

[9] Liu, X., Ye, L., Liu, S., Li, Y., Ji, X., Photocatalytic Reduction of CO_2 by ZnO Micro/nanomaterials with Different Morphologies and Ratios of {0001} Facets, Scientific Reports volume 6, Article number: 38474 (2016). https://doi.org/10.1038/srep38474.

[10] Chen, Y., Kanan, M. W. J., Tin oxide dependence of the CO_2 reduction efficiency on tin electrodes and enhanced activity for tin/tin oxide thin-film catalysts, J. Am. Chem. Soc. 134 (4) (2012) 1986-1989. https://doi.org/10.1021/ja2108799.

[11] Asadi, M., Kumar, B., Behranginia, A., Rosen, B. A., Baskin, A., Repnin, N., Pisasale, D., Phillips, P., Zhu, W., Haasch, R., Klie, R. F., Král, P., Abiade, J., Salehi-Khojin, A., Robust carbon dioxide reduction on molybdenum disulphide edges, Nat. Commun. 5 (2014) Article number: 4470. https://doi.org/10.1038/ncomms5470.

[12] Asadi, M., Kim, K., Liu, C., Addepalli, A. V., Abbasi, P., Yasaei, P., Phillips, P., Behranginia, A., Cerrato, J. M., Haasch, R., Zapol, P., Kumar, B., Klie, R. F., Abiade, J., Curtiss, L. A., Salehi-Khojin, A., Nanostructured transition metal dichalcogenide electrocatalysts for CO_2 reduction in ionic liquid, Science 353 (6298) (2016) 467-470. https://doi.org/10.1126/science.aaf4767.

[13] Collin, J. P., Sauvage, J. P., Electrochemical reduction of carbon dioxide mediated by molecular catalysts, Coord. Chem. Rev. 93 (2) (1989) 245-268. https://doi.org/10.1016/0010-8545(89)80018-9.

[14] Savéant, J.-M., Molecular catalysis of electrochemical reactions. Mechanistic aspects, Chem. Rev. 108 (7) (2008) 2348-2378. https://doi.org/10.1021/cr068079z.

[15] Takeda, H., Cometto, C., Ishitani, O., Robert, M., Electrons, photons, protons and earth-abundant metal complexes for molecular catalysis of CO_2 reduction, ACS Catal. 7 (1) (2017) 70-88. https://doi.org/10.1021/acscatal.6b02181.

[16] Li, L., Yan, J., Wang, T., Zhao, Z. J., Zhang, J., Gong, J., Guan, N., Sub-10 nm rutile titanium dioxide nanoparticles for efficient visible-light-driven photocatalytic hydrogen production, Nat. Commun. 6 article number: 5881 (2015). https://doi.org/10.1038/ncomms6881.

[17] Wang, J. C., Zhang, L., Fang, W. X., Ren, J., Li, Y. Y., Yao, H. C., Wang, J. S., Li, Z. J., Enhanced photoreduction CO_2 activity over direct z-scheme α-Fe_2O_3/Cu_2O heterostructures under visible light irradiation, ACS Appl. Mater. Interfaces 7 (16) (2015) 8631-8639. https://doi.org/10.1021/acsami.5b00822.

[18] Kudo, A., Miseki, Y., Heterogeneous photocatalyst materials for water splitting, Chem.

Soc. Rev. 38 (1) (2009) 253-278. https://doi.org/10.1039/b800489g.

[19] Hisatomi, T., Kubota, J., Domen, K., Recent advances in semiconductors for photocatalytic and photoelectrochemical water splitting, Chem. Soc. Rev. 43 (2014) 7520-7535. https://doi.org/10.1039/C3CS60378D.

[20] Ma, Y., Wang, X., Jia, Y., Chen, X., Han, H., Li, C., Titanium dioxide-based nanomaterials for photocatalytic fuel generations, Chem. Rev. 114 (19) (2014) 9987-10043. https://doi.org/10.1021/cr500008u.

[21] Kang, D., Kim, T. W., Kubota, S. R., Cardiel, A. C., Cha, H. G., Choi, K. S., Electrochemical synthesis of photoelectrodes and catalysts for use in solar water splitting, Chem. Rev. 115 (23) (2015) 12839-12887. https://doi.org/10.1021/acs.chemrev.5b00498.

[22] Tong, H., Ouyang, S., Bi, Y., Umezawa, N., Oshikiri, M., Ye, J., Nano-photocatalytic materials: possibilities and challenges, Adv. Mater. 24 (2) (2012) 229-251. https://doi.org/10.1002/adma.201102752.

[23] Ran, J., Zhang, J., Yu, J., Jaroniec, M., Qiao, S. Z., Earth-abundant cocatalysts for semiconductor-based photocatalytic water splitting, Chem. Soc. Rev. 43 (22) (2014) 7787-7812. https://doi.org/10.1021/jacs.5b04186.

[24] Chang, X., Wang, T., Zhang, P., Zhang, J., Li, A., Gong, J., Enhanced surface reaction kinetics and charge separation of p–n heterojunction $Co_3O_4/BiVO_4$ photoanodes, J. Am. Chem. Soc. 137 (26) (2015) 8356-8359. https://doi.org/10.1021/jacs.5b04186.

[25] England, J., Bill, E., Weyhermüller, T., Neese, F., Atanasov, M., Wieghardt, K., Molecular and electronic structures of homoleptic six-coordinate cobalt(I) complexes of 2,2':6',2"-terpyridine, 2,2'-bipyridine, and 1,10-phenanthroline. An experimental and computational study, Inorg. Chem. 54 (24) (2015) 12002-12018. https://doi.org/10.1021/acs.inorgchem.5b02415.

[26] Wang, M., Weyhermüller, T., Bill, E., Ye, S., Wieghardt, K., Structural and spectroscopic characterization of rhenium complexes containing neutral, monoanionic, and dianionic ligands of 2, 2′-bipyridines and 2,2′:6,2″-Terpyridines: An Experimental and Density Functional Theory (DFT)-Computational Study, Inorg. Chem. 55 (10) (2016) 5019-5036. https://doi.org/10.1021/acs.inorgchem.6b00609.

[27] Wang, M., England, J., Weyhermu, T., Wieghardt, K., Molecular and electronic structures of the members of the electron transfer series $[Mn(bpy)_3]^n$ (n = 2+, 1+, 0, 1−) and $[Mn(tpy)_2]^m$ (m = 4+, 3+, 2+, 1+, 0). An experimental and density functional theory study, Inorg. Chem. 53 (4) (2014) 2276-2287. https://doi.org/10.1021/ic4029854.

[28] Scarborough, C. C., Lancaster, K. M., DeBeer, S., Weyhermueller, T., Sproules, S., Wieghardt, K., Experimental fingerprints for redox-active terpyridine in $[Cr(tpy)_2](PF_6)_n$ (n = 3–0), and the remarkable electronic structure of $[Cr(tpy)_2]^{1-}$, Inorg. Chem. 51 (6) (2012) 3718-3732. https://doi.org/10.1021/ic2027219.

[29] Paddon, C. A., Atobe, M., Fuchigami, T., He, P., Watts, P., Haswell, S. J., Pritchard, G. J., Bull, S. D., Marken, F. J., Towards paired and coupled electrode reactions for clean organic microreactor electrosyntheses, Appl. Electrochem. 36 (6) (2006) 617-634. https://doi.org/10.1007/s10800-006-9122-2.

[30] Pütter, H., Organic Electrochemistry, 4th ed., Lund, H., Hammerich, O., Eds., Marcel Dekker: New York, 2001; 1259-1308.

[31] Frontana-Uribe, B. A., Little, R. D., Ibanez, J. G., Palma, A., Vasquez-Medrano, R., Organic electrosynthesis: a promising green methodology in organic chemistry, Green Chem.

12 (2010) 2099-2119. https://doi.org/10.1039/C0GC00382D.

[32] Tatin, A., Comminges, C., Kokoh, B., Costentin, C., Robert, M., Savéant, J.-M., Efficient electrolyzer for CO_2 splitting in neutral water using earth-abundant materials, Proc. Natl. Acad. Sci. U. S. A. 113 (20) (2016) 5526-5529. https://doi.org/10.1073/pnas.1604628113.

[33] Parajuli, R., Gerken, J. B., Keyshar, K., Sullivan, I., Sivasankar, N., Teamey, K., Stahl, S. S., Cole, E. B, Integration of anodic and cathodic catalysts of earth-abundant materials for efficient, scalable CO_2 reduction, Top. Catal. 58 (1) (2015) 57-66. https://doi.org/10.1007/s11244-014-0345-x.

[34] Kim, B., Ma, S., Molly Jhong, H.-R., Kenis, P. J. A., Influence of dilute feed and pH on electrochemical reduction of CO_2 to CO on Ag in a continuous flow electrolyzer, Electrochim. Acta 166 (2015) 271-276. https://doi.org/10.1016/j.electacta.2015.03.064.

[35] Luc, W., Rosen, J., Jiao, F., An Ir-based anode for a practical CO_2 electrolyzer, Catal. Today 288 (2016) 79-84. https://doi.org/10.1016/j.cattod.2016.06.011.

[36] Sebastián, D., Palella, A., Baglio, V., Spadaro, L., Siracusano, S., Negro, P., Niccoli, F., Arico, A. S., CO_2 reduction to alcohols in a polymer electrolyte membrane co-electrolysis cell operating at low potentials, Electrochim. Acta 241 (2017) 28-40. https://doi.org/10.1016/j.electacta.2017.04.119.

[37] Benson, E. E., Kubiak, C. P., Sathrum, A. J., Smieja, J. M., Electrocatalytic and homogeneous approaches to conversion of CO_2 to liquid fuels, Chem. Soc. Rev. 38 (1) (2009) 89-99. https://doi.org/10.1039/b804323j.

[38] Llorente, M. J., Nguyen, B. H., Kubiak, C. P., Moeller, K. D. J., Paired electrolysis in the simultaneous production of synthetic intermediates and substrates, J. Am. Chem. Soc. 138 (46) (2016) 15110-15113. https://doi.org/10.1021/jacs.6b08667.

[39] Mascetti, J., Carbon dioxide as a chemical feedstock paired electrolysis in the simultaneous production of synthetic intermediates and substrates. In: Carbon dioxide as a chemical feedstock, Aresta, M., Ed., Wiley-VCH, Weinheim 2010, chapter: 4th, pp.55-88.

[40] Gibson, D. H., Carbon dioxide coordination chemistry: metal complexes and surface-bound species. What relationships?, Coord. Chem. Rev. 185 (1) (1999) 335-355. https://doi.org/10.1016/S0010-8545(99)00021-1.

[41] Goedecke, C., Hillebrecht, P., Uhlemann, T., Haunschild, R., Frenking, G., The Dewar–Chatt–Duncanson model reversed — Bonding analysis of group-10 complexes $[(PMe_3)_2M–EX_3]$ (M = Ni, Pd, Pt; E = B, Al, Ga, In, Tl; X = H, F, Cl, Br, I), Can. J. Chem. 87 (10) (2009) 1470-1479. https://doi.org/10.1139/V09-099.

[42] Francke, R., Schille, B., Roemelt, M., Homogeneously catalyzed electroreduction of carbon dioxide-methods, mechanisms, and catalysts, Chem. Rev. 118 (9) (2018) 4631-4701. https://doi.org/10.1021/acs.chemrev.7b00459.

[43] Eisenberg, R., Hendrickson, D. E., The binding and activation of carbon monoxide, carbon dioxide, and nitric oxide and their homogeneously catalyzed reactions, Adv. Catal. 28 (14) (1979) 79-172. https://doi.org/10.1016/S0360-0564(08)60134-0.

[44] (a) Herskovitz, T., Carbon dioxide coordination chemistry. 3. Adducts of carbon dioxide with iridium (I) complexes, J. Am. Chem. Soc. 99 (7) (1977) 2391-2392. https://doi.org/10.1021/ja00449a087; (b) Calabrese, J. C., Herskovitz, T., Kinney, J. B., Carbon dioxide coordination chemistry. 5. The preparation ans structure of the rhodium complex Rh(□1-CO2)(Cl)(diars)2, J. Am. Chem. Soc. 105

Eclética Química Journal, vol. 44, n. 1, 2019, 11-39
ISSN: 1678-4618
DOI: 10.26850/1678-4618eqj.v44.1.2019.p11-39

(1983) 5914-5915. https://doi.org/10.1021/ja00356a033.

[45] Aresta, M., Nobile, C. F., Albano, V. G., Forni, E., Manassero, M., New nickel-carbon dioxide complex: synthesis, properties, and crystallographic characterization of (carbon dioxide)-bis(tricyclohexylphosphine)nickel, J. Chem. Soc. Chem. Commun. 15 (1975) 636-637. https://doi.org/10.1039/C39750000636.

[46] Karsch, H. H., Funktionelle Trimethylphosphinderivate, III. Ambivalentes Verhalten von Tetrakis (trimethylphosphin) eisen: Reaktion mit CO_2, Chem. Ber. 110 (6) (1977) 2213-2221. https://doi.org/10.1002/cber.19771100619.

[47] Komiya, S., Akita, M., Kasuga¸ N., Hirano¸ M., Fukuoka¸ A., Synthesis, structure and reactions of a carbon dioxide complex of iron (0) containing 1,2-bis(diethylphosphino)ethane ligands, J. Chem. Soc. Chem. Commun. 9 (1994) 1115-1116. https://doi.org/10.1039/C39940001115.

[48] Lewis, N. S., Nocera, D. G., Powering the planet: chemical challenges in solar energy utilization, Proc. Natl. Acad. Sci. 103 (43) (2006) 15729-15735. https://doi.org/10.1073/pnas.0603395103.

[49] a) Qiao, J., Liu, Y., Hong, F., Zhang, J., A review of catalysts for the electroreduction of carbon dioxide to produce low-carbon fuels, Chem. Soc. Rev., 43 (2014) 631-675. https://doi.org/10.1039/c3cs60323g; b) Portenkirchner, E., Oppelt, K., Egbe, D. A. M., Knör G., Sariçiftçi, N. S., Electro-and photo-chemistry of rhenium and rhodium complexes for carbon dioxide and proton reduction: a mini review, Nanomaterials and Energy 2 (2013) 134-147. https://doi.org/10.1680/nme.13.00004; c) Lim, R. J., Xie, M., Sk, M. A., Lee, J.-M., Fisher, A., Wang, X., Lim, K. H., A review on the electrochemical reduction of CO_2 in fuel cells, metal electrodes and molecular catalysts, Catal. Today 233 (15) (2014) 169-180. https://doi.org/10.1016/j.cattod.2013.11.037.

[50] a) Lin, S., Diercks, C. S., Zhang, Y.-B., Kornienko, N., Nichols, E. M., Zhao, Y., Paris, A. R., Kim, D., Yang, P., Yaghi, O. M., Chang, C. J., Covalent organic frameworks comprising cobalt porphyrins for catalytic CO_2 reduction in water, Science 349 (6253) (2015) 1208-1213. https://doi.org/10.1126/science.aac8343; b) Matlachowski, C., Braun, B., Tschierlei, S., Schwalbe, M., Photochemical CO_2 Reduction Catalyzed by Phenanthroline Extended Tetramesityl Porphyrin Complexes Linked with a Rhenium(I) Tricarbonyl Unit, Inorg. Chem. 54 (21) (2015) 10351-10360. https://doi.org/10.1021/acs.inorgchem.5b01717; c) Hod, I., Sampson, M. D., Deria, P., Kubiak, C. P., Farha, O. K., Hupp, J. T., Fe-Porphyrin-Based Metal–Organic Framework Films as High-Surface Concentration, Heterogeneous Catalysts for Electrochemical Reduction of CO_2, ACS Catal. 5 (11) (2015) 6302-6309. DOI: 10.1021/acscatal.5b01767; d) Costentin, C., Passard, G., Robert, M., Savéant, J.-M., Ultraefficient homogeneous catalyst for the CO_2-to-CO electrochemical conversion, Proc. Natl. Acad. Sci. 111 (42) (2014) 14990-14994. https://doi.org/10.1073/pnas.1416697111.

[51] [51] Taheri, A., Thompson, E. J., Fettinger, J. C., Berben, L. A., An iron electrocatalyst for selective reduction of CO_2 to formate in water: including thermochemical insights, ACS Catal. 5 (12) (2015) 7140-7151. https://doi.org/10.1021/acscatal.5b01708.

[52] Ambre, R. B., Daniel, Q., Fan, T., Chen, H., Zhang, B., Wang, L., Ahlquist, M. S. G., Duan, L., Sun, L., Molecular engineering for efficient and selective iron porphyrin catalysts for electrochemical reduction of CO_2 to CO, Chem. Commun. 52 (2016) 14478-14481. https://doi.org/10.1039/c6cc08099e.

[53] Bhugun, I., Lexa, D., Savéant, J.-M., Catalysis of the electrochemical reduction of

carbon dioxide by iron (0) porphyrins: Synergystic effect of weak Brönsted acids, J. Am. Chem. Soc. 118 (7) (1996) 1769-1776. https://doi.org/10.1021/ja9534462.

[54] Bhugun, I., Lexa, D., Savéant, J.-M., Ultraefficient selective homogeneous catalysis of the electrochemical reduction of carbon dioxide by an iron (0) porphyrin associated with a weak Broensted acid cocatalyst, J. Am. Chem. Soc. 116 (11) (1994) 5015-5016. https://doi.org/10.1021/ja00090a068.

[55] Costentin, C., Drouet, S., Passard, G., Robert, M., Savéant, J.-M., Proton-coupled electron transfer cleavage of heavy-atom bonds in electrocatalytic processes. Cleavage of a C–O bond in the catalyzed electrochemical reduction of CO_2, J. Am. Chem. Soc. 135 (24) (2013) 9023-9031. https://doi.org/10.1021/ja4030148.

[56] Rao, H., Schmidt, L. C., Bonin, J., Robert, M., Visible-light-driven methane formation from CO_2 with a molecular iron catalyst, Nature 548 (2017) 74-77. https://doi.org/10.1038/nature23016.

[57] Costentin, C., Robert, M., Savéant, J.-M., Tatin, A., Efficient and selective molecular catalyst for the CO_2-to-CO electrochemical conversion in water, Proc. Natl Acad. Sci. USA 112 (2015) 6882-6886. https://doi.org/10.1073/pnas.1507063112.

[58] Azcarate, I., Costentin, C., Robert, M., Savéant, J.-M., Through-Space Charge Interaction Substituent Effects in Molecular Catalysis Leading to the Design of the Most Efficient Catalyst of CO_2-to-CO Electrochemical Conversion, J. Am. Chem. Soc. 138 (51) (2016) 16639-16644. https://doi.org/10.1021/jacs.6b07014.

[59] Bonin, J., Maurin, A., Robert, M., Molecular catalysis of the electrochemical and photochemical reduction of CO_2 with Fe and Co metal based complexes. Recent advances, Coord. Chem. Rev. 334 (2017) 184-198. https://doi.org/10.1016/j.ccr.2016.09.005.

[60] Davies, S. G., Hibberd, J., Simpson, S. J., Disproportionation of the iron carbonyl hydride (η^5-C_5H_5)Fe(CO)H($Ph_2PCH_2CH_2PPh_2$) to the iron methyl (η^5-C_5H_5)Fe$Ph_2PCH_2CH_2PPh_2$)Me., J. Chem. Soc. Chem. Commun. (24) (1982) 1404-1405. https://doi.org/10.1039/C39820001404.

[61] Appel, A. M., Bercaw, J. E., Bocarsly, A. B., Dobbek, H., DuBois, D. L., Dupuis, M., Ferry, J. G., Fujita, E., Hille, R., Kenis, P. J. A., Kerfeld, C. A., Morris, R. H., Peden, C. H. F., Portis, A. R., Ragsdale, S. W., Rauchfuss, T. B., Reek, J. N. H., Seefeldt, L. C., Thauer, R. K., Waldrop, G. L., Frontiers, Opportunities, and Challenges in Biochemical and Chemical Catalysis of CO2 Fixation, Chem. Rev. 113 (8) (2013) 6621-6658. https://doi.org/10.1021/cr300463y.

[62] Pan, F., Zhang, H., Liu, K., Cullen, D., More, K., Wang, M., Feng, Z., Wang, G., Wu, G., Li, Y., Unveiling Active Sites of CO_2 Reduction on Nitrogen-Coordinated and Atomically Dispersed Iron and Cobalt Catalysts, ACS Catal. 8 (4) (2018) 3116-3122. https://doi.org/10.1021/acscatal.8b00398.

[63] Nichols, E. M., Derrick, J. S., Nistanaki, S. K., Smith, P. T., Chang, C. J., Positional effects of second-sphere amide pendants on electrochemical CO_2 reduction catalyzed by iron porphyrins, Chem. Sci. 9 (11) (2018) 2952-2960. https://doi.org/10.1039/c7sc04682k.

[64] Costentin, C., Drouet, S., Robert, M., Savéant, J.-M., Turnover numbers, turnover frequencies, and overpotential in molecular catalysis of electrochemical reactions. Cyclic voltammetry and preparative-scale electrolysis, J. Am. Chem. Soc. 134 (27) (2012) 11235-11242. https://doi.org/10.1021/ja303560c.

[65] Azcarate, I., Costentin, C., Robert, M., Savéant, J.-M., Dissection of Electronic Substituent Effects in Multielectron–Multistep Molecular Catalysis. Electrochemical CO_2-to-CO Conversion Catalyzed by Iron Porphyrins, J. Phys.

Eclética Química Journal, vol. 44, n. 1, 2019, 11-39
ISSN: 1678-4618
DOI: 10.26850/1678-4618eqj.v44.1.2019.p11-39

Chem. C 120 (51) (2016) 28951-28960. https://doi.org/10.1021/acs.jpcc.6b09947.

[66] Pegis, M. L., McKeown, B. A., Kumar, N., Lang, K., Wasylenko, D. J., Zhang, X. P., Raugei, S., Mayer, J. M., Homogenous Electrocatalytic Oxygen Reduction Rates Correlate with Reaction Overpotential in Acidic Organic Solutions, ACS Cent. Sci. 2 (11) (2016) 850-856. https://doi.org/10.1021/acscentsci.6b00261.

[67] Azcarate, I., Costentin, C., Robert, M., Savéant, J.-M., Through-Space Charge Interaction Substituent Effects in Molecular Catalysis Leading to the Design of the Most Efficient Catalyst of CO_2-to-CO Electrochemical, J. Am. Chem. Soc. 138 (51) (2016) 16639-16644. https://doi.org/10.1021/jacs.6b07014.

[68] Specklin, D., Fliedel, C., Gourlaouen, C., Bruyere, J.-C., Avilés, T., Boudon, C., Ruhlmann, L., Dagorne, S., N-Heterocyclic Carbene Based Tri-organyl-Zn–Alkyl Cations: Synthesis, Structures, and Use in CO_2 Functionalization, Chem. Eur. J. 23 (23) 5509-5519. https://doi.org/10.1002/chem.201605907.

[69] Sattler, W., Parkin, G., Zinc catalysts for on-demand hydrogen generation and carbon dioxide functionalization, J. Am. Chem. Soc. 134 (42) (2012) 17462-17465. https://doi.org/10.1021/ja308500s.

[70] Specklin, D., Hild, F., Fliedel, C., Gourlaouen, C., Veiros, L. F., Dagorne, S., Accessing Two-Coordinate Zn^{II} Organocations by NHC Coordination: Synthesis, Structure, and Use as π-Lewis Acids in Alkene, Alkyne, and CO_2 Hydrosilylation, Chem. Eur. J 23 (63) (2017) 15908-15912. https://doi.org/10.1002/chem.201704382.

[71] Rauch, M., Parkin, G., Zinc and Magnesium Catalysts for the Hydrosilylation of Carbon Dioxide, J. Am. Chem. Soc. 139 (50) (2017) 18162-18165. https://doi.org/10.1021/jacs.7b10776.

[72] Rit, A., Zanardi, A., Spaniol, T. P., Maron, L., Okuda, J., A Cationic Zinc Hydride Cluster Stabilized by an N-Heterocyclic Carbene: Synthesis, Reactivity, and Hydrosilylation Catalysis, Angew. Chem. Int. Ed. 53 (48) (2014) 13273-13277. https://doi.org/10.1002/anie.201408346.

[73] Donovan, E. S., Barry, B. M., Larsen, C. A., Wirtz, M. N., Geiger, W. E., Kemp, R. A., Facilitated carbon dioxide reduction using a Zn(II) complex, Chem. Commun. 52 (8) (2016) 1685-1688. https://doi.org/10.1039/C5CC07318A.

[74] Hammouche, M., Lexa, D., Momenteau, M., Savéant, J.-M., Chemical catalysis of electrochemical reactions. Homogeneous catalysis of the electrochemical reduction of carbon dioxide by iron("0") porphyrins. Role of the addition of magnesium cations, J. Am. Chem. Soc. 113 (22) (1991) 8455-8466. https://doi.org/10.1021/ja00022a038.

[75] Wu, Y., Jiang, J., Weng, Z., Wang, M., Broere, D. L. J., Zhong, Y, Brudvig, G. W., Feng, Z., Wang, H., Electroreduction of CO_2 Catalyzed by a Heterogenized Zn-Porphyrin Complex with a Redox-Innocent Metal Center, ACS Central Science 3 (8) (2017) 847-852. https://doi.org/10.1021/acscentsci.7b00160.

[76] Won, D. H., Shin, H., Koh, J., Chung, J., Lee, H. S., Kim, H., Woo, S. I., Highly Efficient, Selective, and Stable CO_2 Electroreduction on a Hexagonal Zn Catalyst, Angew. Chem., Int. Ed. 55 (32) (2016) 9297-9300. https://doi.org/10.1002/anie.201602888.

[77] Hori, Y., Kikuchi, K., Suzuki, S., Production of CO and CH_4 in electrochemical reduction of CO_2 at metal electrodes in aqueous hydrogencarbonate solution, Chem. Lett. 14 (11) (1985) 1695-1698. https://doi.org/10.1246/cl.1985.1695.

[78] Hori, Y., Wakebe, H., Tsukamoto, T., Koga, O., Electrocatalytic process of CO selectivity in

Eclética Química Journal, vol. 44, n. 1, 2019, 11-39
ISSN: 1678-4618
DOI: 10.26850/1678-4618eqj.v44.1.2019.p11-39

electrochemical reduction of CO_2 at metal electrodes in aqueous media, Electrochim. Acta 39 (11-12) (1994) 1833-1839. https://doi.org/10.1016/0013-4686(94)85172-7.

[79] Wei, C., Feng, Z., Baisariyev, M., Yu, L., Zeng, L., Wu, T., Zhao, H., Huang, Y., Bedzyk, M. J., Sritharan, T., Xu, Z., Multifunctional mixed valence N-doped CNT@MFe_2O_4 hybrid nanomaterials: from engineered one-pot coprecipitation to application in energy storage paper supercapacitors, J. Chem. Mater. 28 (12) (2016) 4129-4133. https://doi.org/10.1039/C8NR03533D.

[80] Lin, S., Diercks, C. S., Zhang, Y.-B., Kornienko, N., Nichols, E. M., Zhao, Y., Paris, A. R., Kim, D., Yang, P., Yaghi, O. M., Chang, C. J., Covalent organic frameworks comprising cobalt porphyrins for catalytic CO_2 reduction in water, Science 349 (6253) (2015) 1208-1213. https://doi.org/10.1126/science.aac8343.

[81] Closs, G. L., Closs, L. E., Negative ions of porphin metal complexes, J. Am. Chem. Soc. 85 (6) (1963) 818-819. https://doi.org/10.1021/ja00889a038.

[82] Balducci, G., Chottard, G., Gueutin, C., Lexa, D., Savéant, J.-M., Electrochemistry of iron(I) porphyrins in the presence of carbon monoxide. Comparison with zinc porphyrins, Inorg. Chem. 33 (9) (1994) 1972-1978. https://doi.org/10.1021/ic00087a038.

[83] Lanese, J. G., Wilson, G. S J., Electrochemical studies of zinc tetraphenylporphin, Electrochem. Soc. 119 (8) (1972) 1039-1043. https://doi.org/10.1149/1.2404391.

[84] Lin, C.-L., Fang, M.-Y., Cheng, S.-H J., Substituent and axial ligand effects on the electrochemistry of zinc porphyrins, Electroanal. Chem. 531 (2) (2002) 155-162. https://doi.org/10.1016/S0022-0728(02)01056-2.

[85] Connelly, N. G., Geiger, W. E., Chemical redox agents for organometallic chemistry, Chem. Rev. 96 (2) (1996) 877-910. https://doi.org/10.1021/cr940053x.

[86] Parkhots, O. P., Ivashin, N. V., Study of the structure and spectral properties of radical anions of Zn complexes of porphyrins by the method of density functional theory, Opt. Spectrosc. 106 (2) (2009) 204-212 https://doi.org/10.1134/S0030400X0902009X.

[87] Wang, Y., Hou, P., Wang, Z., Kang, P., Zinc Imidazolate Metal–Organic Frameworks (ZIF-8) for Electrochemical Reduction of CO_2 to CO, ChemPhysChem. 18 (2017) 3142-3147. https://doi.org/10.1002/cphc.201700716.

[88] Kemmitt, R. D. W., Peacock, R. D., The Chemistry of Manganese, Technetium and Rhenium, Pergamon Press, 1973.

[89] Valyaev, D. A., Lavigne, G., Lugan, N., Manganese organometallic compounds in homogeneous catalysis: past, present, and prospects, Coord. Chem. Rev. 308 (2016) 191-235. https://doi.org/10.1016/j.ccr.2015.06.015.

[90] Sinopoli, A., La Porte, N. T., Martinez, J. F., Wasielewski, M. R., Sohail, M., Manganese carbonyl complexes for CO_2 reduction, Coord. Chem. Rev. 365 (2018) 60-74. https://doi.org/10.1016/j.ccr.2018.03.011.

[91] Grice, K. A., Kubiak, C. P., Chapter five – recent studies of rhenium and manganese bipyridine carbonyl catalysts for the electrochemical reduction of CO_2, Advances in Inorg. Chem. 66 (2014) 163-188. https://doi.org/10.1016/B978-0-12-420221-4.00005-6.

[92] Feng, D.-M., Zhu, Y.-P., Chen, P., Ma, T.-Y., Recent Advances in Transition-Metal-Mediated Electrocatalytic CO_2 Reduction: From Homogeneous to Heterogeneous Systems,

Catalysts 7 (12) (2017) 373. https://doi.org/10.3390/catal7120373.

[93] Grice, K. A., Carbon dioxide reduction with homogenous early transition metal complexes: Opportunities and challenges for developing CO_2 catalysis, Coord. Chem. Rev. 336 (2017) 78-95. https://doi.org/10.1016/j.ccr.2017.01.007.

[94] Yamazaki, Y., Takeda, H., Ishitani, O., Photocatalytic reduction of CO_2 using metal complexes C, J. Photochem. Photobiol. 25 (2015) 106-137. https://doi.org/10.1016/j.jphotochemrev.2015.09.001.

[95] Stanbury, M., Compain, J.-D., Chardon-Noblat, S., Electro and photoreduction of CO_2 driven by manganese-carbonyl molecular catalysts, Coord. Chem. Rev. 361 (2018): 120-137. https://doi.org/10.1016/j.ccr.2018.01.014.

[96] Fei, H., Sampson, M. D., Lee, Y., Kubiak, C. P., Cohen, S. M., Photocatalytic CO_2 Reduction to Formate Using a Mn(I) Molecular Catalyst in a Robust Metal–Organic Framework, Inorg. Chem. 54 (14) (2015) 6821-6828. https://doi.org/10.1021/acs.inorgchem.5b00752.

[97] Wang, B., Huang, H., Lv, X.-L., Xie, Y., Li, M.; Li, J.-R., Tuning CO_2 Selective Adsorption over N_2 and CH_4 in UiO-67 Analogues through Ligand Functionalization, Inorg. Chem. 53 (17) (2014) 9254-9259. https://doi.org/10.1021/ic5013473.

[98] Ko, N., Hong, J., Sung, S., Cordova, K. E., Park, H. J., Yang, J. K., Kim, A significant enhancement of water vapour uptake at low pressure by amine-functionalization of UiO-67, J. Dalton Trans. 44 (5) (2015) 2047-2051. https://doi.org/10.1039/C4DT02582B.

[99] Katz, M. J., Brown, Z. J., Colon, Y. J., Siu, P. W., Scheidt, K. A., Snurr, R. Q., Hupp, J. T., Farha, O. K., A facile synthesis of UiO-66, UiO-67 and their derivatives, Chem. Commun. 49 (82) (2013) 9449-9451. https://doi.org/10.1039/c3cc46105j.

[100] Georgopoulos, M., Hoffman, M. Z. J., Cage escape yields in the quenching of tris (2,2'-bipyridine) ruthenium (II) by methylviologen: presence of triethanolamine as a sacrificial electron donor, Phys. Chem. 95 (20) (1991) 7717-7721. https://doi.org/10.1021/j100173a031.

[101] Morimoto, T., Nakajima, T., Sawa, S., Nakanishi, R., Imori, D., Ishitani, O., CO_2 Capture by a Rhenium(I) Complex with the Aid of Triethanolamine, J. Am. Chem. Soc. 135 (45) (2013) 16825-16828. https://doi.org/10.1021/ja409271s.

[102] Hawecker, J., Lehn, J.-M., Ziessel, R., Efficient photochemical reduction of CO_2 to CO by visible light irradiation of systems containing $Re(bipy)(CO)_3X$ or $Ru(bipy)_3^{2+}$–Co^{2+} combinations as homogeneous catalysts, Chem. Soc., Chem. Commun. 0 (9) (1983) 536-538. https://doi.org/10.1039/C39830000536.

[103] Hori, H., Takano, Y., Koike, K., Sasaki, Y., Efficient rhenium-catalyzed photochemical carbon dioxide reduction under high pressure, Inorg. Chem. Commun. 6 (3) (2003) 300-303. https://doi.org/10.1016/S1387-7003(02)00758-X.

[104] Shinozaki, K., Hayashi, Y., Brunschwig, B., Fujita, E., Characterization of transient species and products in photochemical reactions of Re(dmb)$(CO)_3$ Et with and without CO_2, Res. Chem. Intermed. 33 (1-2) (2007) 27-36. https://doi.org/10.1163/156856707779160807.

[105] Fujita, E., Hayashi, Y., Kita, S., Brunschwig, B. S., In Studies in Surface Science and Catalysis; Sang-Eon Park, J.-S. C., Kyu-Wan, L., Eds.; Elsevier: New York, 2004; Vol. 153, p 271.

[106] Agarwal, J., Johnson, R. P., Li, G., A Reduction of CO_2 on a Tricarbonyl Rhenium(I) Complex: Modeling a Catalytic Cycle, J. Phys.

Chem. 115 (13) (2011) 2877-2881. https://doi.org/10.1021/jp111342r.

[107] Hayashi, Y., Kita, S., Brunschwig, B. S., Fujita, E., Involvement of a Binuclear Species with the Re−C(O)O−Re Moiety in CO_2Reduction Catalyzed by Tricarbonyl Rhenium(I) Complexes with Diimine Ligands: Strikingly Slow Formation of the Re−Re and Re−C(O)O−Re Species from Re(dmb)$(CO)_3$S (dmb = 4,4'-Dimethyl-2,2'-bipyridine, S = Solvent), J. Am. Chem. Soc. 125 (39) (2003) 11976-11987. https://doi.org/10.1021/ja035960a.

[108] Franco, F., Pinto, M. F., Royo, B., Lloret-Fillol, J., A Highly Active N-Heterocyclic Carbene Manganese(I) Complex for Selective Electrocatalytic CO_2 Reduction to CO, Angew. Chem. Int. Ed. 57 (17) (2018). https://doi.org/10.1002/anie.201800705.

[109] Bourrez, M., Molton, F., Chardon-Noblat, S., Deronzier, A., [Mn(bipyridyl)$(CO)_3$Br]: An Abundant Metal Carbonyl Complex as Efficient Electrocatalyst for CO_2 Reduction, Angew. Chem. Int. Ed. 123 (2011) 10077-10080. https://doi.org/10.1002/anie.201103616.

[110] Smieja, J. M., Sampson, M. D., Grice, K. A., Benson, E. E., Froehlich, J. D., Kubiak, C. P., Manganese as a substitute for rhenium in CO_2 reduction catalysts: the importance of acids, Inorg. Chem. 52 (5) (2013) 2484-2491. https://doi.org/10.1021/ic302391u.

[111] Sampson, M. D., Nguyen, A. D., Grice, K. A., Moore, C. E., Rheingold, A. L., Kubiak, C. P., Manganese catalysts with bulky bipyridine ligands for the electrocatalytic reduction of carbon dioxide: Eliminating dimerization and altering catalysis, J. Am. Chem. Soc. 136 (14) (2014) 5460-5471. https://doi.org/10.1021/jacs.5b01552.

[112] Franco, F., Cometto, C., Nencini, L., Barolo, C., Sordello, F., Minero, C., Fiedler, J., Robert, M., Gobetto, R., Nervi, C., Local Proton Source in Electrocatalytic CO_2 Reduction with [Mn(bpy–R)$(CO)_3$Br] Complexes, Chem. Eur. J. 23 (20) (2017) 4782. https://doi.org/10.1002/chem.201605546.

[113] Ngo, K. T., McKinnon, M., Mahanti, B., Narayanan, R., Grills, D. C., Ertem, M. Z., J. Rochford J., Turning on the Protonation-First Pathway for Electrocatalytic CO_2 Reduction by Manganese Bipyridyl Tricarbonyl Complexes, J. Am. Chem. Soc. 139 (7) (2017) 2604-2618. https://doi.org/10.1021/jacs.6b08776.

[114] Sampson, M. D., Kubiak, C. P., Manganese Electrocatalysts with Bulky Bipyridine Ligands: Utilizing Lewis Acids To Promote Carbon Dioxide Reduction at Low Overpotentials, J. Am. Chem. Soc. 138 (4) (2016) 1386-1393. https://doi.org/10.1021/jacs.5b12215.

[115] Reuillard, B., Ly, K. H., Rosser, T. E., Kuehnel, M. F., Zebger, I., Reisner, E., Tuning Product Selectivity for Aqueous CO_2 Reduction with a Mn(bipyridine)-pyrene Catalyst Immobilized on a Carbon Nanotube Electrode, J. Am. Chem. Soc. 139 (41) (2017) 14425-14435. https://doi.org/10.1021/jacs.7b06269.

[116] Franco, F., Cometto, C., Vallana, F. F., Sordello, F., Priola, E., Minero, C., Nervi, C., Gobetto, R., A local proton source in a [Mn (bpy-R)$(CO)_3$Br]-type redox catalyst enables CO_2 reduction even in the absence of Brønsted acids, Chem. Commun. 50 (93) (2014) 14670-14673. https://doi.org/10.1039/c4cc05563b.

[117] Smieja, J. M., Sampson, M. D., Grice, K. A., Benson, E. E., Froehlich, J. D., Kubiak, C. P., Manganese as a Substitute for Rhenium in CO_2 Reduction Catalysts: The Importance of Acids, Inorg. Chem. 52 (5) (2013) 2484-2491. https://doi.org/10.1021/ic302391u.

[118] Fei, H., Sampson, M. D., Lee, Y., Kubiak, C. P., Cohen, S. M., Photocatalytic CO_2 Reduction to Formate Using a Mn(I) Molecular Catalyst in a Robust Metal-Organic Framework, Inorg. Chem.

54 (14) (2015) 6821-6828. https://doi.org/10.1021/acs.inorgchem.5b00752.

[119] Agarwal, J., Shaw, T. W., Schaefer, H. F., Bocarsly, A. B., Design of a Catalytic Active Site for Electrochemical CO_2 Reduction with Mn(I)-Tricarbonyl Species, Inorg. Chem. 54 (11) (2015) 5285-5294. https://doi.org/10.1021/acs.inorgchem.5b00233.

[120] Takeda, H., Koizumi, H., Okamoto, K., Ishitani, O., Photocatalytic CO_2 reduction using a Mn complex as a catalyst, Chem. Commun. 50 (12) (2014) 1491-1493. https://doi.org/10.1039/c3cc48122k.

[121] Ngo, K. T., McKinnon, M., Mahanti, B., Narayanan, R., Grills, D. C., Ertem, M. Z., Rochford, Turning on the Protonation-First Pathway for Electrocatalytic CO_2 Reduction by Manganese Bipyridyl Tricarbonyl Complexes, J. J. Am. Chem. Soc. 139 (7) (2017) 2604-2618. https://doi.org/10.1021/jacs.6b08776.

[122] Franco, F., Cometto, C., Nencini, L., Barolo, C., Sordello, F., Minero, C., Fiedler, J., Robert, M., Gobetto, R., Nervi, C., Local Proton Source in Electrocatalytic CO_2 Reduction with [Mn(bpy–R)$(CO)_3$Br] Complexes, Chem. - Eur. J. 23 (20) (2017) 4782-4793. https://doi.org/10.1002/chem.201605546.

[123] Walsh, J. J., Smith, C. L., Neri, G., Whitehead, G. F. S., Robertson, C. M., Cowan, A. J., Improving the efficiency of electrochemical CO_2 reduction using immobilized manganese complexes, Faraday Discuss. 183 (2015) 147-160. https://doi.org/10.1039/c5fd00071h.

[124] Torralba-Peñalver, E.; Luo, Y.; Compain, J.-D.; Chardon-Noblat, S.; Fabre, B., Selective Catalytic Electroreduction of CO_2 at Silicon Nanowires (SiNWs) Photocathodes Using Non-Noble Metal-Based Manganese Carbonyl Bipyridyl Molecular Catalysts in Solution and Grafted onto SiNWs, ACS Catal. 5 (10) (2015) 6138-6147. https://doi.org/10.1021/acscatal.5b01546.

[125] Rosser, T. E., Windle, C. D., Reisner, E., Electrocatalytic and Solar-Driven CO_2 Reduction to CO with a Molecular Manganese Catalyst Immobilized on Mesoporous TiO_2, Angew. Chem., Int. Ed. 55 (26) (2016) 7388. https://doi.org/10.1002/anie.201601038.

[126] Bourrez, M., Orio, M., Molton, F., Vezin, H., Duboc, C., Deronzier, A., Chardon-Noblat, S., Pulsed-EPR Evidence of a Manganese (II) Hydroxycarbonyl Intermediate in the Electrocatalytic Reduction of Carbon Dioxide by a Manganese Bipyridyl Derivative, Angew. Chem., Int. Ed. 53 (1) (2014) 240-243. https://doi.org/10.1002/anie.201306750.

[127] Keim, W., Nickel: an element with wide application in industrial homogeneous catalysis, Angew. Chem. Int. Ed. Engl. 29 (3) (1990) 235-244. https://doi.org/10.1002/anie.199002351.

[128] Rosen, B. M., Quasdorf, K. W., Wilson, D. A., Zhang, N., Resmerita, A.-M., Garg, N. K., Percec, V., Nickel-catalyzed cross-couplings involving carbon-oxygen bonds, Chem. Rev. 111 (3) (2011) 1346-1416. https://doi.org/10.1021/cr100259t.

[129] Wiese, S., Kilgore, U. J., DuBois, D. L., Bullock, R. M., $[Ni(P^{Me}{}_2N^{Ph}{}_2)_2](BF_4)_2$ as an Electrocatalyst for H_2 Production, ACS Catal. 2 (5) (2012) 720-727. https://doi.org/10.1021/cs300019h.

[130] Gan, L., Groy, T. L., Tarakeshwar, P., Mazinani, S. K., Shearer, J., Mujica, V., Jones, A. K., A nickel phosphine complex as a fast and efficient hydrogen production catalyst, J. Am. Chem. Soc. 137 (3) (2015) 1109-1115. https://doi.org/10.1021/ja509779q.

[131] Thoi, V. S., Kornienko, N., Margarit, C. G., Yang, P., Chang, C. J., Visible-Light Photoredox Catalysis: Selective Reduction of Carbon Dioxide

Eclética Química Journal, vol. 44, n. 1, 2019, 11-39
ISSN: 1678-4618
DOI: 10.26850/1678-4618eqj.v44.1.2019.p11-39

to Carbon Monoxide by a Nickel N-Heterocyclic Carbene–Isoquinoline Complex, J. Am. Chem. Soc. 135 (38) (2013) 14413-14424. https://doi.org/10.1021/ja4074003.

[132] Han, Y., Wu, Y., Lai, W., Cao, R., Electrocatalytic water oxidation by a water-soluble nickel porphyrin complex at neutral pH with low overpotential, Inorg. Chem. 54 (11) (2015) 5604-5613. https://doi.org/10.1021/acs.inorgchem.5b00924.

[133] Zhang, M., Zhang, M. T., Hou, C., Ke, Z. F., Lu, T. B., Homogeneous electrocatalytic water oxidation at neutral pH by a robust macrocyclic nickel (II) complex, Angew. Chem. Int. Ed. 53 (48) (2014) 13042-13048. https://doi.org/10.1002/anie.201406983.

[134] Solis, B. H., Maher, A. G., Dogutan, D. K., Nocera, D. G., Hammes-Schiffer, S., Nickel phlorin intermediate formed by proton-coupled electron transfer in hydrogen evolution mechanism, Proc. Natl. Acad. Sci. U.S.A. 113 (3) (2016) 485-492. https://doi.org/10.1073/pnas.1521834112.

[135] Zilbermann, I., Maimon, E., Cohen, H., Meyerstein, D., Redox chemistry of nickel complexes in aqueous solutions, Chem. Rev. 105 (6) (2005) 2609-2626. https://doi.org/10.1021/cr030717f.

[136] Tasker, S. Z., Standley, E. A., Jamison, T. F., Recent advances in homogeneous nickel catalysis, Nature 509 (2014) 299-309. https://doi.org/10.1038/nature13274.

[137] Beley, M., Collin, J. P., Ruppert, R., Sauvage, J. P., Electrocatalytic reduction of carbon dioxide by nickel cyclam^{2+} in water: study of the factors affecting the efficiency and the selectivity of the process, J. Am. Chem. Soc. 108 (4) (1986) 7461-7467. https://doi.org/10.1021/ja00284a003.

[138] Helm, M. L., Stewart, M. P., Bullock, R. M., DuBois, M. R., DuBois, D. L., A synthetic nickel electrocatalyst with a turnover frequency above 100,000 s^{-1} for H_2 production, Science 333 (2011) 863-866. https://doi.org/10.1126/science.1205864.

[139] Shafaat, H. S., Rudiger, O., Ogata, H., Lubitz, W., [NiFe] hydrogenases: a common active site for hydrogen metabolism under diverse conditions, Biochim. Biophys. Acta 1827 (8-9) (2013) 986-1002. https://doi.org/10.1016/j.bbabio.2013.01.015.

[140] Greene, B. L., Wu, C. H., Vansuch, G. E., Adams, M. W., Dyer, R. B., Proton Inventory and Dynamics in the Ni_a-S to Ni_a-C Transition of a [NiFe] Hydrogenase, Biochemistry 55 (12) (2016) 1813-1825. https://doi.org/10.1021/acs.biochem.5b01348.

[141] Jeoung, J. H., Dobbek, H., Carbon dioxide activation at the Ni, Fe-cluster of anaerobic carbon monoxide dehydrogenase, Science 318 (2007) 1461-1464. https://doi.org/10.1126/science.1148481.

[142] Fesseler, J., Jeoung, J.-H., Dobbek, H., How the [$NiFe_4S_4$] Cluster of CO Dehydrogenase Activates CO_2 and NCO^-, Angew. Chem. Int. Ed. 54 (29) (2015) 8560-8564. https://doi.org/10.1002/anie.201501778.

[143] Dempsey, J. L., Brunschwig. B. S., Winkler, J. R., Gray, H. B., Hydrogen evolution catalyzed by cobaloximes, Acc. Chem. Res. 42 (12) (2009) 1995-2004. https://doi.org/10.1021/ar900253e.

[144] Wang, M., Na, Y., Gorlov, M., Sun, L., Light-driven hydrogen production catalysed by transition metal complexes in homogeneous systems, Dalton Trans. (2009) 6458-6467. https://doi.org/10.1039/b903809d.

[145] Mondal, B., Dey, A., Development of air-stable hydrogen evolution catalysts, Chem. Commun. 53 (55) (2017) 7707-7715. https://doi.org/10.1039/c7cc02941a.

[146] Zee, D. Z., Chantarojsiri, T., Long, J. R., Chang, C. J., Metal-polypyridyl catalysts for electro-and photochemical reduction of water to hydrogen, Acc. Chem. Res. 48 (7) (2015) 2027-2036. https://doi.org/10.1021/acs.accounts.5b00082.

[147] Wang, M., Chen, L., Sun, L., Recent progress in electrochemical hydrogen production with earth-abundant metal complexes as catalysts, Energy Environ. Sci. 5 (5) (2012) 6763-6778. https://doi.org/10.1039/C2EE03309G.

[148] Thoi, V. S., Sun, Y., Long, J. R., Chang, C. J., Complexes of earth-abundant metals for catalytic electrochemical hydrogen generation under aqueous conditions, Chem. Soc. Rev. 42 (6) (2013) 2388-2400. https://doi.org/10.1039/c2cs35272a.

[149] Coutard, N., Kaeffer, N., Artero, V., Molecular engineered nanomaterials for catalytic hydrogen evolution and oxidation, Chem. Commun. 52 (95) (2016) 13728-13748. https://doi.org/10.1039/c6cc06311j.

[150] Willkomm, J., Orchard, K. L., Reynal, A., Pastor, E., Durrant, J. R., Reisner, E., Dye-sensitised semiconductors modified with molecular catalysts for light-driven H_2 production, Chem. Soc. Rev. 45 (1) (2016) 9-23. https://doi.org/10.1039/c5cs00733j.

[151] DuBois, D. L., Bullock, R. M., Molecular electrocatalysts for the oxidation of hydrogen and the production of hydrogen – the role of pendant amines as proton relays, Eur. J. Inorg. Chem. 2011 (7) (2011) 1017-1027. https://doi.org/10.1002/ejic.201001081.

[152] Kärkäs, M. D., Verho, O., Johnston, E. V., Åkermark, B., Artificial photosynthesis: molecular systems for catalytic water oxidation, Chem. Rev. 114 (24) (2014) 11863-12001. https://doi.org/10.1021/cr400572f.

[153] Kondo, M., Masaoka, S., Water oxidation catalysts constructed by biorelevant first-row metal complexes, Chem. Lett. 45 (11) (2016) 1220-1231. https://doi.org/10.1246/cl.160639.

[154] Garrido-Barros, P., Gimbert-Surinach, C., Matheu, R., Sala, X., Llobet, A., How to make an efficient and robust molecular catalyst for water oxidation, Chem. Soc. Rev. 46 (20) (2017) 6088-6098. https://doi.org/10.1039/c7cs00248c.

[155] Costentin, C., Robert, M., Savéant, J.-M., Current Issues in Molecular Catalysis Illustrated by Iron Porphyrins as Catalysts of the CO_2-to-CO Electrochemical Conversion, Acc. Chem. Res. 48 (12) (2015) 2996-3006. https://doi.org/10.1021/acs.accounts.5b00262.

[156] Benson, E. E., Kubiak, C. P., Sathrum, A. J., Smieja, J. M., Electrocatalytic and homogeneous approaches to conversion of CO_2 to liquid fuels, Chem. Soc. Rev. 38 (1) (2009) 89-99. https://doi.org/10.1039/b804323j.

[157] Yamazaki, Y., Takeda, H., Ishitani, O., Photocatalytic reduction of CO_2 using metal complexes C, J. Photochem. Photobiol. 25 (2015) 106-137. https://doi.org/10.1016/j.jphotochemrev.2015.09.001.

[158] Morris, A. J., Meyer, G. J., Fujita, E., Molecular approaches to the photocatalytic reduction of carbon dioxide for solar fuels, Acc. Chem. Res. 42 (12) (2009) 1983-1994. https://doi.org/10.1021/ar9001679.

[159] Reithmeier, R., Bruckmeier, C., Rieger, B., Conversion of CO_2 via visible light promoted homogeneous redox catalysis, Catalysts 2 (4) (2012) 544-571. https://doi.org/10.3390/catal2040544.

[160] Kang, P., Chen, Z., Brookhart, M., Meyer, T. J., Electrocatalytic reduction of carbon dioxide: Let the molecules do the work, Top. Catal. 58 (1)

(2014) 30-45. https://doi.org/10.1007/s11244-014-0344-y.

[161] Windle, C. D., Perutz, R. N., Advances in molecular photocatalytic and electrocatalytic CO_2 reduction, Coord. Chem. Rev. 256 (2012) 2562-2570. https://doi.org/10.1016/j.ccr.2012.03.010.

[162] Costentin, C., Robert, M., Savéant, J.-M., Catalysis of the electrochemical reduction of carbon dioxide, Chem. Soc. Rev. 42 (6) (2013) 2423-2436. https://doi.org/10.1039/c2cs35360a.

[163] Wang, J.-W., Zhong, D.-C., Lu, T.-B., Artificial photosynthesis: Catalytic water oxidation and CO_2 reduction by dinuclear non-noble-metal molecular catalysts, Coord. Chem. Rev. 377 (2017) 225-236. https://doi.org/10.1016/j.ccr.2018.09.003.

[164] Niu, K., Xu, Y., Wang, H., Ye, R., Xin, H. L., Lin, F., Tian, C., Lum, Y., Bustillo, K. C., Doeff, M. M., Koper, M. T. M., Ager, J., Xu, R., Zheng, H., A spongy nickel-organic CO_2 reduction photocatalyst for nearly 100% selective CO production, Sci. Adv. 3 (7) (2017) 1-9. https://doi.org/10.1126/sciadv.1700921.

[165] Gao, C., Meng, Q., Zhao, K., Yin, H., Wang, D., Guo, J., Zhao, S., Chang, L., He, M., Li, Q., Zhao, H., Huang, X., Gao, Y., Tang, Z., Co_3O_4 Hexagonal Platelets with Controllable Facets Enabling Highly Efficient Visible-Light Photocatalytic Reduction of CO_2, Adv. Mater. 28 (30) (2016) 6485-6490. https://doi.org/10.1002/adma.201601387.

[166] Kirch, M., Lehn, J.-M., Sauvage, J.-P., Hydrogen generation by visible light irradiation of aqueous solutions of metal complexes. An approach to the photochemical conversion and storage of solar energy, Helv. Chim. Acta 62 (4) (1979) 1345-1384. https://doi.org/10.1002/hlca.19790620449.

[167] Gärtner, F., Sundararaju, B., Surkus, A.-E., Boddien, A., Loges, B., Junge, H., Dixneuf, P. H., Beller, M., Light-Driven Hydrogen Generation: Efficient Iron-Based Water Reduction Catalysts, Angew. Chem. Int. Ed. 48 (52) (2009) 9962-9965. https://doi.org/10.1002/anie.200905115.

[168] Maschmeyer, T., Che, M., Catalytic Aspects of Light-Induced Hydrogen Generation in Water with TiO_2 and Other Photocatalysts: A Simple and Practical Way Towards a Normalization?, Angew. Chem. Int. Ed. 49 (9) (2010) 1536-1539. https://doi.org/10.1002/anie.200903921.

[169] Cheng, T., Xiao, H., Goddard III, W. A., Full atomistic reaction mechanism with kinetics for CO reduction on Cu (100) from ab initio molecular dynamics free-energy calculations at 298 K, Proc. Natl. Acad. Sci. U.S.A. 114 (8) (2017) 1795-1800. https://doi.org/10.1073/pnas.1612106114.

[170] Li, C. W., Ciston, J., Kanan, M. W., Electroreduction of carbon monoxide to liquid fuel on oxide-derived nanocrystalline copper, Nature 508 (2014) 504-507. https://doi.org/10.1038/nature13249.

[171] London, R. E., Walker, T. E., Kollman, V. H., Matwiyoff, N. A., Studies of the pH dependence of carbon-13 shifts and carbon-carbon coupling constants of [U-13C] aspartic and-glutamic acids, J. Am. Chem. Soc. 100 (12) (1978) 3723-3729. https://doi.org/10.1021/ja00480a012.

[172] Kuehnel, M. F., Orchard, K. L., Dalle, K. E., Reisner, E., Selective Photocatalytic CO_2 Reduction in Water through Anchoring of a Molecular Ni Catalyst on CdS Nanocrystals, J. Am. Chem. Soc. 139 (21) (2017) 7217-7223. https://doi.org/10.1021/jacs.7b00369.

Eclética Química Journal

Original article
iq.unesp.br/ecletica

| Vol. 44 | n. 1 | 2019 |

Electrochemical remediation of industrial pharmaceutical wastewater containing hormones in a pilot scale treatment system

Ruiter Lima Morais[1], Luane Ferreira Garcia[1], Emily Kussmaul Gonçalves Moreno[1], Douglas Vieira Thomaz[1], Laís de Brito Rodrigues[1], Lara Barroso Brito[1], Germán Sanz Lobón[2], Gisele Augusto Rodrigues de Oliveira[1], Marcella Ferreira Rodrigues[2], Boniek Gontijo Vaz[2], Eric de Souza Gil[1+]

1 Federal University of Goiás, Faculty of Pharmacy, Goiânia, Goiás, Brazil
2 Federal University of Goiás, Institute of Chemistry, Goiânia, Goiás, Brazil

[+] Corresponding author: Eric de Souza Gil, phone: +55 62 3202-1278, e-mail address: ericsgil@gmail.com

ARTICLE INFO

Article history:
Received: September 25, 2018
Accepted: November 26, 2018
Published: January 28, 2019

Keywords:
1. algestone acetophenide
2. estradiol enanthate
3. electrocoagulation remediation
4. ecotoxicity
5. mass spectrometry

ABSTRACT: The elimination of residual drugs from pharmaceutical and domestic sources is a growing concern, as they are able to reach water and soil resources and can present environmental and health risks even in very low concentrations. Traditional water and wastewater treatment systems have not been efficient in the removal of these compounds, evidencing the importance of the development of new remediation methods. In view of the applicability and versatility of electrocoagulation techniques in the removal of pollutants, the aim of this work is to evaluate the parameters: biochemical oxygen demand (BOD), chemical oxygen demand (COD), color, turbidity, algestone acetophenide (AAc) and estradiol enanthate (EEn) using a pilot treatment system, as well as phytotoxicity and Brine shrimp toxicity. The study showed good removal efficiency, comprising remarkable remediation performance assayed through BOD (61.5%), COD (58.6%), color (83.1%), turbidity (96.7%), AAc (77.0%) and EEn (56.7%) after 30 minutes. For toxicity, raw effluent was considered more phytotoxic for lettuce and cucumber seeds when compared to treated effluent. The results suggest that the pilot prototype was promising, providing an increase in both the germination potential and the root growth of the seeds (*Lactuca sativa* and *Cucumis sativus*) and a significant decrease in the acute toxicity to *Artemia salina*.

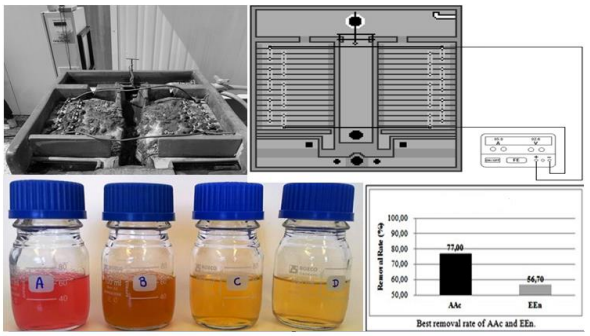

1. Introduction

The residual drugs disposal from pharmaceutical and domestic sources is encompassed among the anthropogenic actions of greater environmental impact[1]. Hence inefficient wastewater treatment, emerging pollutants such as drugs and their metabolites are able to reach water bodies and soil, therefore leading to environmental and health hazards[2].

Residual drugs are usually found in the environment at concentrations of μg L^{-1} (ppb) or ng L^{-1} (ppt)[3], this chronic exposure to subtoxic doses of the drug may result in a number of undesirable effects on both the human organism and the environment[4]. Studies demonstrate the relationship between residual drugs and health problems, which vary upon the class, mental disorders, sexual dysfunctions[5] (Santos *et al.* and resistance to antibiotics[6] are some illustrative examples).

In this context, owing to the widespread occurrence, synthetic hormones are considered major threats. Moreover, such compounds present high stability, being invulnerable to common

Eclética Química Journal, vol. 44, n. 1, 2019, 40-52
ISSN: 1678-4618
DOI: 10.26850/1678-4618eqj.v44.1.2019.p40-52

remediation methods, leading to their omnipresence in pharmaceutical wastewaters[7, 8].

The synthetic hormones AAc and EEn are worldwide consumed drugs used as contraceptive and anti-inflammatory agents[9]. Once these steroids are metabolized in the body, their metabolites are excreted through the urine/feces and dumped in Wastewater Treatment Plants (WWTP)[10] Though steroids like AAc and EEn have been mostly omitted by environmental legislation, they represent a real risk to the environment and human healthy[11]. Therefore, great effort has been done in order to improve the efficiency of current remediation processes[12].

The presence of steroids and their metabolites in aquatic and terrestrial environments can be explained by their non-biodegradable nature, recalcitrance, and by continuous release in environment, which is nonetheless much superior than their removal, henceforth characterizing them as "pseudo-persisted". Thus, conventional biological and chemical treatments become ineffective[13, 14]. Another limiting factor of biodegradation is related to the interconversions between steroids caused by some microorganisms[15].

The use of different advanced oxidation processes (AOP) involving Fenton, photocatalysis, UV-H_2O_2, ozone, ozone-UV, plasma-based processes and sonolysis as promising technologies to deal with some environmental problems has been intensely investigated worldwide by numerous researchers[16, 17]. Even though AOPs appear to be promising and attractive options, handicaps like as high costs (energy, inputs), sustainability (resource use, carbon footprint), by-product formation and experimental level still prevent them from being widely used[18, 19]. Therefore, the use of renewable energy sources to supply processes, the development of less expensive hardware and electrodes and more versatile systems are needed to diffuse and launch the industrial application of these technologies[20, 21].

Hence biodegradation and AOPs limitations to promote steroids removal in waterbodies effluents, methods such as electroremediation by electrocoagulation (EC) are becoming increasingly used due to their wide applicability, low cost and high efficiency. Electrocoagulation is constituted by three main steps: (1) oxidation/reduction reactions at electrode surface, (2) generation of coagulating agents from aluminum or iron (steel) electrodes immersed in the aqueous solution, (3) adsorption of soluble or colloidal pollutant particles on coagulants, and removal by sedimentation and/or flotation. These processes can efficiently mop up pollutants, which would be otherwise unable to undergo degradation through biological remediation methods[22, 23].

Owing to electrocoagulation techniques applicability in treatment of industrial wastewater, the aim of this work is to assess the improvement of BOD, COD, color and turbidity parameters of treated pharmaceutical wastewater, as well as the removal of synthetic hormones AAc and EEn using a pilot electrocoagulation treatment system. In order to evaluate the effluents toxicity, tests concerning phytotoxicity and acute toxicity with *Artemia salina* were henceforth performed.

2. Materials and methods

2.1 Pilot Scale Treatment System (PSTS)

The pilot scale prototype consisted in square aquarium, made in acrylic material, presenting the following dimensions: 38 cm long, 24 cm wide and 30 cm high, in which 16 stain steel 1020 electrodes (20 x 27 x 6.35 cm each) with 1,728 cm^2 of total surface were equally distributed (Figure 1).

The raw effluent sample used was collected in pharmaceutical industry, dedicated to the production of hormonal drugs in Goiânia-Brazil, and the initial treatment conditions were: electric current 14.9-15.4 A (Direct Current – DC); applied potential of 26.5-26.8 V. The inversion of polarity between cathode and anode was performed every 20 minutes. Temperature and electrical parameters were monitored during the treatment regimen/experiment at 10, 20 and 30 minutes. The temperature shifts were monitored in an Infrared Temperature Tester Thermometer GM300 (Benetech, Shenzhen Jumaoyuan Science And Technology Co., Ltd, Shenzhen, China), whereas the current and potential with a Digital Clamp AC/DC Voltmeter F203 (Chauvin Arnoux Metrix, France).

Eclética Química Journal, vol. 44, n. 1, 2019, 40-52
ISSN: 1678-4618
DOI: 10.26850/1678-4618eqj.v44.1.2019.p40-52

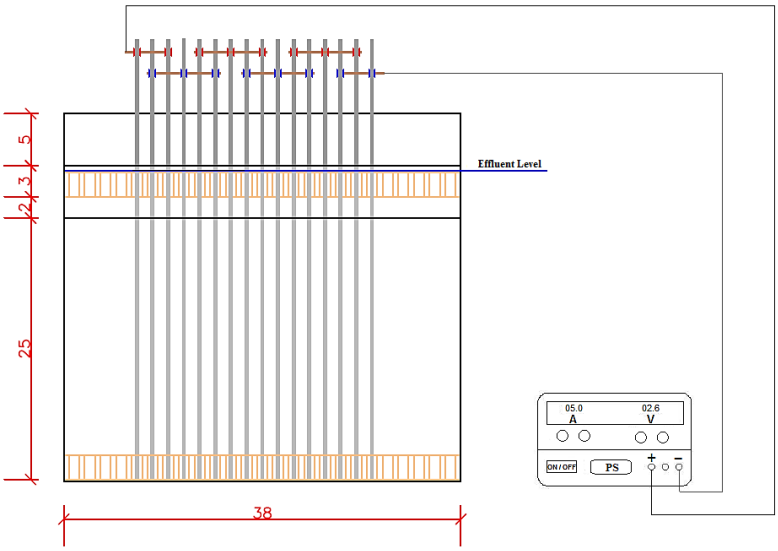

Figure 1. Pilot scale treatment system.

Electrical conductivity, color, BOD, COD, pH, and turbidity were monitored in this study since they are good indicators of wastewater quality. The tests were performed according to the techniques recommended by the Standard Methods for the examination of Water and Wastewater[24].

Some characteristics of synthetic hormones studied are summarized in Table 1.

Table 1. Some characteristics of the synthetic hormones studied.

	Acetophenide Algestone[25]	**Estradiol Enanthate**[26]
Structure	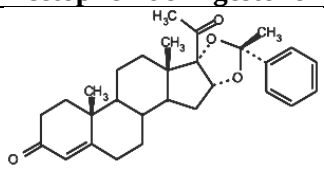	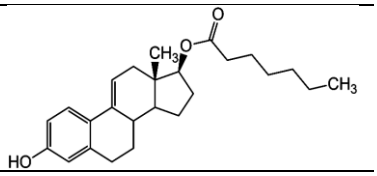
Solubility (mg L^{-1}) (Estimated by Log K_{ow})	0.02864	0.006894
Log K_{ow}	5.53	7.40

The experiment was performed in triplicate (T1, T2 and T3) from the same industrial effluent sample and no additions of chemical compounds were made for correction purposes.

2.2 Mass Spectrometry Analysis

Mass spectrometry (MS) analysis was carried out in a mass spectrometer microTOF III (Brucker Daltonics, Bremen, Germany) equipped with a commercial ESI source (Brucker Daltonics, Bremen, Germany). Samples were methanol-diluted to a (1:1000) ratio, followed by acidification with 0.1% formic acid. The resulting solution was directly injected with a flow rate of 4 µL min^{-1}, all analyses were performed in the positive full scan mode (m/z 100–1000). ESI(+) source conditions were as follows: nebulizer nitrogen gas temperature and pressure of 2.0 bar and 200 °C, capillary voltage of -4 kV, transfer capillary temperature of 200 °C; drying gas of 4 L min^{-1}; end plate offset of -500V; skimmer of 35V and collision voltage of -1.5V. Each spectrum was acquired using 2 microscans per second for one minute. The resolving power (m/Δm50% 16.500,00, where Δm50% is the peak full width at half-maximum peak height). Mass spectra were acquired and processed with Data Analysis software (Brucker Daltonics, Bremen, Germany).

A quantification method by MS was also designed focusing the assessment of pilot scale treatment system efficiency. To avoid matrix effect, calibration curves for AAc using gestodene as secondary standard were constructed. The

Eclética Química Journal, vol. 44, n. 1, 2019, 40-52
ISSN: 1678-4618
DOI: 10.26850/1678-4618eqj.v44.1.2019.p40-52

quantification was possible through calculation of the relation between gestodene and AAc, therefore measuring the intensity in several defined concentration for wastewater and treated water.

To develop calibration curves, 1 mg mL^{-1} AAc and gestodene stocks solutions in methanol were prepared and subsequently diluted to concentrations: 0.5; 2.0; 3.5; 5.0; 6.5 mg L^{-1}. In 500 µL of water sample was added the appropriate volume of the stock solution and finally was added the 0.1% formic acid to helped in ionization process.

Chemicals used were all of ACS grade, and purchased from Sigma-Aldrich, they were used without any further purification. MS and High Performance Liquid Chromatography (HPLC) grade solvents were purchased from J.T. Baker.

2.3 Ecotoxicity Tests

The ecotoxicity tests were performed only on the sample that presented the best result of removal of estrogenic compounds.

2.3.1 Phytotoxicity Tests

Lettuce (*Lactuca sativa*) and cucumber (*Cucumis sativus*) seeds were purchased from an agriculture local supplier. The seed germination and root elongation test on filter paper was performed according to the US Environmental Protection Agency[27] seed germination/root elongation toxicity test. Before the test, the seeds were sterilized with 0.1% sodium hypochlorite solution for 10 min and then rinsed several times in distilled water to prevent fungal growth. Ten seeds of each species were exposed on filter paper (Whatman 2) containing 2.5 mL of raw or treated effluents at 6.25, 12.5, 25, 50 and 100% (v/v) and placed in a Petri dish. Distilled water was used as negative control and zinc sulfate heptahydrate ($ZnSO_4.7H_2O$; 10 mg mL^{-1}) as positive control. Three plates per concentration were prepared and incubated in complete darkness in a growth chamber at 25 ± 1 ºC for 120 h.

After this exposure time, the number of germinated seeds was counted, and the length of the root measured. Tests were only considered valid if 80% of control seeds had germinated and the roots size was at least 5 cm long. The percentage of relative seed germination was calculated by dividing the number of seeds germinated in the exposed groups by the number of seeds geminated in the negative control. The percentage of relative root elongation was calculated by dividing the mean root length in raw or treated effluents exposures by the mean root length in the negative control.

2.3.2 Brine shrimp toxicity assay

The brine shrimp bioassay was performed based on the Meyer[28] method and OECD Guideline 202[29] with modifications. Brine shrimp (*Artemia salina*) nauplii were obtained by hatching dehydrated cysts in artificially prepared seawater (3.5% commercial marine salt [Blue Treasure®] in deionized water) at 27 ± 1 °C, under continuous light and aeration for 48 h. For the test, 20 nauplii divided into 4 groups of 5 organisms each, were exposed to 2 mL of raw and treated effluents at 6.25; 12.5; 25; 50 and 100% (v/v). All test solutions were prepared in artificial seawater. Microplates were incubated in the dark in a climatic chamber for 48 h at 27 ± 1 °C. Artificial seawater was used as the negative control and 10 mg L^{-1} dodecyl sulfate sodium salt (SDS) as the positive control.

After 24 and 48 h, the number of dead nauplii (immobility) in control and exposed groups was counted. The percentage of immobility induced by the effluents was compared with that of the control group. The test was considered valid if the immobilization rate was less than 10% in the negative control group[29].

2.3.3 Statistical analysis

Ecotoxicity tests were evaluated using ANOVA and Dunnett's post hoc test using the GraphPad Prism program. Each experimental value was compared with its corresponding control. Statistical significance was accepted at $p < 0.05$. Toxicity was expressed as effective (EC_{50}) and lethal (LC_{50}) concentrations with their 95% confidence limits.

3. Results and discussion

3.1 Physicochemical Data and Removal Efficiency

The electrics conditions in treatment system are showed on Table 2.

Eclética Química Journal, vol. 44, n. 1, 2019, 40-52
ISSN: 1678-4618
DOI: 10.26850/1678-4618eqj.v44.1.2019.p40-52

Table 2. Electrical conditions during the tests with the pilot system.

Time	Temperature (°C)					Voltage (V)					Current (A)				
(min)	T1	T2	T3	AV	SD	T1	T2	T3	AV	SD	T1	T2	T3	AV	SD
0	28.0	27.9	28.2	28.0	0.2	26.8	26.5	26.6	26.6	0.2	15.4	14.9	15.3	15.2	0.3
10	29.0	28.5	28.9	28.8	0.3	25.5	25.1	25.4	25.3	0.2	26.0	24.0	25.5	25.2	1.0
20	31.0	30.0	30.6	30.5	0.5	26.5	26.1	26.2	26.3	0.2	7.0	6.3	6.8	6.7	0.4
30	32.0	31.0	31.8	31.6	0.5	30.0	28.9	29.8	29.6	0.6	13.0	12.0	12.7	12.6	0.5

T1 = Test nº 1; T2 = Test nº 2; T3 = Test nº 3, AV = Average; SD = Standard Deviation.

In the EC with inversion of polarity, the electrode that behaves as a cathode for a certain time, will behave like anode after the inversion of polarity, in this case, at 20 minutes. This inversion decreases the passivation, increasing electrode lifespan by up to three times, at the same time, reducing the resistivity of the system, thus, the cathode starts to release more OH^- species in the solution, increasing the pH and the pollutant removal efficiency[30].

Despite being under the same initial conditions a small variation of voltage and current (DC) was observed between the tests (T1, T2 and T3) probably due to electrode degradation between one test and another and/or small variations in the composition of the stock effluent.

A variation in voltage and current was also observed during each test. This has occurred due to a variation on the composition of effluent during the assays, as shown at Table 3. Also, these parameters were monitored to assess the electrochemistry removal process.

Table 3. Physicochemical parameters evaluated during the pilot tests.

Time (min)	Test nº	Electrical Conductivity ($\mu S\ cm^{-1}$)	Color ($mg\ L^{-1}$ $CaCO_3$)	BOD ($mg\ L^{-1}$ O_2)	COD ($mg\ L^{-1}$ O_2)	pH	Turbidity (NTU)
0	T1						
	T2	3170.0	2550.0	14342.0	35360.0	5.4	385.0
	T3						
	AV	**3170.0**	**2550.0**	**14342.0**	**35360.0**	**5.4**	**385.0**
	SD	**0**	**0**	**0**	**0**	**0**	**0**
10	T1	3431.0	5700.0	8670.0	22320.0	10.8	520.0
	T2	3216.0	5900.0	9120.0	23055.0	10.2	550.0
	T3	3330.0	5800.0	8950.0	22679.0	10.6	530.0
	AV	**3325.7**	**5800.0**	**8913.3**	**22684.7**	**10.5**	**533.3**
	SD	**107.6**	**100.0**	**227.2**	**367.5**	**0.3**	**15.3**
20	T1	3713.0	650.0	8790.0	22350.0	11.8	19.5
	T2	3564.0	690.0	9240.0	23205.0	11.5	32.0
	T3	3689.0	670.0	8910.0	22780.0	11.7	27.0
	AV	**3655.3**	**670.0**	**8980.0**	**22778.3**	**11.7**	**26.2**
	SD	**80.0**	**20.0**	**233.0**	**427.5**	**0.2**	**6.3**
30	T1	4393.0	430.0	5525.0	14650.0	11.9	12.6
	T2	4139.0	490.0	5930.0	15120.0	11.6	25.0
	T3	4216.0	450.0	5660.0	14840.0	11.8	19.0
	AV	**4249.3**	**456.7**	**5705.0**	**14870.0**	**11.8**	**18.9**
	SD	**130.2**	**30.6**	**206.2**	**236.4**	**0.2**	**6.2**
Avarege Removal Eff. (%)		**-**	**82.1**	**60.2**	**57.9**	**-**	**95.1**

T1 = Test nº 1; **T2** = Test nº 2; **T3** = Test nº 3; **AV** = Average; **SD** = Standard Deviation.

Eclética Química Journal, vol. 44, n. 1, 2019, 40-52
ISSN: 1678-4618
DOI: 10.26850/1678-4618eqj.v44.1.2019.p40-52

A significant decrease of BOD (61.5%), COD (58.6%), turbidity (96.7%) and color (83.1%) after 30 minutes was noticed for the best result (T1). On the other hand, it was possible to observe the increase in electrical conductivity, pH and sludge production. The generation of sludge occurred due to the use of iron anodes and its consequent generation of iron hydroxides, thus playing the same role of flocculation in conventional coagulation treatment systems[22].

When the steel anode is used Fe^{2+} is dissolved in the effluent from the anodic oxidation of Fe, while H_2 gas is generated in the cathode from the reduction of protons in acid medium and/or reduction of water in alkaline medium. Insoluble $Fe(OH)_2$ precipitates at pH > 5.5 remaining in equilibrium with Fe^{2+} to pH 9.5 or with monomeric species such as $Fe(OH)^+$, $Fe(OH)_2$ and $Fe(OH)_3^-$ at high pH values. In the presence of O_2 the dissolved Fe^{2+} is oxidized to insoluble $Fe(OH)_3$ coagulating at pH > 1.0. The insoluble flakes can be in equilibrium with soluble monomeric species such as Fe^{3+}, $Fe(OH)^{2+}$, $Fe(OH)_2^+$, $Fe(OH)_3$ and $Fe(OH)_4^-$ as a function of pH. These species act as coagulants or destabilizing agents that neutralize charges and separate colloids and ionic products from the wastewater by sedimentation or electro-flotation, henceforth producing sludge (Figure 2)[22].

The volume of sludge generated in the EC is reduced compared to conventional chemical coagulation or biological processes. However, hence the importance of pollutants removal, the sludge must be treated and discarded appropriately.

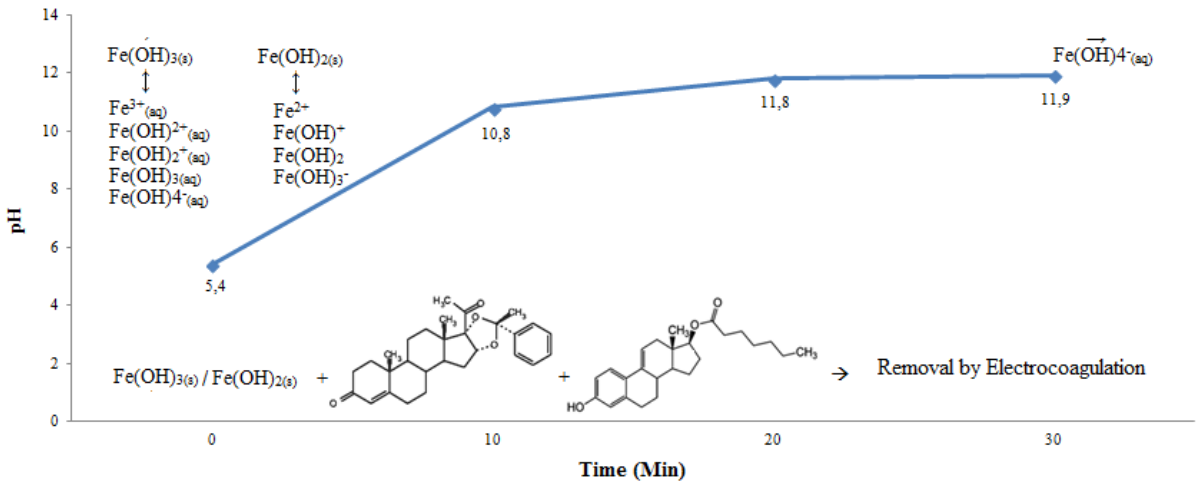

Figure 2. The behavior of pH and possible species formed during the EC of Test 1.

The pH effect of the effluent on the performance of the electrocoagulation process was evaluated throughout the experiments. The initial pH of 5.4 reached 10.8 after 10 minutes with the best removal efficiency of BOD (39.5%) and BOD (36.9%) in this range.

The initial pH of 5.4 may have facilitated the conversion of ferrous ions into ferric ions already in the early stages of electrolysis since this conversion occurs at pH > 4. Ferric ions (Fe^{3+}) undergo hydrolysis reactions and generate insoluble ferric hydroxides (microflocs) which are suspended by removing the contaminants by coagulation. When the pH reaches higher values (pH > 11) the concentration of ferric complexes like $Fe(OH)_4^-$ increases. This complex can remove contaminants through charge neutralization and adsorption, i.e., these precipitates can remove only contaminants from the water, which are positively charged[31]. This fact explains the increase in the efficiency of BOD and COD removal with pH > 11.8.

From a physicochemical point of view, these results suggest that the pilot prototype was promising. This fact was supported by HPLC-MS analyzes of algestone acetophenide and estradiol enanthate, where the best removal rate was 77.0% and 56.7% respectively in the Test 1 (Table 4 and Figure 3).

Eclética Química Journal, vol. 44, n. 1, 2019, 40-52
ISSN: 1678-4618
DOI: 10.26850/1678-4618eqj.v44.1.2019.p40-52

Table 4. Data regarding the removal of Algestone Acetophenide and Estradiol Enanthate taken from HPLC-MS.

Test	Removal Efficiency (%)	
	Algestone Acetophenide	Estradiol Enanthate
T1	**77.0**	**56.7**
T2	76.1	53.2
T3	76.7	55.2
AV	76.6	55.0
SD	0.46	1.76

T1 = Test nº 1; **T2** = Test nº 2; **T3** = Test nº 3; **AV** = Average; **SD** = Standard Deviation.

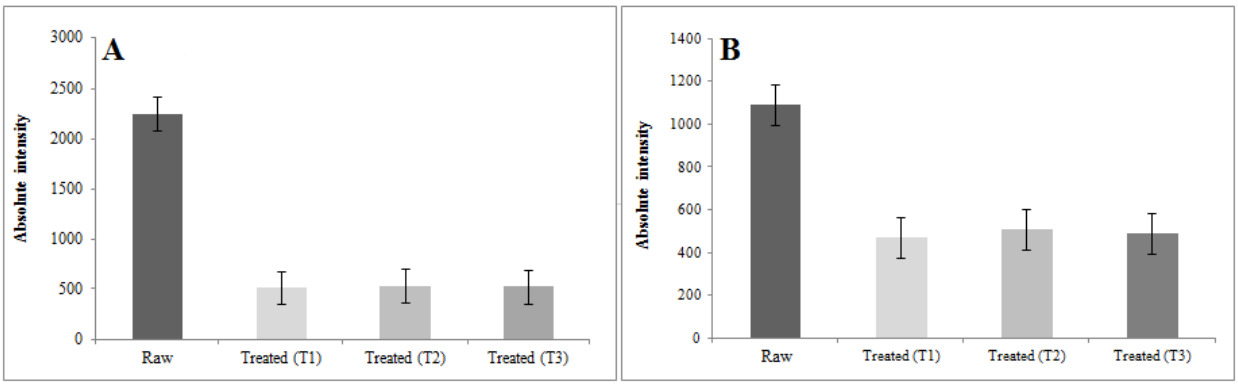

Figure 3. Removal rate of Algestone Acetophenide – 471.2441 m/z **(A)** and Estradiol Enanthate – 433.2645 m/z **(B)**

These results can be corroborating the quantification method by MS. The initial and final concentrations of AAc and EEn were calculated, 4.58 ppm ($y = 0.0758x + 0.3487$; $r^2 > 0.93$) in wastewater and 0.98 ppm ($y = 0.064x + 0.0063$; $r^2 > 0.97$).

The results found in the literature for treatment by electrocoagulation of estrogens are shown in Table 5.

Table 5. EC studies for hormones removal (best conditions).

Hormone	Removal efficiency (%)	Electrodes	Time (min)	Voltage (V)	Reference
Algestone Acetophenide	77.0	Steel	30	26.8	This study
Estradiol Enanthate	56.7				
Estrone	61.0	Aluminium	20	98.0	32
17β-Estradiol	63.0				
17α-Ethinylestradiol	64.0				
Estriol	56.0				
17α-Ethinylestradiol	22.7	Aluminium	40	5.0	33

Understanding the physicochemical properties of steroidal compounds is crucial to predicting their fate in the aquatic or terrestrial environment. The distribution of organic pollutants between water and natural solids is often considered as a process of partitioning between the aqueous and organic phases. The water partition coefficient (K_{ow}) is the ratio between the concentration of a compound in n-octanol and the water under equilibrium conditions at a given temperature. Compounds with high molecular weight and log $K_{ow} > 5$, such as AAc and EEn (Table 1), are easily adsorbed to sediments and can be removed mainly by coagulation[34].

Eclética Química Journal, vol. 44, n. 1, 2019, 40-52
ISSN: 1678-4618
DOI: 10.26850/1678-4618eqj.v44.1.2019.p40-52

Every treatment system can generate toxic byproducts and monitoring both the primary compound and its degradation products is a complex and often unfeasible task. The use of toxicological assays can be considered a simple and efficient way to monitor these contaminants[35, 36]. In this sense, toxicity tests were performed in the sample that presented the best compounds removal result (T1).

3.2 Phytotoxicity

Short-term toxicological tests are useful tools for predicting ecotoxicological risks, estimating acute toxicity, and establishing maximum acceptable concentrations of chemicals and by-products released into the environment[37, 38]. In the ecotoxicological assessment, phytotoxicity tests play an important role because plants are the basis of terrestrial and aquatic ecosystems, also acting as primary producers in the food chain[39, 40]. Seed germination and root elongation test being the simplest one, however is sensitive and representative of the action of the toxicant at the first interface of the developing plant (seed) and its environment[40-42]. However, there is a lack of data on the effects of effluents generated by the pharmaceutical industry on seed germination and root elongation.

The effects of raw and treated effluents on seed germination and root length are presented in Figure 4. Both effluents induced significant effects on seed germination (Fig. 4A) and root elongation of *L. sativa* (Fig. 4B). Raw effluent inhibited the development of all species tested in a concentration-dependent manner (Fig. 4B and 4D). Only raw effluent at 100% (v/v) significantly reduced the seed germination rate of *C. sativus* and considering treated effluent had no significant effect on *C. sativus* germination (Fig. 4C). Treated effluent was less toxic for root length when compared to raw effluent, with effect significantly only at 100% (v/v) (Fig. 4D).

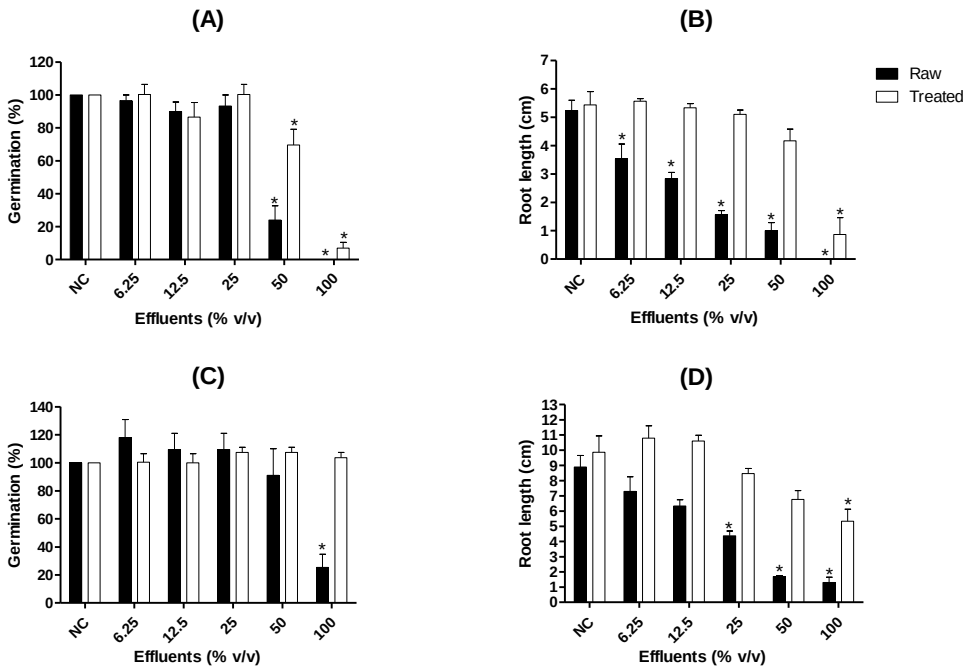

Figure 4. Seed germination and root length of *Lactuca sativa* (A and B) and *Cucumis sativus* (C and D) exposed to different concentrations of raw and treated effluents. Error bars represent ± standard deviation of 3 replicates. Asterisk (*) represents statistical difference ($p < 0.05$) from the respective negative control (NC).

The potential toxicity of raw and treated effluents was expressed as the EC_{50} value (Table 6). For both species tested, raw effluent was more toxic than treated effluent with lower EC_{50} values, mainly in relation to root length parameter (13.15% and 22.80% for *L. sativa* and *C. sativus*, respectively; Table 6).

Eclética Química Journal, vol. 44, n. 1, 2019, 40-52
ISSN: 1678-4618
DOI: 10.26850/1678-4618eqj.v44.1.2019.p40-52

Table 6. Effects of raw and treated effluents on germination and on root length. Median effective concentration (EC_{50}) values with their respective confidence intervals are presented in % v/v at *Lactuca sativa* and *Cucumis sativus* seed after 120 h of exposure.

	EC_{50} % v/v (CI)			
Effluents	*Lactuca sativa*		*Cucumis sativus*	
	Seed germination	Root length	Seed germination	Root length
Raw	40.36 (35.08 – 46.44)	13.15 (9.91 – 17.46)	80.62(59.10 – 110.00)	22.80 (17.43 – 29.81)
Treated	59.16 (49.21 – 71.09)	67.32 (52.78 – 85.88)	>100	>100

D'Abrosca[43] assessed the phytotoxicity of some pharmaceuticals including ethinyl estradiol on several species. The authors observed that *L. sativa* was the most sensitive species for both tested endpoints, inhibiting more than 50% of seed germination and 25% of root elongation in the highest tested concentration (10^{-3} mol L^{-1}). Our results also showed that *L. sativa* was more sensitive than *C. sativus.* Additionally, we observed a reduction in the toxicity of the raw effluent for both specie tested after the treatment (Fig. 4 and Table 6).

3.3 Brine shrimp toxicity assay

Artemia spp. (brine shrimp) presents several advantages, such as a short life cycle and adaptability to wide ranges of salinity, which have contributed to increasing the use of brine shrimps in ecotoxicological studies[40, 44, 45]. Moreover, ecotoxicity tests with different organisms may be used to determine the effect level of effluents and thus their environmental impacts[46].

Table 7 shows the percent of mortality (immobility) of *A. salina* nauplii after 24 h of exposure to raw and treated effluents. The raw effluent was highly toxic to *A. salina* nauplii with LC_{50}-24 h of 0.58% whereas the treated samples caused no mortality after 24h of exposure (Table 7). Raw effluent induced significant toxicity to *A. salina* nauplii in concentration- and time-dependent manners with LC_{50}-48 h of 0.31% (Table 8). However, the treated effluent also caused significant mortality to *A. salina* in highest tested concentrations (50% and 100%) after 48 h of exposure, which suggests the generation of toxic by-products.

Table 7. Immobilization rate of *Artemia salina* nauplii after 24 h of exposure to raw and treated effluents and their median lethal concentrations (LC_{50}) causing 50% of immobilization. NC: negative control; SD: standard deviation of four replicates.

Concentration (% v/v)	**Number of immobilized organisms at 24 h**					**Immobilization**		**LC_{50} (%v/v)**
Raw effluent	1	2	3	4	SD	Total	%	0.58
NC	0	0	0	0	0.0	0/20	0	
0.01	0	0	1	0	0.5	1/20	5	
0.10	0	0	1	0	0.5	1/20	5	
1.00	5	3	4	2	1.3	14/20	70*	
5.00	4	5	5	4	0.6	18/20	90*	
10.0	5	5	5	5	0.0	20/20	100*	
Treated effluent	1	2	3	4	SD	Total	%	>100
NC	0	0	0	0	0.0	0/20	0	
6.25	0	0	0	0	0.0	0/20	0	
12.5	0	0	0	0	0.0	0/20	0	
25.0	0	0	0	0	0.0	0/20	0	
50.0	0	0	0	0	0.0	0/20	0	
100.0	0	0	0	0	0.0	0/20	0	

*Statistically different ($p<0.05$) from the respective negative control (NC).

Eclética Química Journal, vol. 44, n. 1, 2019, 40-52
ISSN: 1678-4618
DOI: 10.26850/1678-4618eqj.v44.1.2019.p40-52

Table 8. Immobilization rate of *Artemia salina* nauplii after 48 h of exposure to raw and treated effluents and their median lethal concentrations (LC_{50}) causing 50% of immobilization. NC: negative control; SD: standard deviation of four replicates.

Concentration (% v/v)	Number of immobilized organisms at 48 h					Immobilization		LC_{50} (%v/v)
Raw effluent	1	2	3	4	SD	Total	%	0.31
NC	0	0	0	0	0.0	0/20	0	
0.01	0	0	2	0	1.0	2/20	10	
0.10	0	2	1	0	0.9	3/20	15	
1.00	5	4	5	3	0.9	17/20	85*	
5.00	5	5	5	5	0.0	20/20	100*	
10.0	5	5	5	5	0.0	20/20	100*	
Treated effluent	1	2	3	4	SD	Total	%	53.88
NC	0	0	0	0	0.0	0/20	0	
6.25	0	0	0	0	0.0	0/20	0	
12.5	0	0	1	0	0.5	1/20	5	
25.0	0	1	1	0	0.6	2/20	10	
50.0	3	1	2	0	1.3	6/20	30*	
100.0	5	5	4	5	0.5	19/20	95*	

*Statistically different ($p<0.05$) from the respective negative control (NC).

Ecotoxicity evaluation with different organisms is useful to determine the toxic effect potential of pharmaceutical effluents and thus their environmental impacts[46]. Additionally, ecotoxicity assays for effluents are mandatory in many countries including Brazil[47, 48]. The ecotoxicity test proved that toxicity of the synthetic hormones present in the raw effluent was reduced by electrocoagulation technique herein employed.

4. Conclusions

The results obtained allowed to conclude that the electrochemical treatment of the hormonal effluent generated by pharmaceutical industries was efficient in the removal of the compounds studied, in the reduction of organic load, color and turbidity, as well as in the reduction of toxicity to lettuce and cucumber seeds and *Artemia salina*. Besides that, despite the differences between the used species, *A. salina* was more sensitive than seeds to detect toxicity. Therefore, the physicochemical analyses carried out in conjunction with bioassays were able to provide valuable information on the quality of synthetic hormones containing effluents, in order to reduce their impact on the environment.

Electrocoagulation may be a promising method in the treatment process of industrial pharmaceutical effluents since it provides electrolytic, physicochemical or electrochemical precipitation of the sludge. Even though it does not entirely remove recalcitrant compounds, electrochemical processes can increase the degree of biodegradability, facilitating degradation by biological processes, reducing their toxicity.

5. Acknowledgments

The authors wish to thank Conselho Nacional de Desenvolvimento Científico e Tecnológico (CNPq) [grant number 471109/2013-4] and Financiadora de Estudos e Pesquisas (FINEP) [grant number 01.14.0140.00] for the financial support to this work. Coordenadoria de Aperfeiçoamento de Pessoal (CAPES) for Luane Ferreira Garcia, Emily Kussmaul Gonçalves Moreno and Laís de Brito Rodrigues scholarships. Fundação de Amparo à Pesquisa do Estado de Goiás (FAPEG) and Programa Mobilidade Docente AUGM to assist the participation of events abroad.

6. References

[1] Pereira, L. C., de Souza, A. O., Bernardes, M. F. F., A perspective on the potential risks of emerging contaminants to human and environmental health, Environ. Sci. Pollut. Re. Int. 22 (2015) 13800-13823. https://doi.org/10.1007/s11356-015-4896-6.

[2] Archer, E., Petrie, B., Kasprzyk-Hordern, B., Wolfaardt, G. M., The fate of pharmaceuticals and personal care products (PPCPs), endocrine disrupting contaminants (EDCs), metabolites and illicit drugs in a WWTW and environmental waters, Chemosphere 174 (2017) 437-446. https://doi.org/10.1016/j.chemosphere.2017.01.101.

[3] Hilton, M. J., Thomas, K. V., Determination of selected human pharmaceutical compounds in effluent and surface water samples by high-performance liquid chromatography–electrospray tandem mass spectrometry. J. Chromatography A. 1015 (2003)129–141. https://doi.org/10.1016/S0021-9673(03)01213-5.

[4] Hari, A. C., Paruchuri, R. A., Sabatini, D. A., Kibbey, T. C. G., Effects of pH and Cationic and Nonionic Surfactants on the Adsorption of Pharmaceuticals to a Natural Aquifer Material, Environ. Sci. Technol. 39 (2005) 2592-2598. https://doi.org/10.1021/es048992m.

[5] Santos, L. H. M. L. M., Araújo, A. N., Fachini, A., Ecotoxicological aspects related to the presence of pharmaceuticals in the aquatic environment., J. Hazard. Mater 175 (2010) 45-95. https://doi.org/10.1016/j.jhazmat.2009.10.100.

[6] Xu, J., Xu, Y., Wang, H. Occurrence of antibiotics and antibiotic resistance genes in a sewage treatment plant and its effluent-receiving river, Chemosphere 119 (2015) 1379–1385. https://doi.org/10.1016/j.chemosphere.2014.02.040.

[7] Liu, J-L., Wong, M-H., Pharmaceuticals and personal care products (PPCPs): A review on environmental contamination in China, Environment International, 59 (2013) 208-222. https://doi.org/10.1016/j.envint.2013.06.012.

[8] Yang, Y-Y., Liu, W-R., Liu, Y-S., Suitability of pharmaceuticals and personal care products (PPCPs) and artificial sweeteners (ASs) as wastewater indicators in the Pearl River Delta, South China, Sci. Total Environ. 590-591 (2017) 611-619. https://doi.org/10.1016/j.scitotenv.2017.03.001.

[9] Joseph, E., The dictionary of drugs: chemical data, structures and bibliographies, Springer, 2014.

[10] Liu, Z.-H., Kanjo, Y., Mizutani, S., Urinary excretion rates of natural estrogens and androgens from humans, and their occurrence and fate in the environment: a review, Sci. Total Environ. 407 (2009) 4975–4985. https://doi.org/10.1016/j.scitotenv.2009.06.001.

[11] Kanakaraju, D., Glass, B. D., Oelgemöller, M., Advanced oxidation process-mediated removal of pharmaceuticals from water: a review, J. Environ. Manage. 219 (2018) 189-207. https://doi.org/10.1016/j.jenvman.2018.04.103.

[12] Aquino, S. F., Brandt, E. M. F., Chernicharo, C. A. L., Removal of drugs and endocrine disrupters in sewage treatment plants: literature review, Eng. Sanit. Ambient. 18 (2013) 187-204. https://doi.org/10.1590/S1413-41522013000300002.

[13] Mirzaei, R., Yunesian, M., Nasseri, S., Occurrence and fate of most prescribed antibiotics in different water environments of Tehran, Iran, Sci. Total Environ. 619-620 (2018) 446-459. https://doi.org/10.1016/j.scitotenv.2017.07.272.

[14] Xiang, J., Wu, M., Lei, J., Fu, C., Gu, J., Xu, G., The fate and risk assessment of psychiatric pharmaceuticals from psychiatric hospital effluent, Ecotox. Environ. Safe. 150 (2019) 289-296. https://doi.org/10.1016/j.ecoenv.2017.12.049.

[15] Xuan, R., Blassengale, A. A., Wang, Q., Degradation of estrogenic hormones in silt loam soil, J. Agric. Food Chem. 56 (2008) 9152–9158. https://doi.org/10.1021/jf8016942.

[16] Tijani, J. O., Fatoba, O. O., Madzivire, G., Petrik, L. F., A review of combined advanced oxidation technologies for the removal of organic pollutants from water, Water Air Soil Pollut. 225 (2014) 2102. https://doi.org/10.1007/s11270-014-2012-y.

[17] Ribeiro, A. R., Nunes, O. C., Pereira, M. F. R., Silva, A. M. T., An overview on the advanced oxidation processes applied for the treatment of water pollutants defined in the recently launched Directive 2013/39/EU, Environ. Int. 75 (2015) 33-51. https://doi.org/10.1016/j.envint.2014.10.027.

[18] Arvanitoyannis, I. S., Kassaveti, A., Stefanatos, S., Olive oil waste treatment: a

comparative and critical presentation of methods, advantages & disadvantages, Crit. Rev. Food Sci. Nutr. 47 (3) (2007) 187-229. https://doi.org/10.1080/10408390600695300.

[19] Miklos, D. B., Remy, C., Jekel, M., Linden, K. G., Drewes, J. E., Hübner, U., Evaluation of advanced oxidation processes for water and wastewater treatment - A critical review, Water Research 139 (2018) 118-131. https://doi.org/10.1016/j.watres.2018.03.042.

[20] Moreira, F. C., Boaventura, R. A. R., Brillas, E., Vilar, V. J. P., Electrochemical advanced oxidation processes: A review on their application to synthetic and real wastewaters, Applied Catalysis B: Environmental 202 (2017) 217-261. https://doi.org/10.1016/j.apcatb.2016.08.037.

[21] Klavarioti, M., Mantzavinos, D., Kassinos, D., Removal of residual pharmaceuticals from aqueous systems by advanced oxidation processes, Environment International 35 (2009) 402-417. https://doi.org/10.1016/j.envint.2008.07.009.

[22] Sirés, I., Brillas, E., Remediation of water pollution caused by pharmaceutical residues based on electrochemical separation and degradation technologies: a review, Environ. Int 40 (2012) 212-229. https://doi.org/10.1016/j.envint.2011.07.012.

[23] Cañizares, P., Jiménez, C., Martínez, F., Saez, C., Rodrigo, M. A., Study of the electrocoagulation process using aluminum and iron electrodes, Ind. Eng. Chem. Res. 46 (2007) 6189-6195. https://doi.org/10.1021/ie070059f.

[24] APHA, AWWA, WEF, Standard Methods for examination of water and wastewater, Washington DC, 22nd ed., 2012.

[25] ChemSpider Search and Share Chemistry, Algestone acetophenide, 2018. Database: http://www.chemspider.com/Chemical-Structure.4447595.html. Accessed 20 May 2018.

[26] ChemSpider Search and share chemistry, Estradiol enanthate, 2018. Database: http://www.chemspider.com/Chemical-Structure.19815.html. Accessed 20 May 2018.

[27] USEPA, United States Environmental Protection Agency. Ecological effects test guidelines. OPPTS 850.4200, Seed Germination/Root Elongation Toxicity Test. EPA 712 C (1996) 96-154.

[28] Meyer, B. N., Ferrigni, N. R., Putnam, J. E., Jacobsen, L. B., Nichols, D. E., McLaughlin, J. L., Brine Shrimp: a convenient general bioassay for active plant constituents, Journal of Medicinal Plant Research, 45 (1982) 31-34. https://doi.org/10.1055/s-2007-971236.

[29] Organization For Economic Cooperation And Development [OECD], Guideline for testing of chemicals, Daphnia sp. Acute Immobilization Test, France, Guideline No. 202, 2004.

[30] Crespilho, F. N., Santana, C. G., Rezende, M. O. O., Tratamento de efluente da indústria de processamento de coco utilizando eletroflotação, Quim. Nova, 27 (2004) 387-392. https://doi.org/10.1590/S0100-40422004000300005.

[31] Benefield, L. D., Judkins, J. F., Weand, B. L., Process Chemistry for Water and Wastewater Treatment, Prentice-Hall, Englewood Cliffs, N.J., 1982.

[32] Cook, M. M., Symonds, E. M., Gerber, B., Hoare, A., Van-Vleet, E. S., Breitbart, M., Removal of Six Estrogenic Endocrine-Disrupting Compounds (EDCs) from Municipal Wastewater Using Aluminum Electrocoagulation, Water 8 (2016) 128. https://doi.org/10.3390/w8040128.

[33] Garcia, L. F., Morais, R. L., Santos, W. T. P., Pacheco, C., Santiago, M. F., Gil, E. S., Low Cost Commercial Anodes on the Electrochemical Remediation of the Estrogen 17α-ethinylestradiol. J. Chem. Pharm. Res. 8 (2016) 958-96l.

[34] Pal, A., Gin, KY-H., Lin, AY-C., Reinhard, M., Impacts of emerging organic contaminants on freshwater resources: review of recent occurrences, sources, fate and effects, Sci. Total Environ. 408 (2010) 6062-6069. https://doi.org/10.1016/j.scitotenv.2010.09.026.

[35] Kerr, J. L., Guo, Z., Smith, D. W., Goss, G. G., Belosevic, M. (2008) Use of goldfish to monitor wastewater and reuse water for xenobiotics, J. Environ. Eng. Sci. 7 (4) (2008) 369-383. https://doi.org/10.1139/S08-011.

[36] Leusch, F. D. L., Khan, S. J., Gagnon, M. M., Quayle, P., Trinh, T., Coleman, H., Rawson, C., Chapman, H. F., Blair, P., Nice, H., Reitsema, T., Assessment of wastewater and recycled water quality: a comparison of lines of evidence from in vitro, in vivo and chemical analyses, Water Res. 50 (2014) 420-431. https://doi.org/10.1016/j.watres.2013.10.056.

[37] Klauck, C. R., Giacobbo, A., Oliveira, E. D. L., Silva, L. B., Rodrigues, M. A. S., Evaluation of acute toxicity, cytotoxicity and genotoxicity of landfill leachate treated by biological lagoon and advanced oxidation processes, J. Environ. Chemic. Eng. 5 (2017) 6188-6193. https://doi.org/10.1016/j.jece.2017.11.058.

[38] Zhang, W., Liu, W., Zhang, J., Zhao, H., Zhang, Y., Quan, X., Jin, Y., Characterization of acute toxicity, genotoxicity and oxidative stress posed by textile effluent on zebrafish, J. Environ. Sci. 24 (2012) 2019-2027.

[39] Boutin, C., Strandberg, B., Carpenter, D., Mathiassen, S. K., Thomas, P. J., Herbicide impact on non-target plant reproduction: what are the toxicological and ecological implications? Environ. Pollut. 185 (2014) 295-306. https://doi.org/10.1016/j.envpol.2013.10.009.

[40] Oliveira, G. A. R., Leme, D. M., de Lapuente, J., Brito, L. B., Porredón, C., Rodrigues, L. B., Brull, N., Serret, J. T., Borràs, M., Disner, G. R., Cestari, M. M., Oliveira, D. P., A test battery for assessing the ecotoxic effects of textile dyes, Chem Biol Interact., 291 (2018) 171-179. https://doi.org/10.1016/j.cbi.2018.06.026.

[41] Wang, X., Sun, C., Gao, S., Wang, L., Shuokui, H., Validation of germination rate and root elongation as indicator to assess phytotoxicity with *Cucumis sativus*. Chemosphere 44 (2001) 1711-1721. https://doi.org/10.1016/s0045-6535(00)00520-8.

[42] Lyu, J., Park, J., Pandey, L. K., Choi, S., Lee, H., De Saeger, J., Depuydt, S., Han, T., Testing the toxicity of metals, phenol, effluents, and receiving waters by root elongation in Lactuca sativa L., Ecotoxicol. Environ. Saf. 149 (2018) 225-232. https://doi.org/10.1016/j.ecoenv.2017.11.006

[43] D'Abrosca, B., Fiorentino, A., Izzo, A., Cefarelli, G., Pascarella, M. T., Uzzo, P., Monaco, P., Phytotoxicity evaluation of five pharmaceutical pollutants detected in surface water on germination and growth of cultivated and spontaneous plants, J. Environ. Sci. Health A, 43 (2008) 285-294. https://doi.org/10.1080/10934520701792803.

[44] Nunes, B. S., Carvalho, F. D., Guilhermino, L. M., Stappen, G. B., Use of the genus Artemia in ecotoxicity testing, Environ. Pollut. 144 (2006) 453-462. https://doi.org/10.1016/j.envpol.2005.12.037.

[45] Libralato, G., Prato, E., Migliore, L., Cicero, A. M., Manfra, L., A review of toxicity testing protocols and endpoints with Artemia spp, Ecol. Indicat. 69 (2016) 35-49. https://doi.org/10.1016/j.ecolind.2016.04.017.

[46] Maselli, B. de S., Luna, L. A. V., Palmeira, J. de O., Tavares, K. P., Barbosa, S., Beijo, L. A., Umbuzeiro, G. A., Kummrow, F., Ecotoxicity of raw and treated effluents generated by a veterinary pharmaceutical company: a comparison of the sensitivities of different standardized tests, Ecotoxicology 24 (2015) 795-804. https://doi.org/10.1007/s10646-015-1425-9.

[47] Pessala, P., Schultz, E., Nakari, T., Joutti, A., Herve. S., Evaluation of wastewater effluents by small-scale biotests and a fractionation procedure, Ecotoxicol. Environ. Saf. 59 (2004) 263–272. https://doi.org/10.1016/j.ecoenv.2003.10.002.

[48] CONAMA, Conselho Nacional do Meio ambiente, Resolucão CONAMA nº 430, de 13 de maio de 2011.

Eclética Química Journal, vol. 44, n. 1, 2019, 40-52
ISSN: 1678-4618
DOI: 10.26850/1678-4618eqj.v44.1.2019.p40-52

Eclética Química Journal

Original article
iq.unesp.br/ecletica

| Vol. 44 | n. 1 | 2019 |

Voltammetric method for the quantification of cadmium using non-commercial electrodes and minimal instrumentation

Javier Ernesto Vilasó Cadre[1+], Alejandro Céspedes Martínez[2], María de los Ángeles Arada Pérez[1], José Alejandro Baeza Reyes[3]

1 Universidad de Oriente, Faculty of Natural and Exact Sciences, Sede Antonio Maceo, Santiago de Cuba, Cuba
2 Empresa Nacional de Análisis y Servicios Técnicos, 18401 Las Palmas Av, Havana, Cuba
3 Universidad Nacional Autónoma de México, 33 República de Brasil St., Ciudad de México, México

+ Corresponding author: Javier Ernesto Vilasó Cadre, e-mail address: javiere@uo.edu.cu

ARTICLE INFO

Article history:
Received: September 5, 2018
Accepted: December 13, 2018
Published: January 28, 2019

Keywords:
1. voltammetry
2. cadmium
3. non-commercial graphite electrodes
4. minimal instrumentation

ABSTRACT: A voltammetric method for the cadmium quantification was developed using minimal instrumentation. A manual homemade potentiostat for linear voltammetry was used. An Ag reference electrode and auxiliary and working electrodes of writing graphite were employed for the electroanalysis. The electrolytic conditions for the quantification were stablished. Linearity, detection and quantification limits, precision and accuracy were evaluated. The conditions for the quantification were KCl 1 mol L^{-1} as supporting electrolyte and pH 5. The range of quantification was from 10^{-3} to $1.5\cdot10^{-2}$ mol L^{-1}. The linear correlation (r), determination (R^2) and adjusted ($R^2_{adj.}$) coefficients were 0.9986, 0.9972 and 0.9970. The detection and quantification limits were $3\cdot10^{-4}$ mol L^{-1} and 10^{-3} mol L^{-1}. Results showed an acceptable repeatability, with coefficients of variation from 1.5 to 5.8% depending on the concentration. Uncertainty associated with the cadmium concentration was in the range of $1.2\cdot10^{-4}$ to $7\cdot10^{-5}$ mol L^{-1}, diminishing with the increasing of the concentration. A good accuracy was observed, with recoveries between 86.84 and 109.64%.

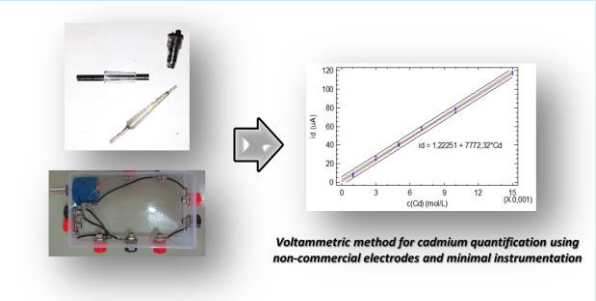

1. Introduction

Voltammetry is an electroanalytical method based on the measurement of the current intensity during an electrolysis provoked by a controlled variable of potential over time. Voltammogram is a current-potential curve that shows the current increase due to analyte diffusion to and reaction on the electrode surface. This is caused by the concentration gradients between the bulk solution and the electrode. Voltammetric analysis is simple and not destructive; sample treatments are unnecessary in many cases. Furthermore, voltammetry techniques allow speciation and simultaneous determination[1-3]. This method has been widely used in metal quantification in different samples[4-8].

Cadmium is one of the most monitored metals in the environment and wastewaters. Cadmium control is important due to its wide industrial applications, but its presence in ecosystems generates significant effects. This metal is used in batteries and as additive for plastics and glasses; it is also employed for galvanization and coating of surfaces due to its resistance to corrosion. Moreover, cadmium works as mordant in tincture and impression of textile materials, among other applications. However, cadmium compounds are toxic even in low concentrations. They may cause renal problems, infertility, immunologic and nervous affliction, cancer, and others[9]. Cadmium

Eclética Química Journal, vol. 44, n. 1, 2019, 53-61
ISSN: 1678-4618
DOI: 10.26850/1678-4618eqj.v44.1.2019.p53-61

is easily bioaccumulated by fish, crustaceans and plants[8, 10, 11]. Electrochemical reduction of cadmium may be used for its voltammetric quantification. The reaction of the process is provided in Equation 1.

$$Cd^{2+}_{(ac)} + 2e^- = Cd_{(s)} \quad (1)$$

Although voltammetry is cheaper than other methods of instrumental analysis, commercial instrumentation for its development is inaccessible for many laboratories of low economic resources. Some researchers have shown that construction of instrumentation for electrochemical methods is possible, from selective electrodes[12, 13] to potentiostats[14-16]. A non-commercial instrumentation may be considered as minimal when it consists of the basic components to generate an electrochemical process. Voltammetric determination of cadmium has been reported[7], however, the quantification using non-commercial instrumentation has not been widely reported. Bearing in mind this context, the objective of this work is to evaluate the analytic parameters for the voltammetric quantification of cadmium by using non-commercial electrodes and a minimal instrumentation potentiostat reported by the authors[17]. For future application of the method, the concentration ranges of the determinations have been selected in correspondence with the common amount of cadmium in the solution from the digestion of Ni-Cd rechargeable batteries[18].

2. Materials and methods

2.1. Electrochemical instrumentation and chemical reagents

A homemade minimal instrumentation manual micropotentiostat for linear sweep voltammetry was employed to develop the voltammetric method. The scheme of the circuit is shown in the Figure 1[17]. This consists of two parallel circuits. One allows the measurement the current between the working electrode and the auxiliary electrode. The other allows to measure the virtual potential between the working electrode and the reference. The potential sweep is made using a rheostat, which causes a potential fall through the electrolytic cell.

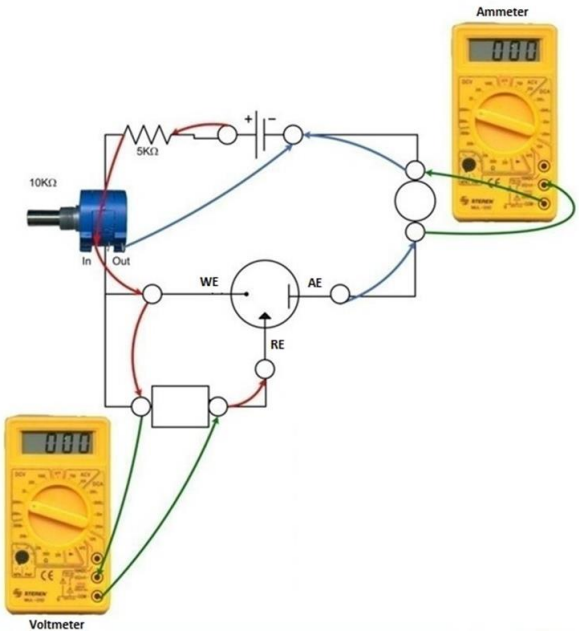

Figure 1. Circuit scheme for the voltammetric method for cadmium quantification using minimal instrumentation[17].

Figure 2 shows the electrodes design. A microdisc of graphite (d=2.03 mm) for writing was employed as a non-commercial working electrode. A bar of the same material was used as auxiliary electrode. The reference was an Ag wire. Linear potential sweeps were done from -10 to -1500 mV. All the chemical reagents used were for analytic use (Uni-Chem, Serbia).

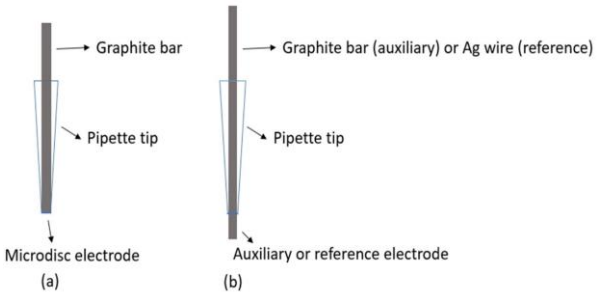

Figure 2. Electrodes design for the voltammetric method for cadmium quantification using minimal instrumentation: (a) Working electrode, (b) Auxiliary and reference electrodes.

2.2. Study of conditions for the voltammetric method for cadmium quantification

Supporting electrolyte concentration and pH were studied for the voltammetric determination of cadmium. The effect of the KCl concentration over the limiting current was studied at 0.1, 1.0 and 2.0

Eclética Química Journal, vol. 44, n. 1, 2019, 53-61
ISSN: 1678-4618
DOI: 10.26850/1678-4618eqj.v44.1.2019.p53-61

mol L^{-1} [19]. The effect of the pH was studied at the values of 3, 4 and 5, in the KCl concentration fixed previously[20]. pH was fixed using an acetic acid/acetate buffer, which was prepared according to a reported methodology[21]. Three voltammograms were registered for each KCl concertation and pH, then, the average limiting current was calculated. Furthermore, simple Analysis of Variance (ANOVA) was used to compare the currents between the different values of KCl concentration and pH respectively. A cadmium solution 0.01 mol L^{-1} was use for the study.

2.3. Linearity

A calibration curve was built registering the voltammograms to reduce Cd^{2+} at 0.001, 0.005, 0.007, 0.01 and 0.015 mol L^{-1}. Diffusion current (difference between limiting current and residual current) was represented as a function of the concentration, and a linear regression was plotted to obtain the coefficients and the equation of the curve. The curve generated was the result of the mean of three currents for each concentration of Cd^{2+} [22].

2.4. Detection and quantification limits

In order to determine the detection and quantification limits, 20 voltammograms from the electrolysis medium (without analyte) were generated. The residual current was determined from the voltammograms, and the concentration associated to each value was calculated using the calibration plot. The detection limit was calculated as three times the standard deviation and the quantification limit was calculated as ten times the standard deviation[23].

2.5. Precision

Precision was evaluated as the repeatability of the method. Ten voltammograms were registered at the Cd^{2+} concentrations: $3\cdot10^{-3}$, $5\cdot10^{-3}$ and $7\cdot10^{-3}$ mol L^{-1}. The variation coefficient was calculated as a dispersion criterion[23]. The uncertainty associated to the repeatability was estimated according to the reported metrologic characterization of the potentiostat[17], where the results showed that it is the most significant source of uncertainty.

2.6. Accuracy

Recovery essays were conducted to estimate the accuracy of the method. Solutions of Cd^{2+} of concentrations: $3\cdot10^{-3}$, $5\cdot10^{-3}$ and $7\cdot10^{-3}$ mol L^{-1} were prepared, voltammograms were registered and then, an amount of $CdCl_2$ corresponding to a concentration of $5\cdot10^{-4}$ mol L^{-1} was added. The voltammograms were registered once more. Experiments were conducted five times, and ANOVA was used to compare the recoveries at different concentrations. Recovery percentage was calculated according to Equation 2[23].

$$\%R = \frac{AA-BA}{A} \cdot 100 \qquad (2)$$

where:
%R: Recovery percentage
AA: Concentration of the solution after the addition
BA: Concentration of the solution before the addition
A: Concentration of the addition.

2.7. Data processing

Statgraphics Centurion XVI and Microsoft Office Excel were used to process the experimental data and the statistical tests.

3. Results and discussion

3.1. Conditions for the voltammetric method for cadmium quantification

Figure 3 shows the behavior of the limiting current from the Cd^{2+} reduction with the changes of KCl concentration. An increase of the current is observed from 0.1 to 1 mol L^{-1} of supporting electrolyte. From 1 mol L^{-1} on, the current maintains almost constant.

Eclética Química Journal, vol. 44, n. 1, 2019, 53-61
ISSN: 1678-4618
DOI: 10.26850/1678-4618eqj.v44.1.2019.p53-61

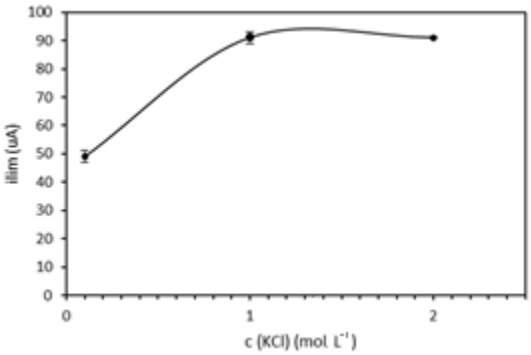

Figure 3. Limiting current for Cd^{2+} 0.01 mol L^{-1} reduction as a function of the KCl concentration in the electrolysis medium.

The Cochran test for the comparison of variances did not show differences statistically significant (p-value=0.8995 > α=0.05). As a result of comparing the limiting currents at each concentration of KCl, ANOVA showed differences statistically significant between them (p-value=0.0000 < α=0.05). Table 1 shows the identification of homogeneous currents using a multiple ranges contrast through a LSD test of Fisher for a 95% of confidence.

Table 1. LSD test of Fisher for the identification of homogeneous limiting currents to different KCl concentrations (95% of confidence).

c(KCl)	Cases	Mean	Homogeneous groups	
0.1 mol L^{-1}	3	49.3	X	
1 mol L^{-1}	3	91.0		X
2 mol L^{-1}	3	91.3		X

The supporting electrolyte allows the analyte to reach predominantly the electrode from the bulk solution by diffusion. This result is mainly because the ions of the electrolyte assume the mass transport by migration. The current will be independent of the supporting electrolyte concentration when the maximum migration mass transport is reached[1]. The currents corresponding to 1 and 2 mol L^{-1} do not show differences statistically significant. Therefore, any of the homogeneous values can be selected to develop the voltammetric electrolysis in order to reduce Cd^{2+}. KCl 1 mol L^{-1} was selected.

Figure 4 shows the limiting current as a function of the pH of the medium. It is possible to observe that the three current values are similar.

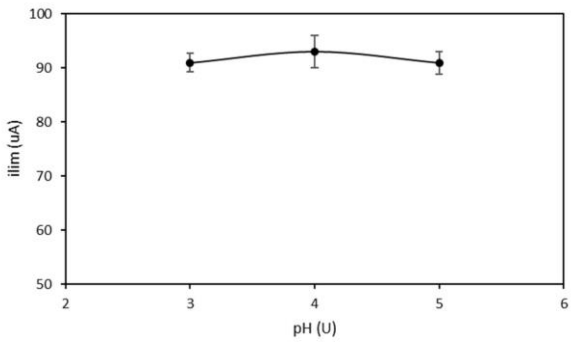

Figure 4. Limiting current for Cd^{2+} 0.01 mol L^{-1} reduction as a function of the pH of the medium.

After comparing the variances, the Cochran test did not show differences statistically significant (p-value=0.6047 > α=0.05). The comparison of the currents using ANOVA did not show differences statistically significant (p-value=0.5632 > α=0.05) either. This result demonstrates that it is possible to select any of the pH values to develop the voltammetric method. The stability of the limiting current matches the species distribution diagram for cadmium[24], where Cd^{2+} is stable until pH 8. However, several voltammetric determinations of cadmium are carried out at pH 5[8, 25]; that is the reason why this value was selected to develop the method.

3.2. Linearity

Figure 5 shows the voltammograms for the reduction of cadmium at different concentrations using the minimal instrumentation. The sigmoid form of the linear voltammograms is observed and the limiting current increases with the concentration.

Eclética Química Journal, vol. 44, n. 1, 2019, 53-61
ISSN: 1678-4618
DOI: 10.26850/1678-4618eqj.v44.1.2019.p53-61

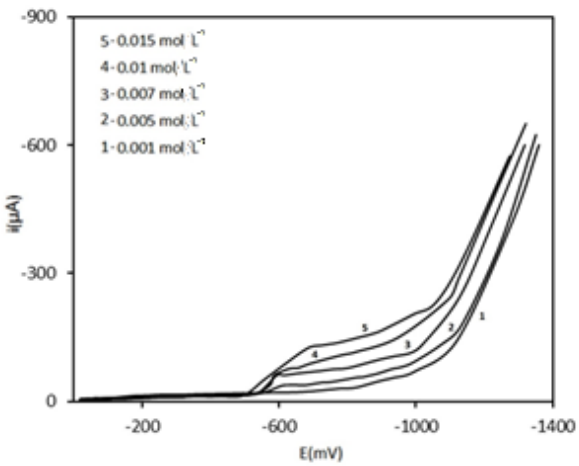

Figure 5. Voltammograms for the Cd^{2+} reduction using minimal instrumentation.

Figure 6 shows the calibration plot obtained from the voltammograms. The linear range of the voltammetric method is from 10^{-3} to $1.5 \cdot 10^{-2}$ mol L^{-1}. The linear correlation coefficient (r) of the curve is 0.9987, which demonstrates a strong linear correlation between the current and the concentration of cadmium. The determination coefficient (R^2) is 0.9975, demonstrating that the mathematic model explains the 99.75% of the variability between both variables. The adjusted coefficient ($R^2_{adj.}$) is 0.9973.

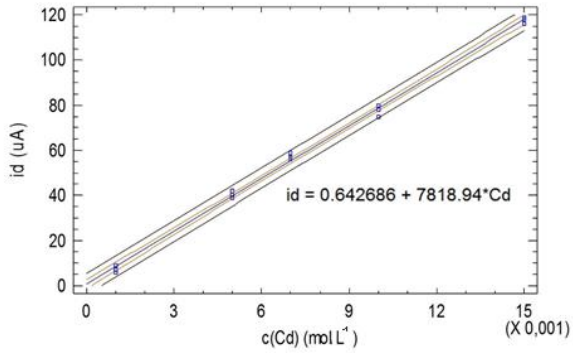

Figure 6. Calibration plot and equation for the voltammetric method for cadmium quantification using minimal instrumentation.

Table 2 shows the ANOVA for the calibration plot for the voltammetric method for cadmium quantification. The p-value is inferior to the significance level (α=0.05), which demonstrates a statistically significant relationship between the current and the concentration.

Table 2. ANOVA for the calibration plot for the voltammetric method for cadmium quantification using minimal instrumentation (95% of confidence).

Source	SS	DF	MS	F	p-value
Model	20394.9	1	20394.9	5098.9	0.0000
Residue	51.9	13	3.9		
Total (Corr.)	20446.9	14			

SS: Sum of squares, DF: Degrees of freedom, MS: Mean square

A representation of the residues as a function of the concentration allows corroborating the linearity of a calibration plot. Figure 7 does not show a defined tendency of the residues, demonstrating the linearity of the curve in the range of concentrations.

Table 3 shows the regression parameters of the calibration plot for the 95% of confidence. Errors and the p-values associated with the slope and the intercept are the most important.

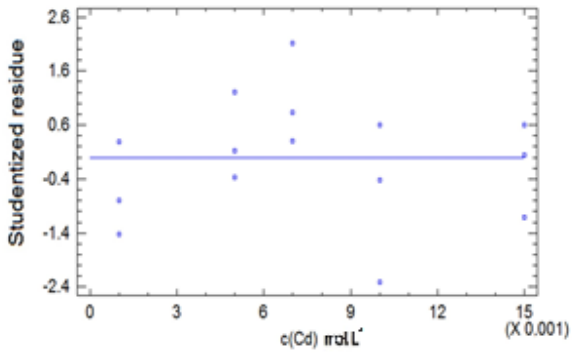

Figure 7. Studentized residues as a function of the Cd^{2+} concentration for the calibration plot for the voltammetric method for cadmium quantification using minimal instrumentation.

Eclética Química Journal, vol. 44, n. 1, 2019, 53-61
ISSN: 1678-4618
DOI: 10.26850/1678-4618eqj.v44.1.2019.p53-61

Table 3. Parameters of the calibration plot regression for the voltammetric method for cadmium quantification using minimal instrumentation (95% of confidence).

Parameter	Minimal Square Estimated	Standard Error	Statistical T	p-value
Intercept	0.6427	0.9794	0.6562	0.5231
Slope	7818.94	109.50	71.4071	0.0000

The p-value of the intercept is superior to the level of significance (α=0.05), indicating that the intercept is statistically equal to zero. It demonstrates the adequate correction of the limiting current by the subtraction of the residual current. The slope of the calibration plot indicates the sensibility of the method. The value reported is 7818.94 μA·mol L^{-1}, which demonstrates a high variation of the current with Cd^{2+} concentration changes.

3.3. Detection and quantification limits

Table 4 shows the detection and quantification limits of the voltammetric method for the quantification of cadmium using minimal instrumentation. The detection limit is in the order commonly reported for linear voltammetry (10^{-4} mol L^{-1})[1].

Table 4. Detection and quantification limits of the voltammetric method for cadmium quantification using minimal instrumentation.

Limit	Value
Detection	$3\cdot10^{-4}$ mol L^{-1}
Quantification	10^{-3} mol L^{-1}

3.4. Precision

Table 5 shows the results of the repeatability for three cadmium concentrations. Results of 10 essays and the statistical parameters as well as uncertainty are shown.

Table 5. Repeatability of the voltammetric method for the cadmium quantification using minimal instrumentation.

Essay	Concentration (mol L^{-1}) 0.003	0.005	0.007
1	0.0033	0.0050	0.0072
2	0.0031	0.0049	0.0073
3	0.0030	0.0050	0.0070
4	0.0033	0.0050	0.0073
5	0.0030	0.0054	0.0070
6	0.0033	0.0052	0.0072
7	0.0035	0.0050	0.0070
8	0.0033	0.0050	0.0070
9	0.0033	0.0052	0.0072
10	0.0033	0.0052	0.0072
Mean	0.0033	0.0051	0.0071
SD	0.00019	0.00017	0.00011
CV	5.8%	3.3%	1.5%
Uncertainty	$1.2\cdot10^{-4}$ mol L^{-1}	10^{-4} mol L^{-1}	$7\cdot10^{-5}$ mol L^{-1}

SD: Standard deviation, CV: Coefficient of variation

Eclética Química Journal, vol. 44, n. 1, 2019, 53-61
ISSN: 1678-4618
DOI: 10.26850/1678-4618eqj.v44.1.2019.p53-61

The deviation of the results obtained under similar conditions (repeatability) for voltammetric methods is due to fundamentally to the reproducibility of the electrode surface. The electrolysis is a surface phenomenon, and the surface homogeneity influences the current repeatability. When a new electrode surface is generated, it is not exactly equal to the previous one. Therefore, both the amount and shape of the active sites where the electrolysis occurs are not equal either. Consequently, it provokes the measured currents between different electrode surfaces to differ in some degree. Nowadays, vitreous carbon is the most commonly used material as carbon electrode due to the homogeneity of the surface and therefore, the good repeatability of the current values[26]. However, the non-commercial graphite electrode used in this voltammetric method shows an acceptable repeatability.

Uncertainty diminishes with the increase of the concentration. It bears correspondence to results presented by other authors[27, 28]. This tendency is associated with the major magnitude of the errors when the concentration diminishes[29].

3.5. Accuracy

Table 6 shows the recovery percentages for cadmium quantification using minimal instrumentation. An amount of $CdCl_2$ was added to standard solutions to increase concentration in 0.0005 mol L^{-1}. In all cases, the recovery percentages were between 80 and 110%; the range reported by the Guidelines for Validation of Chemical Testing Methods[23]. This demonstrates a good accuracy for cadmium quantification by means of the voltammetric method with the non-commercial electrodes and potentiostat.

Table 6. Recovery percentages for the voltammetric cadmium quantification using minimal instrumentation.

Concentration	Essay	AA	BA	A	%R	
0.003 mol L^{-1}	1	0.0035	0.0030	0.0005	104.7	$\%R_{mean}$ 101.2
	2	0.0038	0.0033	0.0005	106.9	
	3	0.0038	0.0033	0.0005	100.5	CV 8.30%
	4	0.0037	0.0033	0.0005	86.84	
	5	0.004	0.0035	0.0005	106.9	
	Essay	**AA**	**BA**	**A**	**%R**	
0.005 mol L^{-1}	1	0.0059	0.0054	0.0005	99.36	$\%R_{mean}$ 99.64
	2	0.0055	0.0050	0.0005	94.37	
	3	0.0059	0.0054	0.0005	100.8	CV 6.10%
	4	0.0054	0.0049	0.0005	109.2	
	5	0.0056	0.0051	0.0005	94.49	
	Essay	**AA**	**BA**	**A**	**%R**	
0.007 mol L^{-1}	1	0.0077	0.0073	0.0005	99.52	$\%R_{mean}$ 99.52
	2	0.0077	0.0072	0.0005	94.22	
	3	0.0075	0.0070	0.0005	94.47	CV 6.30%
	4	0.0078	0.0073	0.0005	109.64	
	5	0.0076	0.0071	0.0005	99.77	

AA: Concentration of the solution after the addition, BA: Concentration of the solution before the addition, A: Concentration of the addition, %R: Recovery percentages.

The Cochran test did not show differences statistically significant between the variances of the recovery percentages in the three concentrations (p-value=0.6260> α=0.05). The comparison of the recovery percentages in the three concentrations using ANOVA did not show differences statistically significant (p-value=0.9183 > α=0.05). Thus, it demonstrates that the accuracy does not vary with concentration for the levels of these essays.

Eclética Química Journal, vol. 44, n. 1, 2019, 53-61
ISSN: 1678-4618
DOI: 10.26850/1678-4618eqj.v44.1.2019.p53-61

4. Conclusions

A voltammetric method for the quantification of cadmium using minimal instrumentation was developed. Supporting electrolyte KCl 1 mol L^{-1} and pH 5 were selected as working conditions. Regression coefficients superior to 99% showed a good linearity of the method using the non-commercial electrodes and the manual homemade potentiostat. The limits of detection and quantification were in correspondence with the results reported for the linear sweep voltammetry. Results showed an acceptable repeatability. Uncertainty associated with the cadmium concentration diminished with the increase of concentration. A good accuracy was observed, with recovery percentages complying with the established standards. The accuracy was independent of the concentration for the studied range.

5. Acknowledgments

Authors are thankful to Geisa Dávila for the language correction.

6. References

[1] Skoog, D. A., Holler, F. J., Crouch, S. R., Principles of Instrumental Analysis, McGraw Hill, New York, 6th ed., 2008, Ch. 25.

[2] Bard, A. J., Faulkner, L. R., Electrochemical Methods, John Wiley & Sons Inc., New York, 2001, Ch 6.

[3] Kounaves, S., Voltammetric Techniques, In: Handbook of Instrumental Techniques for Analytical Chemistry, Settle, F., ed., Prentice Hall, New York, 1997, Ch 37.

[4] Leon-Rojas, C., Optimización y puesta a punto de un método de mineralización de muestras ambientales para la determinación de ultratrazas de platino, rodio y paladio, Rev. Int. Contam. Amb. 21 (3) (2005) 107-113. Available in: <https://www.redalyc.org/articulo.oa>.

[5] Alvarado-Gámez, A. L., Campos-Fernandéz, J., Development and validation of a voltammetry method to determine traces of iron in water and other matrixes, Port. Electrochim. Acta 23 (1) (2005) 209-221.

[6] Espinosa-Castellón, E. R., Alvarado-Gámez, A. L., Desarrollo y validación de un método voltamperométrico para determinar estaño total en agua, Rev. Int. Contam. Ambie. 28 (1) (2012) 61-72.

[7] Farghaly, O. A., Abdel Hameed, R. S., Abu-Nawwas, H., Analytical application using modern electrochemical techniques, Int. J. Electrochem. Sci. 9 (2014) 3287-3318.

[8] Moreno, Y. L., García, J. M., Chaparro, S. P., Cuantificación voltamétrica de plomo y cadmio en papa fresca, Rev. U. D. C. A. Act. & Div. Cient. 19 (1) (2016) 97-104.

[9] Nordberg, G., Metals: Chemical properties and toxicity, In: Encyclopedia of health and security in the work, Mayer, J., ed., Chantal Dufresne BA, Geneva, 1998, Ch. 63.

[10] Hernández Moreno, D., García Fernandéz, M. A., Alonso Díaz, J., Melgar Riol, M. J., Pérez López, M., Concentraciones de metales pesados (plomo y cadmio) en conservas de almeja, berberecho y navaja comercializadas en España, Ciencia y Tecnología Alimentaria 4 (3) (2004) 197-205.

[11] Chang, C. Y., Yu, H. Y., Chen, J. J., Li, F. B., Zhang, H. H., Liu, C. P., Accumulation of heavy metals in leaf vegetables from agricultural soils and associated potential health risks in the Pearl River Delta, South China, Environ. Monit. Assess. 186 (3) (2014) 1547-1560. https://doi.org/10.1007/s10661-013-3472-0.

[12] Zhenning, Y., Lub, Y., Li, X., Silver ion-selective electrodes based on bis(dialkyldithiocarbamates) as neutral ionophores, Sens. Actuators B 122 (1) (2007) 174-181. https://doi.org/10.1016/j.snb.2006.05.020.

[13] Guo, S. X., Khoo, S. B., Highly selective and sensitive determination of silver(I) at a poly(8-mercaptoquinoline) film modified glassy carbon electrode, Electroanalysis 11 (12) (1999) 891-898. https://doi.org/10.1002/(SICI)1521-4109(199908)11:12%3C891::AID-ELAN891%3E3.0.CO;2-9.

[14] Khan, F., Khanam, A., Study of complexes of cadmium with some L-amino acids and vitamin-C

by voltammetric technique, Ecl. Quím. J. 33 (2) (2008) 29-36. https://doi.org/10.1590/S0100-46702008000200004.

[15] Economou, A., Bolis, S.D., Efstathiou, C.E., Volikakis, G.J., A "virtual" electroanalytical instrument for square wave voltammetry, Analytica Chimica Acta 467 (2) (2002) 179-188. https://doi.org/10.1016/S0003-2670(02)00191-5.

[16] Baltuano, O., Hernández, Y., Montoya, E., Desarrollo de un potenciostato analítico de bajo costo y altas prestaciones, Informe Científico 12 (2012) 165-169.

[17] Vilasó, J. E., Arada, M. A., Baeza, J. A., Céspedes, A., Construction and metrological characterization of a minimal instrumentation micropolarograph, Port. Electrochim. Acta 34 (5) (2016) 309-320. https://doi.org/10.4152/pea.201605309.

[18] Nogueira, C. A., Delmas, F., New flowsheet for the recovery of cadmium, cobalt and nickel from spent Ni–Cd batteries by solvent extraction, Hydrometallurgy 52 (3) (1999) 267-287. https://doi.org/10.1016/S0304-386X(99)00026-2.

[19] Copeland, T. R., Christie, J. H., Skogerboe, R. K., Osteryoung, R.A., Effect of supporting electrolyte concentration in pulsed stripping voltammetry at the thin film mercury electrode, Analytical Chemistry 45 (6) (1973) 995-996. https://doi.org/10.1021/ac60328a017.

[20] Zeng, A., Liu, E., Tan, S. N., Zhang, S., Gao, J., Stripping voltammetric analysis of heavy metals at nitrogen doped diamond-like carbon film electrodes, Electroanalysis 14 (18) (2002) 1294-1298. https://doi.org/1040-0397/02/1809-1294.

[21] Lurie, J., Handbook of Analytical Chemistry, Mir Publishers, Moscow, 1975.

[22] Dieker, J. W., Van Der Linden, W. E., Poppe, H., Behaviour of solid electrodes in normal and differential pulse voltammetric methods, Talanta 25 (1978) 151-155. https://doi.org/10.1016@0039-9140(78)80104-0.

[23] NC Guideline, Guidelines for validation of chemical testing methods, NC, NC Proyecto (2001) 23.

[24] Choi, J., Ide, A., Truong, Y. B., Kyratzis, I. L., Caruso, R. A., High surface area mesoporous titanium–zirconium oxide nanofibrous web: a heavy metal ion adsorbent, J. Mater. Chem. A (2013) 5847-5853. https://doi.org/10.1039/c3ta00030c.

[25] Rajawat, D. S., Kumar, N., Satsangee, S. P., Trace determination of cadmium in water using anodic stripping voltammetry at a carbon paste electrode modified with coconut shell powder, Journal of Analytical Science and Technology 5 (19) (2014). https://doi.org/10.1186/s40543-014-0019-0.

[26] Uslu, B., Ozkan, S. A., Solid electrodes in Electroanalytical Chemistry: Present applications and prospects for high throughput screening of drug compounds, Combinatorial Chemistry & High Throughput Screening 10 (7) (2007) 495-513. https://doi.org/1386-2073/07.

[27] Thomson, M., The Characteristic Function, a method-specific alternative to the Horwitz Function, Journal of AOAC International 95 (6) (2012) 1803-1806.

[28] Hechavarría, A., Arada, M.A., Estimación de la incertidumbre de la medición en análisis químico, un caso de estudio, Rev. Cubana Quím. 29 (1) (2017) 54-72.

[29] EURACHEM/CITAC Guideline, Quantifying uncertainty in analytical measurement, EURACHEM/CITAC, CG4 (2000) 120.

Eclética Química Journal

Original article
iq.unesp.br/ecletica

| Vol. 44 | n. 1 | 2019 |

Chromium speciation in leather samples: an experiment using digital images, mobile phones and environmental concepts

Vinícius Costa[1], Ariane Neiva[1], Edenir Pereira-Filho[1+]

[1] Federal University of São Carlos - UFSCar, São Paulo, Brazil

[+] Corresponding author: Edenir Pereira-Filho, e-mail address: erpf@ufscar.br

ARTICLE INFO

Article history:
Received: October 03, 2018
Accepted: December 11, 2018
Published: January 28, 2019

Keywords:
1. PhotoMetrix
2. digital image
3. mobile phone
4. leather and Cr(VI)

ABSTRACT: This study proposes a new and simple method for Cr speciation and Cr(VI) determination in leather samples using digital images. The experiments were performed using a mobile phone and a free app called PhotoMetrix that was used to obtain and process data. The results obtained from PhotoMetrix were compared to reference methods using UV−Vis. A statistical evaluation between both proposed and the reference methods using two-sample t-test did not show a significant difference at a 95% confidence level. Bovine leather samples (4 samples) tanned with Cr salts and ovine leather samples (3 samples) tanned with vegetable tannin were analyzed. The proposed method presented limits of detection (LOD) and quantification (LOQ) of 0.6 and 2 mg/kg, respectively. In addition, the proposed method using PhotoMetrix and digital images can provide undergraduate students an opportunity to learn topics such as quantitative analyses, environmental chemistry, speciation chemistry, image processing and treatment of statistical data. The results demonstrated that the proposed method can be applied to routine analyses and in experimental analytical chemistry courses.

The use of the smartphone is an excellent tool for the introduction of quantitative analysis

1. Introduction

Quantitative instrumental methods based on atomic spectrometry are commonly used to determine Cr(VI), however these techniques are expensive and are not available in several universities, especially those located in developing countries[1-3]. An image for analysis can be obtained from a mobile phone, scanner or webcam that are versatile instruments and easy to operate. Undergraduate students enjoy interactive and attractive classes, and the use of these tools can be an interesting approach for the experimental part of a laboratory exercise. In recent years, several research groups have used mobile phones and scanners in laboratory classes for determination of metals in several samples[4-6].

Digital images can provide a large amount of data from the extraction of picture elements called pixels, where each pixel is characterized by different channels. The color system most commonly used for color images is red (R), green (G) and blue (B). Although RGB is the most frequently used color model, there are others that can be generated from it, such as hue, saturation and value (HSV); hue, saturation and lightness (HSL); cyan, magenta, yellow, key or black (CMYK) color space; and hue, saturation and intensity (HSI). In these models, hue (H) is associated with how most people recognize a color, for example, the differentiation between red and yellow. Saturation (S) is the amount of the color that is present in an image, for example, the differentiation between red and pink. Value (V), lightness (L), or intensity (I) are related to the amount of light, such as the distinction between dark and light red or between dark and light gray. Value is defined as the highest amount among R, G

or B, intensity as the average of R, G or B colors, and lightness is defined as the average of the maximum and minimum amounts of R, G or B[7].

In 2016, a new free app called PhotoMetrix for image analysis was proposed by Grasel and co-authors[8]. The authors used PhotoMetrix for the identification of tannins according the source type (chestnut, valonea, quebracho, black wattle, tara and myrobalan). PhotoMetrix was used in module multivariate analysis, and images were analyzed using RGB histograms and HSI channels. Principal component analysis (PCA) was employed to verify separation among sample groups. In other study using PhotoMetrix, Helffer and collaborators[9] proposed a simple method for determination of Fe in supplements. The determination of Fe in these samples was performed in univariate mode and differentiation among them was performed in multivariate mode using PCA.

In this sense, the present study proposed a new method for Cr speciation and Cr(VI) determination in leather samples by digital images using the PhotoMetrix app and a mobile phone to obtain, prepare, handle the data, and perform the calculations. This method is simple and obeys the principles of green chemistry as it requires minimum number and quantity of reagents and can be performed in a fast, non-destructive and inexpensive manner. In addition, the method can be applied in laboratory classes and several chemical concepts can be addressed with students.

2. Materials and methods

2.1 Experimental details

The experiments related to image analysis, data processing and treatment were accomplished in an analytical chemistry laboratory course with 15 students. The students were divided into groups, and each one was responsible for part of the activities. Group 1 was responsible for standard solutions preparation, Group 2 was responsible for alkaline Cr(VI) extraction in leather samples and Group 3 was related to data acquisition, processing, and results compilation and organization. A total of 4 hours was needed to carry out the experiments. The results obtained by ICP OES (inductively coupled optical emission spectrometry) for total Cr determination were previously provided to the students.

2.2 Instrumentation

Digital images were obtained using the PhotoMetrix app version 1.0.5 using a cell phone. The PhotoMetrix application in the "Univariate Analysis" mode captures images using the camera of the mobile device. The images can be analyzed using two modes, vector RGB and multi-channel. In vector RGB mode, R, G, B average values are used to calculate the Euclidean norm of the values. In multi-channel mode, each color channels (R, G, B, H, S, V, L, I) is used individually. PhotoMetrix also allows the use of different spot sizes (32 x 32; 64 x 64; 96 x 96 pixels) to obtain images. The mobile phone was mounted on an apparatus made from a wooden box (16.5 × 29.5 and 9.5 cm in height), with a holder to attach the phone (similar to those found in cars to mount a mobile phone) and a hole for the phone camera, as shown in Figure S1 (see Supplementary Material).

Reference concentrations of total Cr were obtained with an ICP OES (iCAP 6000, Thermo Scientific, Waltham, MA, USA), after acid extraction of the samples (n=3). This instrument allows collection of sequential emission signals, using both axial and radial viewings. Argon (99.996%, White Martins-Praxair, Sertãozinho, SP, Brazil) was used as a plasma gas for ICP OES and additional instrumental parameters are shown in Table S1 (see Supplementary Material). Reference concentrations of Cr(VI) were obtained using a spectrophotometer (Thermo Fisher, Shanghai, China), in 540 nm wavelength and a quartz cuvette with 1 cm of optical path.

2.3 Reagents, solutions and samples

All solutions were prepared by students. Ultrapure water (18.2 MΩ cm resistivity) produced by a Milli-Q Plus Total Water System (Millipore Corp., Bedford, MA, USA) was used to prepare all the aqueous solutions. Nitric acid (HNO_3) was previously purified using a sub-boiling distillation system, Distillacid BSB-939-IR (Berghof, Eningen, Germany), and hydrogen peroxide, (H_2O_2) 30% w/w (Synth, Diadema, Brazil), was used for the digestion of samples to determine total Cr. The analytical curve for determination of total Cr was prepared in the range 0.005 to 60 mg L^{-1}. All glassware and polypropylene flasks were washed with soap, soaked in 10% v/v HNO_3 for 24 h, and rinsed with deionized water prior to use.

Eclética Química Journal, vol. 44, n. 1, 2019, 62-74
ISSN: 1678-4618
DOI: 10.26850/1678-4618eqj.v44.1.2019.p62-74

A standard stock solution containing 1000 mg L^{-1} of Cr(VI) was prepared by weighing an adequate mass of a primary standard, potassium dichromate ($K_2Cr_2O_7$) (Synth, São Paulo, Brazil), previously dried at 160 °C for 2 h. The reagents sodium hydroxide (NaOH), sulfuric acid (H_2SO_4), 1,5-diphenylcarbazide (DPC) and acetone were purchased from Merck (Darmstadt, Germany).

The alkaline extraction of Cr(VI) was performed using a 0.1 mol L^{-1} NaOH solution. A 5.0 mol L^{-1} H_2SO_4 solution was prepared to adjust the pH of the extracts. In addition, a DPC solution was prepared daily by dissolving 0.2 g of the reagent in 10 mL of acetone and diluting to 100 mL with deionized water. The DPC solution was then stored in an amber flask to avoid degradation by the environmental light. The calibration curve to determine Cr(VI) concentration by digital images was prepared in the range from 0.05 to 0.75 mg L^{-1} and a Cr(III) solution (Qhemis, Jundiaí, SP, Brazil) containing 50 mg $L^{-1}$was prepared and used in the addition and recovery tests. Seven leather samples were acquired from Embrapa Pecuária Sudeste (São Carlos, SP, Brazil) and analyzed in this study. The leathers were tanned with Cr salts (bovine samples: 1 to 4) and vegetable tannin (ovine samples: 5 to 7). Additional details about the process of leather tanned using Cr salts are available in publication of Dixit *et al.*[10].

2.4 Sample preparation to determine total Cr and Cr(VI)

To determine total Cr, a reference extraction procedure proposed by Neiva and Pereira-Filho[11] was used. The extraction procedure for determination of Cr(VI) using the reference method by UV−Vis and proposed procedure using digital images is described below. The general procedure is represented in Figure 1.

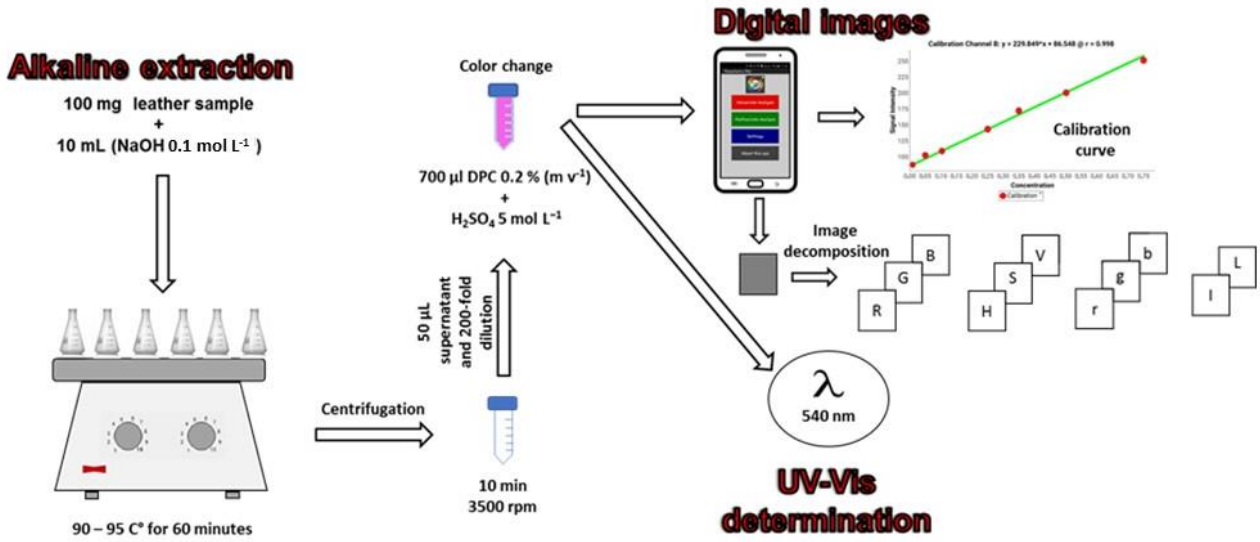

Figure 1. Pictorial for procedure of extraction to Cr(VI), for determination by digital images acquisition and UV-Vis determination.

For Cr(VI) extraction, 100 mg of leather samples were weighed in Erlenmeyer flasks, and 10 mL of 0.1 mol L^{-1} NaOH solution were added. This solution was placed on a hot plate (208-2 D, Nova Ética, São Paulo, Brazil) for 60 min at 90-95 °C with sporadic shaking. When it reached room temperature, the solution was transferred to plastic tubes and centrifuged (3500 rpm for 3 min). A 50 µL aliquot of the supernatant solution was collected and diluted 200-fold. Later, 700 µL of 0.2% (w/v) DPC solution was added and, after this, the pH was adjusted to 1.0 with 5 mol L^{-1} H_2SO_4 solution until the solution changed to a pink color[12]. To verify the performance of the proposed method, addition and recovery experiments were employed. In the recovery tests, a known concentration of

Eclética Química Journal, vol. 44, n. 1, 2019, 62-74
ISSN: 1678-4618
DOI: 10.26850/1678-4618eqj.v44.1.2019.p62-74

Cr(III) and Cr(VI) was added to the samples before the alkaline extraction and the determinations were carried by UV−Vis and digital images.

2.5 Hazard

The students were advised to use safety goggles, gloves and lab vests during the experimental procedure and to take extreme care in acid and solutions preparation and manipulations. The Cr(VI) extraction was performed in a fume hood. In addition, all the Cr (VI) waste were separated for proper treatment and disposal.

3. Results and discussion

3.1 Optimization of the PhotoMetrix parameters

Initially, some experiments were performed to verify the influence of spot size (number of pixels) in the recording of the digital images. To select the best spot size, the linear determination coefficient (R^2) of the analytical curves was used. The spot size that presented the best R^2 value of the analytical curves was 64 x 64 pixels. To select the best color parameter (*vector RGB* and *multi-channel*), we used a standard solution of Cr(VI) at 0.35 mg L^{-1}, and from the analytical curve obtained, the standard concentration was predicted. The parameters obtained for *vector RGB* and *multi-channel* histograms are presented in Table 1.

Table 1. Analytical parameters obtained for the different color channels.

Histograms	Channel	Linear equation	R^2	% recovery
Vector RGB	RGB	y= 212.122x +12.361	0.981	60
Multi-channel	B (Blue)	y= 203.404x + 106.733	0.993	109
	V (Value)	y= 0.893x + 0.343	0.991	120
	L (Lightness)	y= 0.390x + 0.342	0.985	122
	I (Intensity)	y= 0.246x + 0.343	0.963	122
	S (Saturation)	y= 1.000x + 0.104	0.932	115
	H (Hue)	y= 87.406x + 191.671	0.546	38
	G (Green)	y= -14.204x + 88.399	-0.392	-213
	R (Red)	Y= -27.707x + 87.105	-0.806	-235

The color channel B (blue) showed the best trueness (109%) and so was selected for the further experiments. In addition, channel B presented an R^2 of 0.993 and a linear analytical curve equation of y = 203.404x + 106.733. After images decomposition it was observed that channel B presented the highest values when compared with R and G, being the most sensitive channel among the 8 tested.

Figure 2a shows the analytical curve for color channel B, and Figure 2b show the colors of the standard solutions used in the analytical curve. An attractive feature of PhotoMetrix is that the analytical curves are obtained on the app (Figure 2a). In addition, the concentrations predicted by the colors can be also observed in the app. The pink/violet coloration, shown in Figure 2b, is derived from the colorimetric reaction between Cr(VI) and the chromogenic reagent DPC. The overall reaction between Cr(VI) and DPC is presented in Equation 1.

$$2\ CrO_4^{2-} + 3H_4L + 8H^+ \longrightarrow [Cr(III)(HL)_2]^+ + Cr^{3+} + H_2L + 8H_2O \quad (1)$$

The DPC (H_4L) is oxidized to diphenylcarbazone (H_2L), whereas Cr(VI) is reduced to Cr(III) forming the pink/violet color complex Cr(III) - diphenylcarbazone $[Cr(III)(HL)_2]^+$, the reaction occurs in acid medium and the complex has maximum absorbance at 540 nm.

Eclética Química Journal, vol. 44, n. 1, 2019, 62-74
ISSN: 1678-4618
DOI: 10.26850/1678-4618eqj.v44.1.2019.p62-74

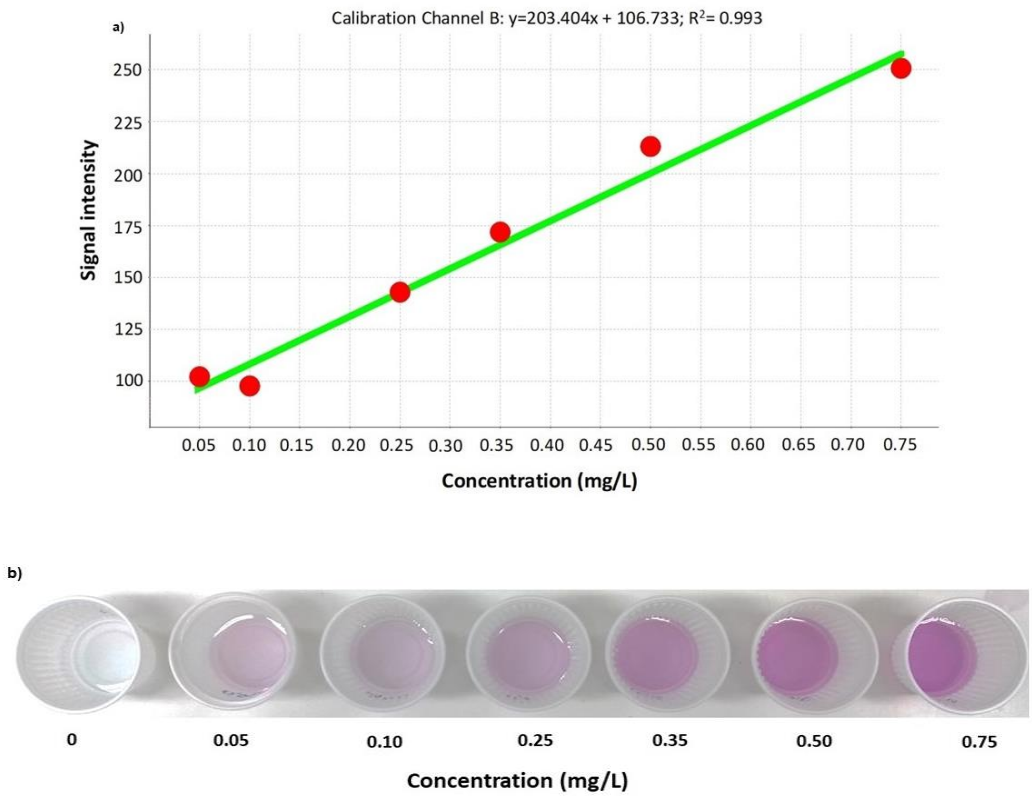

Figure 2. a) Analytical curve in the range of 0.05 - 0.75 mg L^{-1}; b) colors related with standards used in analytical curve.

3.2 Validation and application

The limits of detection (LOD) and quantification (LOQ) were calculated according International Union of Pure and Applied Chemistry (IUPAC) recommendations[13]. The LOD and LOQ of method proposed were 0.6 and 2 mg kg^{-1}, respectively. These values were obtained after multiplying the LOD and LOQ values from the analytical curve by the dilution factor (20,000-fold). The precision estimated as the relative standard deviation (%RSD, n=7) was determined from seven measurements for the extractions performed on a sample of leather with a concentration of 14 mg L^{-1} of Cr(VI), and the RSD obtained was 7.5%. To evaluate the accuracy of the proposed method, addition and recovery experiments were employed. Samples were spiked with standard solutions of 50 mg L^{-1} Cr(III) and 50 mg L^{-1} Cr(VI) before alkaline extraction, and the obtained recoveries were in the range 98-124%. The results are shown in Table 2. No species conversion (oxidation) from III to VI was observed.

In addition, the results obtained through the method developed in this research were compared to those obtained by a reference method using UV-Vis, and the results of the concentrations of total Cr, Cr(III) and Cr(VI) are presented in Table 3.

A statistical evaluation using two-sample t-test showed that there is no difference between the Cr(VI) values obtained with the use of the proposed and the reference method at the 95% confidence level. The concentrations of Cr(VI) determined in the bovine leather samples tanned with Cr salts showed, as expected, the highest values, varying from 1420 – 2100 mg kg^{-1}. On the other hand, the ovine leather samples tanned with vegetable tannins presented Cr(VI) concentration lower than the LOQ of the proposed method. The samples analyzed show values of Cr(VI) concentration above the limits set by the European Union that established a maximum concentration of Cr(VI) of 3 mg kg^{1} [14]. The use of vegetable tannins shows this treatment is in accordance with principles of green chemistry.

Eclética Química Journal, vol. 44, n. 1, 2019, 62-74
ISSN: 1678-4618
DOI: 10.26850/1678-4618eqj.v44.1.2019.p62-74

Table 2. Samples spiked with standard solutions of Cr(III) and Cr(VI) before alkaline extraction and % trueness of Cr(VI) (mean ± standard deviation; n=3).

Leather samples	Simultaneous addition (mg L^{-1}) of Cr(III) and Cr(VI)	Found (mg L^{-1}) Cr (VI)	% recovery (CrVI)
Sample 1 (bovine)	0	18 ± 1	-
	50	76 ± 5	116
Sample 2 (bovine)	0	21 ± 1	-
	50	76 ± 4	110
Sample 3 (bovine)	0	14 ± 1	-
	50	67 ± 2	106
Sample 4 (bovine)	0	19 ± 1	-
	50	69 ± 3	100
Sample 5 (ovine)	0	-	-
	50	57 ± 3	114
Sample 6 (ovine)	0	-	
	50	62 ± 4	124
Sample 7 (ovine)	0	-	
	50	49 ± 3	98

Table 3. Determination of total Cr by ICP OES and Cr(VI) in leather samples by UV-Vis and proposed method.

Leather samples	Concentration (mg kg^{-1})			
	Total Cr	Cr(III)	Cr(VI)	
	Reference method (ICP OES)	Total Cr - Cr VI	Proposed method (digital image)	Reference method (UV-Vis)
Sample 1 (bovine)	16419 ± 435	14609 ± 545	1810 ± 113	1728 ± 105
Sample 2 (bovine)	16917± 261	14817 ± 345	2100 ± 85	2006 ± 87
Sample 3 (bovine)	15091± 471	13671 ± 528	1420 ± 57	1337 ± 112
Sample 4 (bovine)	20445 ± 688	18535 ± 815	1910 ± 127	1795 ± 96
Sample 5 (ovine)	19 ± 2	-	<LOQ	<LOQ
Sample 6 (ovine)	25 ± 2	-	<LOQ	<LOQ
Sample 7 (ovine)	10 ± 3	-	<LOQ	<LOQ

The Cr(VI) values found are high and worrisome, since studies with sensitized individuals revealed that at a level of 5 mg kg^{-1} of Cr, half of the people evaluated presented allergic skin reactions[15]. Normally, leather tanning involves the use of Cr(III). However, there have been many reports that Cr(VI) has been abnormally detected in some leather samples, but this has been widely debated[16]. In time, the chemicals used in production and other environmental factors, such as heat and light, may cause changes and deformations in leather products, e.g., oxidation of Cr(III) to Cr(VI), a decrease in shrinkage temperature, fading or yellowing color, a loss of

Eclética Química Journal, vol. 44, n. 1, 2019, 62-74
ISSN: 1678-4618
DOI: 10.26850/1678-4618eqj.v44.1.2019.p62-74

physical resistance, and odor problems due to oxidation of fat liquors or formaldehyde release. These deformations generally occur due to oxidant groups – free radicals**,** which arise depending on these factors.

3.3 Note to faculty

In technological terms, our society has changed substantially in the last decades. Not only did computers become ubiquitously part of school space or homes, but mobile phone also invaded the hands of students and teachers. It is well known in the literature that teacher can use tools accessible to students, aiming at a contextualized teaching. Contextual teaching draws the attention of students, since the reality of their day can be lived in the classroom. Nowadays every student has a mobile phone, and this may be an opportunity for the teacher to introduce chemical concepts from colorimetric experiments, in which students use their mobile phone as an instrument of analysis. This type of activity addresses the concept of contextualized teaching.

In the experiments proposed in this study using a mobile phone, we highlight the importance of the used app (PhotoMetrix), which facilitates the development of the class and student learning. In this sense, the use of these tools can be a strategy used by teachers in experimental classes, with the purpose of contributing to the intellectual development and awakening the scientific interest of these students who could become future researchers.

From this experiment, several chemical concepts can be approached in the classroom and are listed below:

- Quantitative analysis;
- Chemical speciation;
- Environmental chemistry;
- Solution preparation and construction of a calibration curve;
- Sample preparation;
- Planning and executing experiments through the use of appropriate chemical literature and electronic resources;
- The use of statistical tools can also be approached from analyzing data statistically, assessing the reliability of experimental results, and discussing the sources of systematic and random error in experiments;
- Validation of the analytical procedure.

3.4 Students opinion about the use of Photometrix in experimental class

Currently, many students have a mobile phone and are willing to install a free app, such as the PhotoMetrix. This approach shows that it is possible to use materials in the daily lives of students in the classroom. The utility of this method lies not only in its efficacy for determining Cr(VI) concentration via the measurement of a color change but also in its robustness in a range of factors, including lighting conditions and picture quality, which can vary dramatically from one classroom to another. In addition, the samples used in this experiment can be easily obtained and are present in the daily lives of the students. The students found the experiment interesting, mainly because they could compare the results obtained with PhotoMetrix with those obtained with an equipment, such as a UV-Vis as was performed in this study.

The students' evaluation from the experimental procedure was very positive, mainly due to the fact they used their own mobile phones in data acquisition and treatment. This experiment was performed in a course named "Qualitative and Quantitative Analysis in Chemistry" and at the end of at least 4 experimental classes performed in different semesters, 20 students answered some questions about the use of Photometrix in the experimental classes. Figure 2S summarizes the students' opinions.

4. Conclusions

The proposed method for Cr(VI) speciation and determination in leather samples using digital images from mobile phones was shown to be very efficient. The results obtained with the proposed procedure demonstrated good accuracy with values obtained from a reference method by UV-Vis. This method can be used in routine analyses for determination of Cr(VI) in leather samples. In addition, the method can be used in experimental analytical chemistry courses. The students can be motivated by learning that their mobile phones can be used as effective analytical devices. Another benefit of this approach is that students can see with their eyes what they are measuring and understand.

Eclética Química Journal, vol. 44, n. 1, 2019, 62-74
ISSN: 1678-4618
DOI: 10.26850/1678-4618eqj.v44.1.2019.p62-74

5. Acknowledgments

This study was supported by the São Paulo Research Foundation (FAPESP, 2016/01513-0), the Conselho Nacional de Desenvolvimento Científico e Tecnológico (CNPq, 401074/2014-5 and 305637/2015-0), and Embrapa. This study was financed in part by the Coordenação de Aperfeiçoamento de Pessoal de Nível Superior - Brasil (CAPES) - Finance Code 001.

6. References

[1] Sussulini, A., Arruda, M. A. Z., Determinação de cromo (VI) por espectrometria de absorção atômica com chama após a extração e pré-concentração no ponto, Eclet. Quím. J. 31 (2006) 73-80. https://doi.org/10.1590/S0100-46702006000100009.

[2] Capitán-Vallvey, L. F., López-Ruiz, N., Martínez-Olmos, A., Erenas, M. M., Palma, A. J., Recent developments in computer vision-based analytical chemistry: A tutorial review. Anal. Chim. Acta, 899 (2015) 23-56. https://doi.org/10.1016/j.aca.2015.10.009.

[3] Santos, P. M., Pereira-Filho, E. R., Digital image analysis – an alternative tool for monitoring milk authenticity, Anal. Methods. 5 (2013) 3669-3674. https://doi.org/10.1039/C3AY40561C.

[4] Colzani, H., Rodrigues, Q. E. A. G., Fogaça, C., Gelinski, L. N., Pereira-Filho, E. R., Borges, E. M., Determinação de fosfato em refrigerantes utilizando um scanner de mesa e análise automatizada de dados: um exemplo didático para ensino de química, Quim. Nova. 40 (2017) 833-839. https://doi.org/10.21577/0100-4042.20170035.

[5] Montangero, M., Determining the Amount of Copper (II) Ions in a Solution Using a Smartphone, J. Chem. Educ. 92 (2015) 1759-1762. https://doi.org/10.1021/acs.jchemed.5b00167.

[6] Moraes, E. P., Confessor, M. R., Gasparotto, L. H. S., Low-Cost Method for Quantifying Sodium in Coconut Water and Seawater for the Undergraduate Analytical Chemistry Laboratory: Flame Test, a Mobile Phone Camera, and Image Processing, J. Chem. Educ. 92 (2015) 1696-1699. https://doi.org/10.1021/ed400797k.

[7] Gomes, M. S., Trevisan, L. C., Nóbrega, J. A., Kamogawa, M. Y., Uso de scanner em espectrofotometria de absorção molecular: aplicação em experimento didático enfocando a determinação de ácido ascórbico, Quim. Nova. 31 (2008) 1577-1581. https://doi.org/10.1590/S0100-40422008000600050.

[8] Grasel, F. S., Ferrão, M. F., Helfer, G. A., Costa, A. B., Principal Component Analysis of Commercial Tannin Extracts Using Digital Images on Mobile Devices, J. Braz. Chem. Soc. 27 (2016) 2372-2377. https://doi.org/10.5935/0103-5053.20160135.

[9] Helfer, G. A., Magnus, V. S., Bock, F. A., Teichmann, A., Ferrão, M. F., Da Costa, A. B., PhotoMetrix: An Application for Univariate Calibration and Principal Components Analysis Using Colorimetry on Mobile Devices, J. Braz. Chem. Soc. 28 (2017) 328-335. https://doi.org/10.5935/0103-5053.20160182.

[10] Dixit, S., Yadav, A., Dwivedy, P. D., Das, M., Toxic hazards of leather industry and technologies to combat threat: a review, J. Clean. Prod. 87 (2015) 39-49. https://doi.org/10.1016/j.jclepro.2014.10.017.

[11] Neiva, A. N., Pereira-Filho, E. R., Evaluation of the Chemical Composition of Synthetic Leather Using Spectroscopy Techniques. Appl. Spectrosc. 72 (2018) 921-932. https://doi.org/10.1177/0003702818764922.

[12] Oliveira, L. F., Canevari, N. T., Guerra, M. B. B., Pereira, F. M. V., Schaefer, C. E. G. R., Pereira-Filho, E. R., Proposition of a simple method for chromium (VI) determination in soils from remote places applying digital images: A case study from Brazilian Antarctic Station, Microchem J. 109 (2013) 165-169. https://doi.org/10.1016/j.microc.2012.03.007.

[13] Belter, M., Sajnog, A., Barałkiewicz, D., Over a century of detection and quantification capabilities in analytical chemistry-historical overview and trends. Talanta, 129 (2014) 606-616. https://doi.org/10.1016/j.talanta.2014.05.018.

[14] ISO 17075. (2007). Leather – Chemical Tests – Determination of Chromium (VI) Content. International Organization for Standardization.

[15] BFR (Bundesinstitut fur Risikobewertung). Chromium (VI) in leather clothing and shoes problematic for allergy sufferers. (2007) <http://www.bfr.bund.de/cd/9575>. Accessed 10 December 2017.

[16] Neiva, A. M., Sperança, M. A., Costa, V. C., Jacinto, M. A. C., Pereira-Filho, E. R., Determination of toxic metals in leather by wavelength dispersive X-ray fluorescence (WDXRF) and inductively coupled plasma optical emission spectrometry (ICP OES) with emphasis on chromium. Environ. Monit. Assess. 190, (2018) 618-631. https://doi.org/10.1007/s10661-018-6990-y.

Eclética Química Journal, vol. 44, n. 1, 2019, 62-74
ISSN: 1678-4618
DOI: 10.26850/1678-4618eqj.v44.1.2019.p62-74

Supplementary Material

Chromium speciation in leather samples: an experiment using digital images, mobile phones and environmental concepts

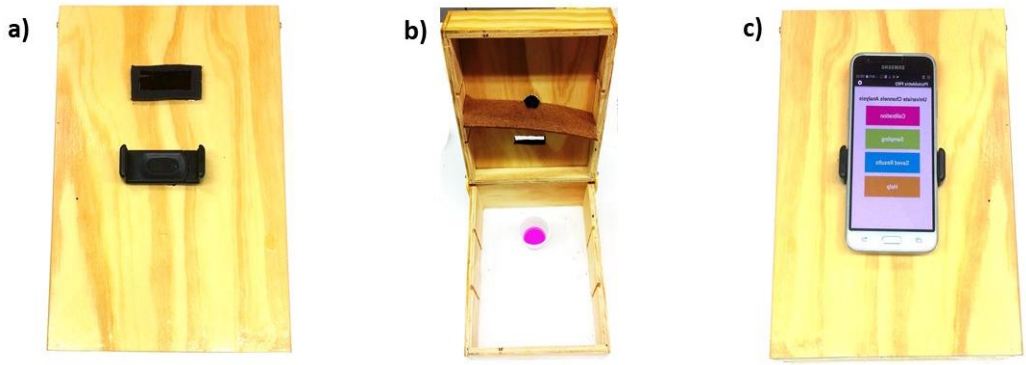

Figure 1S. a) Wooden box with a holder to attach the phone and a hole for the phone camera; b) profile of the interior of the wooden box with the sample; c) wooden box with the phone in the holder.

Eclética Química Journal, vol. 44, n. 1, 2019, 62-74
ISSN: 1678-4618
DOI: 10.26850/1678-4618eqj.v44.1.2019.p62-74

Question

1 – What is your opinion about the operation and results interpretation obtained from Photometrix?

Summary

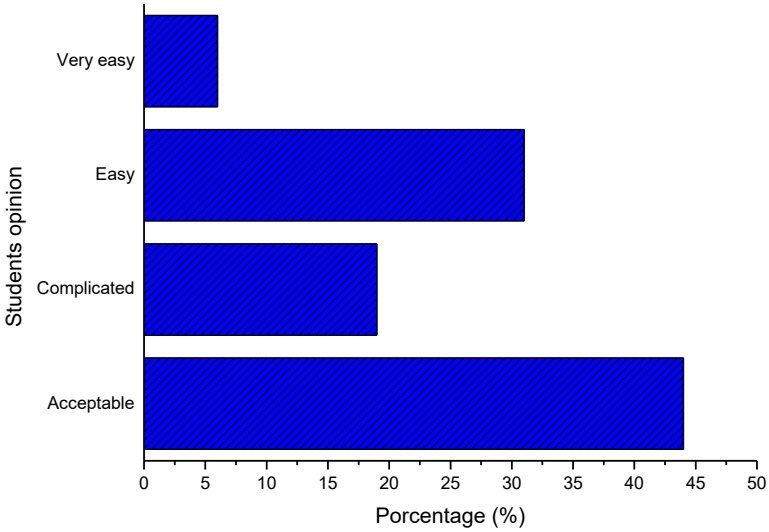

2 – Did you have an idea about this type of mobile phone application before this experimental class?

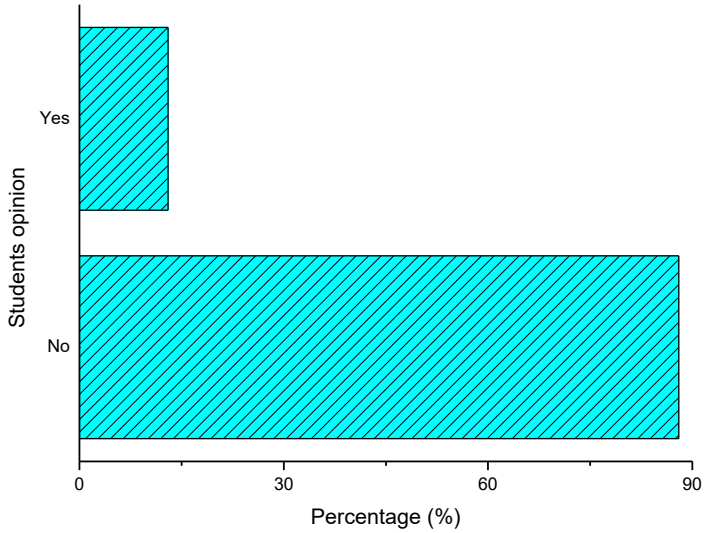

3 – Could you use Photometrix in your other classes?

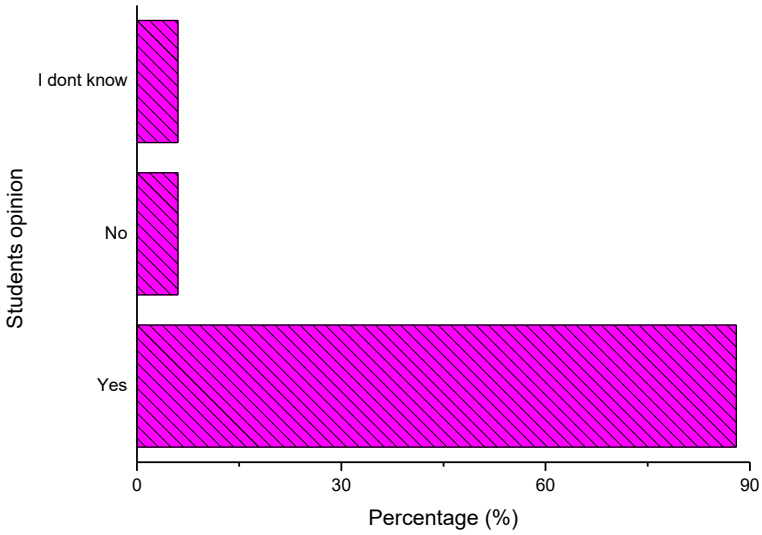

Eclética Química Journal, vol. 44, n. 1, 2019, 62-74
ISSN: 1678-4618
DOI: 10.26850/1678-4618eqj.v44.1.2019.p62-74

4 – Would you like Photometrix to be used in other experimental classes?

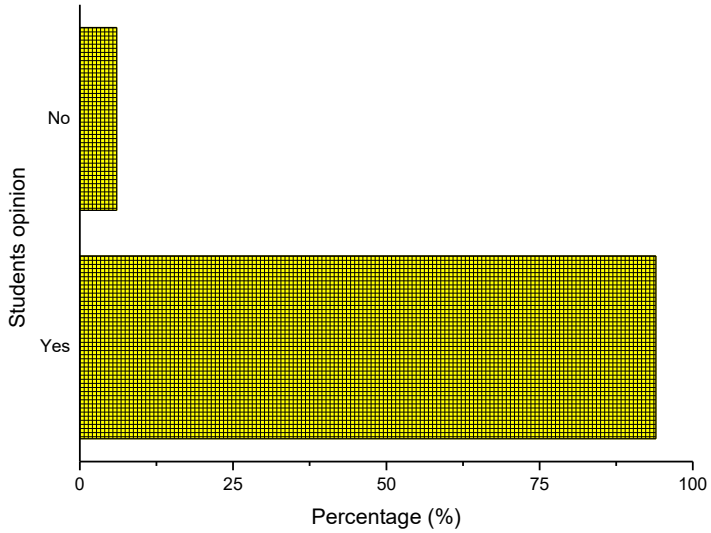

5 – What is your opinion about the use of Photometrix and instrumental techniques?

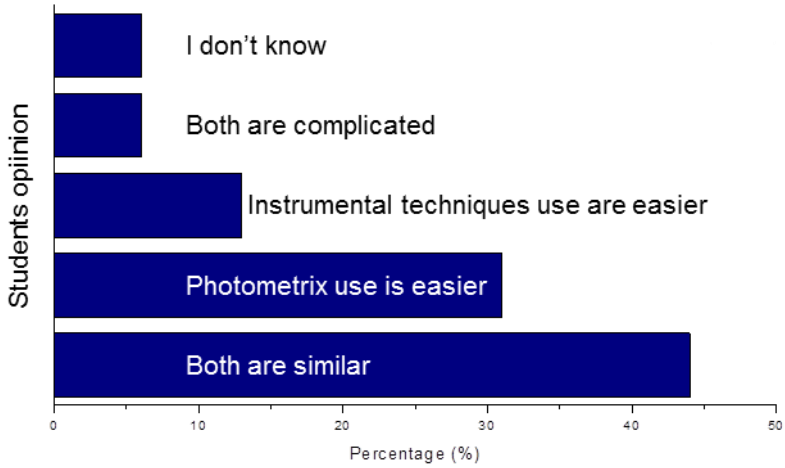

Figure 2S. Students' opinions about the use of Photometrix in the experimental class.

Eclética Química Journal, vol. 44, n. 1, 2019, 62-74
ISSN: 1678-4618
DOI: 10.26850/1678-4618eqj.v44.1.2019.p62-74

Table S1. Operational parameters for ICP OES determinations.

Instrument parameter	Operational conditions
Radio frequency applied power (kW)	1.15
Integration time for low emission line (s)	15
Integration time for high emission line (s)	5
Sample introduction flow rate (mL min^{-1})	2.1
Pump stabilization time (s)	5
Argon auxiliary flow rate (L min^{-1})	0.5
Argon plasma flow rate (L min^{-1})	12
Argon nebulizer flow rate (L min^{-1})	0.7
Replicates	3
Element and wavelength (nm); View modes: axial and radial.	Cr I (283.5)

Eclética Química Journal, vol. 44, n. 1, 2019, 62-74
ISSN: 1678-4618
DOI: 10.26850/1678-4618eqj.v44.1.2019.p62-74

ISSN: 1678-4618
DOI: 10.26850/1678-4618eqj.v44.1.2019.p62-74